Computing modal parameters of fluid-loaded panels using the coupling coefficient

A project report submitted in partial fulfilment
of the requirements for the degree
in

Master of Technology (M.Tech)
in
Mechanical Engineering

by

Tarun Singh Baghel

Advisor: Dr. Venkata R. Sonti

Department of Mechanical Engineering
Indian Institute of Science
Bangalore - 560012, India

July 2019

This thesis is dedicated to my loving wife *Dr. Seema*, whose support, enthusiasm and tolerance enabled me to complete the work. For the past 19 months she has taken all the pain to raise our daughter *Tivisha* which helped me to complete the project in time.

Declaration

I hereby declare that this thesis entitled as "**Computing modal parameters of fluid-loaded panels using the coupling coefficient**" is a original research work carried out by me under the guidance of **Prof. Venkata R. Sonti**,*Vibro Acoustics Lab, Department of Mechanical Engineering, IISc.* Since this is extension of the work carried out by one of senior student Anoop A. M. (PHD thesis), certain contents of report in chapter 3 and 4 has been taken from his thesis. To the best of my knowledge the contents of this dissertation except where some specific reference is made have not been submitted in whole or part for consideration for any other degree or qualification in this, or any other university.

Tarun Singh Baghel
Vibro Acoustics Lab
Mechanical Engineering Department
IISc, Bangalore

Acknowledgements

Foremost, I would like to express my sincere gratitude to my adviser **Prof. Venkata R. Sonti** for continous support during my M.Tech study, for his patience, enthusiasm and motivation. His guidance and courses on Vibration and Acoustics helped me in all the time of reserch and writing this thesis.
Beside my advisor, I would like to thank the following individuals, group of individuals, institutions etc for encouragement and advise. This thesis would not have been what it is without their support.

- **Space Applications Centre (SAC)**-*ISRO, DOS, Govt. Of India*
- **Shri A. K. Lal**-*Deputy Director-SRA/SAC ISRO*
- **Shri K. B. Vyas**- Group Director-MQAG/SRA/SAC ISRO
- **Shri B. Satyanarayana**- Head-QAMD/MQAG/SRA/SAC ISRO
- **Faculty and Students** - Dept. of Mechanical Engg. - IISc
- **Space Technology Cell (STC)** - IISc
- **Anoop A. M.** -Vibro Acoustics Lab, Dept. of ME. IISc
- **All the labmates** - Vibro Acoustics Lab, Dept. of ME. IISc
- **Taxpayers of India**

Last but not the least, I would like to thank my family and friends for supporting and helping me in direct and indirect way to complete this research.

Abstract

The purpose of this study is to derive closed form expressions for the resonance frequencies (and subsequently the modeshapes) of a flexible simply-supported fluid-loaded panel set in an infinite rigid baffle. The coupled equation of motion is derived for a panel excited by a harmonic force and radiating sound. When this force is set to zero, the equation for the eigenvalue problem (or free vibration problem) is obtained. This equation carries a term called the modal coupling coefficient, which is an improper double integral. This integral is computed in a closed form using branch cuts in the complex plane. Once this coupling coefficient is obtained in a closed form, the homogeneous equation above is amenable for computing the coupled natural frequencies and modeshapes.

It is in the nature of panel radiation that several types of interactions surface depending upon the frequency of excitation. Thus, for a standard size panel, keeping 10000 Hz as the upper limit of the excitation frequency, analytical expressions of the coupling coefficient are derived for the corner-corner and the edge-edge interactions. Using these expressions, the coupled equation is written in the matrix form. The natural frequency is then determined by equating the real part of determinant to zero. Further, the mode shapes are evaluated and it is found that cross modal coupling is minimal. Thus, only the diagonal terms of the coupled matrix are sufficient for natural frequency evaluation.

The closed form expressions for the coupled resonances are presented. The frequency evaluated is validated considering two different plates of size 0.455m $\times$0.546m and 1.5m $\times$1.8m . A close match between the frequencies obtained from the coupled equation and LMS virtual lab simulation is observed.

Table of contents

List of figures

List of tables

Chapter 1

Introduction

1.1 Motivation

Sound and structure interaction is a subject that finds relevance in applications such as aircraft structures, nuclear reactor components, marine platforms, hull of the ships, turbines, dams, launch vehicles, etc. The structural vibration creates the sound field that in turn influences the vibration field and modifies it. Hence, this is a coupled problem. When structures radiate sound into a light fluid such as air, one could consider it largely uncoupled (or one way coupled). This implies that the vibration field of the structure can be computed first (assuming that it is placed in a vacuum) and then the results can be used to compute the sound pressure field. However, if the structure is placed in a heavy fluid such as water, then a fully coupled (or two-way coupled) problem has to be solved. Here, the vibration field and the sound pressure field are simultaneously unknown. Occasionally, even in light fluids, under certain conditions (such as enclosed air) one has to solve a coupled problem.

In this context, sound radiation from a rectangular panel (or plate) placed in a baffle (or an infinite rigid wall) in contact with a fluid has been a topic of research for several decades. The one way coupled problem is tractable analytically and numerically and is already available in the literature and textbooks. The two way coupled problem is also solvable numerically. However, the analytical solution is a complicated one, remaining partially addressed and it is the topic of this document.

1.2 Objective

The main objective of this thesis is to obtain analytical expressions for the natural frequencies and also to identify the mode shapes of a fluid-loaded finite simply-supported rectangular thin panel (or plate) placed in a baffle (i.e., a rigid wall). The objective is achieved in the following way:

- First, the free vibration eigenvalue problem for a fluid-loaded rectangular panel is derived [12].
- The eigenvalue problem derivation brings about a term called the modal coupling coefficient (which is an improper double integral). This coupling coefficient integral is computed in a closed form through an L-shaped branch cut in the complex plane (as done by a senior student Anoop).
- These closed form expressions obtained above are then used to find the natural frequencies of the fluid-loaded panel.

1.3 The work carried out as part of the M.Tech degree

This work is an extension of research carried out by a former student Mr. Anoop Mana. The following are the details of the work carried out:

- The relevant portions of PhD thesis of Mr. Anoop were rederived.
- The results of a relevant paper by Pope and Leibowitz [15] that presents the coupling coefficent in a different way were also derived. A few results that were missing in this paper were also computed.
- The coupling coefficient was numerically computed and compared with the closed form expressions.
- A study was done to compare the magnitudes of self modal coupling coefficients with the cross modal coupling coefficients.
- After ascertaining that the self modal coefficients are adequate, the closed form expressions for the coupled resonances were derived that are valid across the entire frequency range.

- The natural frequencies for the fluid-loaded panel were numerically computed and compared with those obtained from a commercial package (LMS).

1.4 Organization of Thesis

This thesis is presented in 6 chapters. Original work done is discussed in the chapter 3 and 5 . A brief summary of each chapter is given here:

- **Chapter 2** :- In this chapter, the relevant literature on the structural acoustics of a panel is reviewed. The additional background material which helps in reading this thesis is also presented. Finally, a brief introduction on one way and fully coupled analysis is presented.

- **Chapter 3** :- The coupled partial differential equations governing the vibrations of a fluid loaded panel driven by a harmonic point force and that of the radiated sound field are derived in this chapter. A single coupled equation is derived for the panel vibration driven by the point force. Setting the point force to zero results in the free vibration eigenvalue problem amenable for computing the natural frequencies. In order to compute the natural frequencies, the equations are arranged in a matrix form.

- **Chapter 4** :- This chapter is devoted to finding the closed form expressions of the modal coupling coefficient using branch cuts in the complex plane. Expressions for the corner-corner modes and the edge-edge modes are derived. These expressions are general in the sense that they can be used for panels of any size under fluid loading conditions.

- **Chapter 5** :- Numerical results are presented in this chapter. Closed form expressions for the coupled natural frequencies of the panel are presented. The numerical natural frequency values are compared with those computed from a commercial package (LMS). A comparison with the *in vacuo* natural frequency values of the panel is also presented.

- **Chapter 6** :- In this chapter, relevant conclusions are drawn from all the important results obtained in the thesis. The avenues for future work are also briefly mentioned in this chapter. Appendices are provided at the end of the thesis which detail the step by step derivation of the expressions given in the main text.

1.5 Conclusions

In this chapter, we have discussed the motivation behind evaluating the modal parameters of a fluid loaded panel. Objective of the study is presented along with novelty in the task done for completing project. At last, the outline of thesis organization is presented, before going in details of the work. In the next chapter, a brief theory of panel radiation and fully coupled systems is presented which helps in understanding the thesis.

Chapter 2

Background and literature survey

2.1 Introduction

This chapter presents material which helps in reading of the thesis. The idea being that the reader should not need to refer too much outside material in following the reported work. In addition, this chapter also presents the literature survey of the previous works done in the field of fully coupled systems.
Initially, a brief introduction to the structural acoustics of the finite panel is presented in section 2.2. Related governing differential equations are also presented. In section 2.3, one way coupled analysis is discussed, in which different modes of the panel radiation are presented. Discussion on the two way coupled analysis is done in section 2.4 along with mathematical formulation of the coupled sound radiation and sound transmission.

2.2 Structural acoustics of finite panels

Acoustic waves are generated by the flexural modes of the panel vibration subjected to direct mechanical force excitation. For a finite panel, the flexural vibration can be expressed as a superposition of the *in vacuo* natural modes. Each mode is associated with a certain wave number in the panel. In radiation problem, the panel set in an infinite rigid baffle is excited by an external force and the acoustic pressure field generated by the panel vibration is obtained by solving the Helmholtz equation with the boundary condition imposed at the panel-fluid boundary (Eqs. (2.2), (2.3)). Problems of fluid-structure interactions can be solved using the following equations

$$\text{Structure} : \{\mathcal{L}\mathbf{u}_s = \mathbf{f}, \tag{2.1}$$

$$\text{Fluid} : \{(\Delta^2 + k^2)p(x, y, z, t) = 0 \ , \tag{2.2}$$

$$\text{Coupling} : \{\dot{u}_s\,|_{int} = \dot{u}_a|_{int} \ . \tag{2.3}$$

In the Eq.(2.1), $\mathcal{L}$ represents a differential operator specific to the structure model [14], $\mathbf{u}_\mathrm{s}$ the generalized displacement vector and $\mathbf{f}$, the generalized force vector. The generalized force is composed of the direct excitation by any mechanical loading on the structure, denoted as f_s , and the force exerted by the surrounding acoustic medium at the fluid-structure interface, denoted as $f_{\text{ int}}$ [17]. Thus, we have

$$\mathbf{f} = \mathbf{f}_\mathrm{s} + \mathbf{f}_\mathrm{int}. \tag{2.4}$$

The kinematic boundary condition at the fluid-structure interface insists that the fluid and the structural velocity at the interface in the normal direction be the same, which is stated in Eq. (2.3).

The effectiveness of flexural waves in a structure in radiating sound depends on whether the waves, which essentially act as a source against the fluid, are subsonic (slower than the wave speed in the fluid) or supersonic (faster than the wave speed in the fluid). The frequency which separates subsonic and supersonic waves in the structural acoustics is known as coincident (critical) frequency (Fig. 2.1). Hatched portion in the figure represents subsonic region.

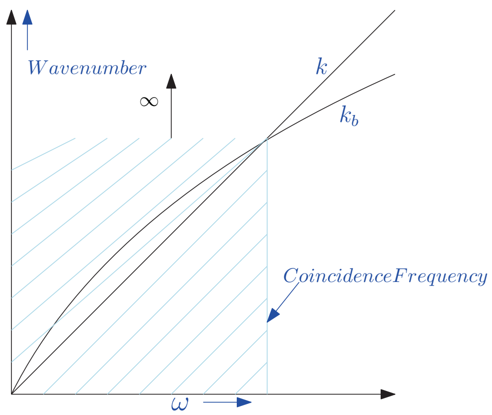

Fig. 2.1 Coincidence frequency

When a panel is excited at a frequency above coincidence frequency, acoustic waves are radiated from the full panel area. However, sound cancellation is a dominant phenomenon in case of subsonic waves on the panel.

In the structural acoustics, there are two methods for analyzing the sound radiation. In the first method i.e., one way coupled analysis, the structure is assumed to be present in vacuum and the velocity response is computed. The structure is then placed in the acoustic medium and the velocity obtained earlier is used to compute the acoustic pressure. In the second method i.e., fully coupled analysis, the fluid and structural domains PDEs are solved simultaneously, i.e., the fluid pressure and the structural velocity are simultaneously unknowns. This method is used when the fluid loading cannot be ignored [4, 7].

2.3 One way coupled analysis

As discussed in the section 2.2, acoustic waves are generated by the flexural modes of panel vibration subjected to direct mechanical force excitation. Bulk fluid response over the panel depends on the frequency of excitation. For a finite panel, the flexural vibration of panel can be expressed as a superposition of the *in vacuo* natural modes. Each mode is associated with a certain wavenumber in the panel. Maidanik classified the panel modes with respect to their modal wavenumbers in the wave number space [13].

Following the work of Maidanik [13], a similar classification of the panel wave numbers is used in this thesis and is illustrated in Fig. 2.2. In this figure , k_m and k_n are the panel modal wave numbers in the x and y directions, respectively, when it is vibrating in the $(m,n)^{th}$ mode.

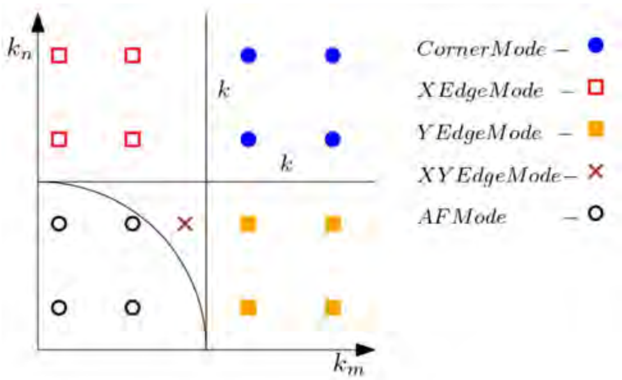

Fig. 2.2 Panel modes classification in the wavenumber space with respect to the acoustic wave number.

Based on the panel wave numbers k_m and k_n, the modes of a vibrating panel can be classified into four categories: corner modes, X/Y edge (single edge) modes, XY edge (double edge) modes and acoustically fast (AF) modes [13, 6, 15]. The associated panel wave numbers definition compared with the acoustic wave number is given in the Table 2.1.

Type	Panel wave numbers
Corner	$k_m > k, k_n > k$
X edge	$k_m < k, k_n > k$
Y edge	$k_m > k, k_n < k$
XY edge	$k_m < k, k_n < k, k_m^2 + k_n^2 > k^2$
Acoustically fast (AF)	$k_m < k, k_n < k, k_m^2 + k_n^2 < k^2$

Table 2.1 Types of panel modes based on the panel wavenumbers

In corner modes (Fig. 2.3 (3)), only the corner quarter cells in the panel contribute significantly to the sound radiation. The X edge and the Y edge (Fig. 2.3 (1), (2)) modes are more efficient radiators than the corner modes. In these cases, a strip of half-cell width along the X or the Y edges of the panel radiates efficiently. For the XY edge modes (Fig. 2.3 (4)) [7], significant radiation is due to the edge strips extending over the entire perimeter. The above modes are responsible for the sound radiation below the critical frequency. Above the critical frequency, the whole panel surface radiates efficiently and the sound radiation is due to the acoustically fast modes.

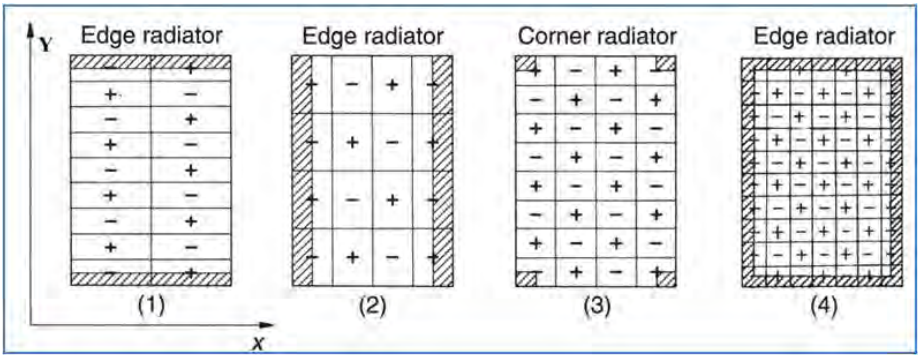

Fig. 2.3 Pictorial representation of the panel modes [7].

2.4 Two way coupled analysis

In the two-way coupled analysis, the effect of the radiated pressure field is taken into account while finding the panel response. The radiated pressure field can be obtained by solving the Helmholtz equation with the boundary condition in terms of the panel velocity. Thus, both the structure and the acoustic domains are now coupled and one needs to solve both the domains simultaneously. The panel response can still be expressed as the superposition of the *in vacuo* modes [6]. The problem of fully coupled analysis is studied through sound radiation and sound transmission problems.

2.4.1 The sound radiation problem

For a sound radiation problem, a direct mechanical force excites the structure and the pressure field in the acoustic medium is generated by the structural vibrations alone (radiated pressure field). The associated pressure loading on the structure can be represented as $\mathrm{f}_{\mathrm{int}} = \mathrm{f}_{\mathrm{rad}}$ (Eq. 2.4). Thus,

$$\mathbf{f} = \mathbf{f_s} + \mathbf{f}_{\mathrm{rad}}. \tag{2.5}$$

While solving the structure domain equation (Eq.(2.1)) for one way coupled formulation, the radiated pressure loading from the acoustic domain is neglected, i.e., $\mathrm{f}=\mathrm{f}_s$. Now, the acoustic pressure field can be obtained using Eqs. (2.2) and (2.3). In the two-way coupled formulation, we do not neglect the radiated pressure field. We solve Eqs. (2.1), (2.2) and (2.5) with the boundary condition Eq. (2.3), simultaneously.

2.4.2 The sound transmission problem

For a sound transmission problem, the structure is excited by an acoustic wave alone. No direct mechanical loading on the structure is considered for the transmission problem, i.e., $\mathrm{f}_s = 0$. The total pressure in the acoustic medium consists of the contributions from the incident and the radiated pressure fields. Hence, we can write $\mathrm{f}_{\mathrm{int}} = \mathrm{f}_{\mathrm{inc}} + \mathrm{f}_{\mathrm{rad}}$ (Eq. 2.4). Thus,

$$\mathbf{f} = \mathbf{f}_{\mathrm{inc}} + \mathbf{f}_{\mathrm{rad}}. \tag{2.6}$$

In the case of one-way coupled formulation, we neglect the radiated pressure field and have $\mathrm{f} = \mathrm{f}_{\mathrm{inc}}$. Structural velocity can be computed by solving Eq. (2.1) and the acoustic pressure field is obtained by solving Eqs. (2.2) and (2.3). While, for the two-way coupled formulation, we solve Eqs. (2.1), (2.2) and (2.6) with the boundary condition Eq. (2.3), simultaneously.

For a fully coupled systems, the radiated pressure field induces coupling between the *in vacuo* modes of the structure. The coupling is expressed in the form of a modal coupling coefficient in the resulting equation of motion for the panel.

Davies developed an analytical expression for the modal coupling coefficient of a simply supported panel set in an infinite rigid baffle with the fluid loading on one side [6]. However, his analytical expressions were valid only at low frequencies where the panel modal wave numbers were greater than the acoustic wave number [13]. The real parts of the coupling coefficients were related to the radiation damping on the panel response and the imaginary parts led to a virtual mass addition to the panel mass. Davies observed that the effect of the cross modal inertia coupling terms in determining the coupled natural frequencies of the water-loaded panel was negligible [6]. It was largely influenced by the self inertia terms.

Pope and Leibowitz presented a more complete calculations for the modal coupling coefficients [15] than that given by Davies [6]. They derived approximate expressions for the coupling coefficients involving corner, edge and the acoustically fast modes. However, some key coupling coefficient expressions involving acoustic fast-double edge and single edge-double edge interactions were not presented in his paper.

Sandman [16] studied the vibration and the resulting sound radiation from a water-loaded finite panel with a concentrated mass, set in an infinite rigid baffle. He formulated the panel response assuming it to be a linear combination of the *in vacuo* modes. Both the fluid loading and the concentrated mass induced the coupling between the *in vacuo* panel modes. He further evaluated the modal coupling coefficient at low frequency using numerical method and considering only 10 modes in the truncated equation of motion. Sandman concluded that the effects of the concentrated mass are significant only at relatively high frequencies and it causes change in the directivity of sound radiation.

The low frequency acoustic radiation from a fluid-loaded panel, elastically restrained against rotation at the edges was studied by Lomas and Hayek [11]. He further compared the self and cross modal coupling coefficients for the lower order modes (obtained numerically) with Davies' approximations for the corner-corner interactions [6] and found a good match. The coupled natural frequencies of a few lower order modes were also obtained for both the simply supported and the clamped boundary conditions.

Berry et al. [3] analyzed the radiation of sound from a baffled, rectangular plate with the edges elastically restrained against deflection and rotation. A variational method was used to model the fluid-structure interactions. The modal coupling coefficients were expressed as an integral involving simple Taylor functions and were evaluated numerically. The paper also discussed the mean quadratic velocity of a water-loaded panel and the resulting radiated power for various boundary conditions [2].

Graham [8, 9] presented an asymptotic analytical solution for a simply supported plates using contour integration to replace the impedance in double Fourier transform and obtained asymptotic expressions for the modal coupling coefficients. The results were validated against the numerical solutions. The expressions derived for the radiation coupling coefficients were found to be asymptotically equivalent to that derived earlier for the corner - corner modal interactions by Davies [6].

Crighton and Innes studied the effect of the fluid loading on the response of a thin infinite panel at low frequencies using the asymptotic method [5]. The authors also considered the response of a panel of finite width but of infinite length to a line excitation. It was found that the modes of the fluid-loaded finite panel were of the same shape as that of the *in vacuo* case, however of a different scale due to the fluid loading. Takahashi found the approximate expressions for the self modal coupling coefficients and discussed the sound transmission loss at different frequencies [18]. The cross modal coupling was ignored in his analysis.

Recently, modal sound transmission coefficients were formulated for a single leaf panel by Wang [19] and derived an expression for the equivalent self modal coupling coefficient. Wang incorporated the modal coupling effect into the modal sound transmission coefficient of each structural mode by introducing the equivalent modal impedance. The effect of the cross modal coupling on the overall transmission coefficient was found to be significant only when the participating modes were subsonic. Fahy [7] gave approximate expression for the frequency of a fluid-loaded panel. However, his expression were valid only when the plate bending wave number is much greater than the acoustic wave number, or rather when the fluid loading on the panel is reactive.

In the literature as mentioned above, a few key paper discusses about the coupled resonance frequency and modal coupling coefficient. These discussions have limitations as: Davies analytical expressions for the modal coupling coefficient are valid only at low frequencies [6]. Pope and Leibowitz [15] does not presented some key modal coupling coefficient expressions involving acoustic fast-double edge and edge-double edge interactions. Sandman [16] evaluated the modal coupling coefficients numerically at low frequency, considering only 10 modes in the truncated equation of motion. Evaluation of modal coupling coefficient by Berry [2], Lomas and Hayek [2] is done numerically. Anoop [12] used mean quadratic velocity plots for evaluation of the coupled resonance frequency. Fahy's [7] approximate expression for the coupled resonance frequency is valid at low frequencies only.

Above mentioned limitations will be addressed in the report and generalized expression for evaluation of coupled resonance frequency will be presented which will be valid for entire frequency range.

2.5 Conclusions

In this chapter we have discussed the relevant literature associated with the fully coupled systems. Brief introduction of one way and two way coupled system was also presented. Mathematical formulation of the radiation and transmission problem was discussed in the section 2.4. We have also presented the governing differential equations of structures and acoustics. In the next chapter, we will be presenting the formulation of the coupled equation using governing differential equations of structures and acoustics.

Chapter 3

Vibration of a fluid loaded panel

3.1 Introduction

Consider a finite thin elastic rectangular panel ($-a/2 \leq x \leq a/2, -b/2 \leq y \leq b/2$) lying in the plane z=0, set in an infinite rigid baffle with simply supported boundary conditions Fig. 3.1.

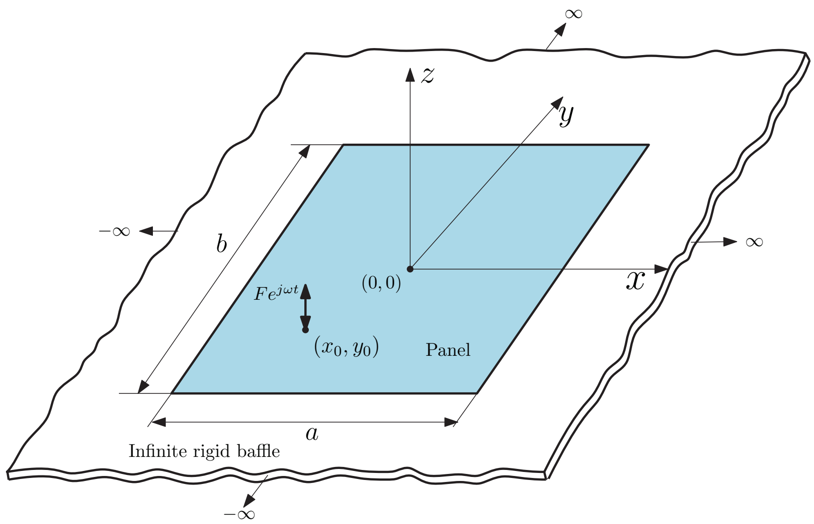

Fig. 3.1 Rectangular plate in a rigid baffle

The plate partition separates the fluid (water) into two regions of acoustic impedance ($\rho_0 c$). The plate is excited by a point harmonic force of magnitude $\tilde{F}$ and angular frequency ω at a point x_0 and y_0. The resulting flexural vibration of the plate radiate sound in the surrounding fluid medium. The associated pressure field for $z < 0$ and $z > 0$ is assumed to be $\mathrm{p}_1(x, y, z, t)$ and $\mathrm{p}_2(x, y, z, t)$ respectively. At the plate interface, pressure can be written as

$$p_1(x,y,z,t) = p^-(x,y,z,t), \tag{3.1}$$
$$p_2(x,y,z,t) = p^+(x,y,z,t), \tag{3.2}$$

however

$$p^-(x,y,z,t) = -p^+(x,y,-z,t). \tag{3.3}$$

Hence,

$$p_1(x,y,z,t) = -p^+(x,y,-z,t). \tag{3.4}$$

Pressure difference across the plate interface is

$$\Delta p(x,y,z=0,t) = p_1(x,y,z=0,t) - p_2(x,y,z=0,t) = -2p^+(x,y,z=0,t). \tag{3.5}$$

3.2 Pressure field surrounding the panel

Here onward time expression will be omitted in the discussion. The radiated pressure $p^+(x,y,z)$ must satisfy the 3-D Helmholtz equation

$$(\Delta^2 + k^2)p^+(x,y,z) = 0. \tag{3.6}$$

Taking a double Fourier transforms of the above equation in the x and y directions results in

$$\left(\frac{d^2}{dz^2} + \left(k^2 - \lambda^2 - \mu^2\right)\right)\frac{1}{2\pi}\int_{-\infty}^{\infty}\int_{-\infty}^{\infty} p^+(x,y,z)\mathrm{e}^{-\mathrm{i}\lambda x - \mathrm{i}\mu y}\mathrm{d}x\mathrm{d}y. \tag{3.7}$$

Lets define

$$P^+(\lambda,\mu,z) = \frac{1}{2\pi}\int_{-\infty}^{\infty}\int_{-\infty}^{\infty} p^+(x,y,z)\mathrm{e}^{-\mathrm{i}\lambda x - \mathrm{i}\mu y}\mathrm{d}x\mathrm{d}y. \tag{3.8}$$

Eq. 3.8 can be solved for $P^+(\lambda,\mu,z)$ as

$$P^+(\lambda,\mu,z) = A(\lambda,\mu)e^{-\mathrm{i}\sqrt{k^2-\lambda^2-\mu^2}z} + B(\lambda,\mu)e^{\mathrm{i}\sqrt{k^2-\lambda^2-\mu^2}z}. \tag{3.9}$$

From causality $A(\lambda,\mu)=0$. Hence, for a forward traveling wave (in the region $z>0$), the solution takes the form

$$P^{+}(\lambda,\mu,z)=B(\lambda,\mu)e^{\mathrm{i}\sqrt{k^2-\lambda^2-\mu^2}z}. \tag{3.10}$$

For evaluating the unknown $B(\lambda,\mu)$, we invoke the boundary condition at z=0 in the Fourier transform domain as

$$\frac{\partial}{\partial z}P^{+}(\lambda,\mu,z=0)=\mathrm{i}\rho_0 ckV_a(\lambda,\mu,z)|_{z=0}, \tag{3.11}$$

where ρ_0 is fluid density and $V_a(\lambda,\mu,z)$ is the double Fourier transforms of the fluid particle velocity $v_a(x,y,z)$.
Using Eqs. 3.10 and 3.11, we can write

$$\sqrt{k^2-\lambda^2-\mu^2}P^{+}(\lambda,\mu,z=0)=\rho_0 ckV_a(\lambda,\mu,z)|_{z=0}. \tag{3.12}$$

Or

$$B(\lambda,\mu)=P^{+}(\lambda,\mu,z=0)=Z_a(\lambda,\mu)V_a(\lambda,\mu,z=0). \tag{3.13}$$

Here we call $Z_a(\lambda,\mu)$ as acoustic impedance defined as

$$Z_a(\lambda,\mu)=\frac{\rho_0 ck}{\sqrt{k^2-\lambda^2-\mu^2}}. \tag{3.14}$$

Hence,

$$P^{+}(\lambda,\mu,z)=Z_a(\lambda,\mu)V_a(\lambda,\mu,z=0)e^{\mathrm{i}\sqrt{k^2-\lambda^2-\mu^2}z}. \tag{3.15}$$

3.3 Coupled equation of motion

The panel is assumed to be simply supported. A very important conclusion is drawn by the Davies [6] which states that, the modes in case of heavy fluid loading remains to be *in vacuo* modes. Hence, panel velocity as a modal sum can be written as

$$v_p(x,y)=\sum_{m,n=1}^{\infty}B_{mn}\phi_{mn}(x,y). \tag{3.16}$$

Where B_{mn} is the modal coefficient and ϕ_{mn} is the $(m,n)^{th}$mode shape. For current system, mode shape is given as

$$\phi_{mn}(x,y) = \sin\frac{m\pi(x+a/2)}{a}\sin\frac{n\pi(y+b/2)}{b}. \tag{3.17}$$

Taking a double Fourier transform of Eq. (3.16), it results in

$$V_p(\lambda,\mu) = \sum_{m,n=1}^{\infty} B_{mn}\Phi_{mn}(\lambda,\mu). \tag{3.18}$$

Consider a thin panel excited at (x_0, y_0) by a point harmonic force of amplitude $\tilde{F}$ and frequency ω (Fig. (3.1)). Equation of motion for the panel is

$$D(1-\mathrm{i}\eta)\nabla^4 v_p(x,y,t) + m_p\frac{\partial^2 v_p(x,y,t)}{\partial t^2} = -\mathrm{i}\omega\left[\Delta p(x,y,z=0,t) + \tilde{F}\delta\left(x-x_0\right)\delta\left(y-y_0\right)\mathrm{e}^{-\mathrm{i}\omega t}\right].$$

Neglecting material damping

$$D\nabla^4 v_p(x,y,t) + m_p\frac{\partial^2 v_p(x,y,t)}{\partial t^2} = -\mathrm{i}\omega\left[\Delta p(x,y,z=0,t) + \tilde{F}\delta\left(x-x_0\right)\delta\left(y-y_0\right)\mathrm{e}^{-\mathrm{i}\omega t}\right], \tag{3.19}$$

where D is the bending stiffness, m_p is the mass per unit area $(\rho_p h)$ and η is the damping loss factor of the panel. Pressure difference $\Delta p(x,y,z=0)$ across the panel is given by

$$\Delta p(\lambda,\mu) = \frac{1}{2\pi}\int_{-\infty}^{\infty}\int_{-\infty}^{\infty}\Delta P(x,y)\mathrm{e}^{-\mathrm{i}\lambda x-\mathrm{i}\mu y}\mathrm{d}x\mathrm{d}y. \tag{3.20}$$

Substituting Eqs. 3.16 and 3.17 into Eq. 3.19 we get

$$\sum_{m,n}\left[D\left\{\left(\frac{m\pi}{a}\right)^2 + \left(\frac{n\pi}{b}\right)^2\right\}^2 - m_p\omega^2\right]B_{mn}\phi_{mn}(x,y) = -\mathrm{i}\omega\left[\Delta p(x,y,z=0,t) + \tilde{F}\delta\left(x-x_0\right)\delta\left(y-y_0\right)\mathrm{e}^{-\mathrm{i}\omega t}\right].$$

In the wavenumber domain above equation is

$$\sum_{m,n}\left[D\left\{\left(\frac{m\pi}{a}\right)^2+\left(\frac{n\pi}{b}\right)^2\right\}^2-m_p\omega^2\right]B_{mn}\Phi_{mn}(\lambda,\mu)$$
$$=-i\omega\Delta P(\lambda,\mu)-\frac{\mathrm{i}\omega\tilde{F}}{2\pi}\mathrm{e}^{\mathrm{i}\lambda x_0+\mathrm{i}\mu y_0}, \tag{3.21}$$

where $\Phi_{mn}(\lambda,\mu)$ and $\Delta P(\lambda,\mu)$ are [12]

$$\Phi_{mn}(\lambda,\mu)=\frac{k_m k_n}{2\pi}\frac{\left[(-1)^m\mathrm{e}^{\mathrm{i}\lambda a/2}-\mathrm{e}^{-\mathrm{i}\lambda a/2}\right]}{(\lambda^2-k_m^2)}\frac{\left[(-1)^n\mathrm{e}^{\mathrm{i}\mu b/2}-\mathrm{e}^{-\mathrm{i}\mu b/2}\right]}{(\mu^2-k_n^2)}, \tag{3.22}$$

and

$$\Delta P(\lambda,\mu)=P^-(\lambda,\mu,z=0)-P^+(\lambda,\mu,z=0)=-2Z_a(\lambda,\mu)V_a(\lambda,\mu,z=0). \tag{3.23}$$

Here, $k_m=m\pi/a$, $k_n=n\pi/b$, $Z_a(\lambda,\mu)=\rho_0 ck/\sqrt{k^2-\lambda^2-\mu^2}$. $V_a(\lambda,\mu,z=0)$ is the fluid velocity over the panel surface, equivalent to the panel velocity.

Substituting $\Delta P(\lambda,\mu)$ into Eq. 3.21.

$$\sum_{m,n}\left[D\left\{\left(\frac{m\pi}{a}\right)^2+\left(\frac{n\pi}{b}\right)^2\right\}^2-m_p\omega^2\right]B_{mn}\Phi_{mn}(\lambda,\mu)$$
$$=2\mathrm{i}\omega Z_a(\lambda,\mu)V_a(\lambda,\mu,z=0)-\frac{\mathrm{i}\omega\tilde{F}}{2\pi}\mathrm{e}^{\mathrm{i}\lambda x_0+\mathrm{i}\mu y_0}. \tag{3.24}$$

Using the fact that

$$V_a(\lambda,\mu,z=0)=V_p(\lambda,\mu), \tag{3.25}$$

and combining Eqs. 3.18 and 3.24 , coupled equation becomes

$$\sum_{m,n}\left[D\left\{\left(\frac{m\pi}{a}\right)^2+\left(\frac{n\pi}{b}\right)^2\right\}^2-m_p\omega^2\right]B_{mn}\Phi_{mn}(\lambda,\mu)$$
$$=2\mathrm{i}\omega Z_a(\lambda,\mu)\sum_{m,n=1}^{\infty}B_{mn}\Phi_{mn}(\lambda,\mu)-\frac{\mathrm{i}\omega\tilde{F}}{2\pi}\mathrm{e}^{\mathrm{i}\lambda x_0+\mathrm{i}\mu y_0}. \tag{3.26}$$

Multiplying above equation with $\sum_{p,q=1}^{\infty} \Phi_{pq}(-\lambda,-\mu)$ and integrating over λ and μ domain we get

$$\frac{1}{2i\omega}\sum_{m,n}\sum_{p,q} B_{mn}K_{mn}\overline{\Theta}_{mnpq} - \sum_{m,n}\sum_{p,q} B_{mn}\int_{-\infty}^{\infty}\int_{-\infty}^{\infty}\Phi_{mn}(\lambda,\mu)\Phi_{pq}(-\lambda,-\mu)d\lambda\mathrm{d}\mu = -\frac{\tilde{F}}{4\pi}\sum_{p,q}\int_{-\infty}^{\infty}\int_{-\infty}^{\infty}\frac{\Phi_{pq}(-\lambda,-\mu)}{Z_a(\lambda,\mu)}\mathrm{e}^{\mathrm{i}x_0+\mathrm{i}\mu y_0}\mathrm{d}\lambda\mathrm{d}\mu, \tag{3.27}$$

where

$$\overline{\Theta}_{mnpq} = \int_{-\infty}^{\infty}\int_{-\infty}^{\infty}\frac{\Phi_{mn}(\lambda,\mu)\Phi_{pq}(-\lambda,-\mu)}{Z_a(\lambda,\mu)}\mathrm{d}\lambda\mathrm{d}\mu, \tag{3.28}$$

and

$$K_{mn} = \left[D\left\{\left(\frac{m\pi}{a}\right)^2 + \left(\frac{n\pi}{b}\right)^2\right\}^2 - m_p\omega^2\right]. \tag{3.29}$$

The second term integral of Eq. (3.27) can be solved as [12]

$$\int_{-\infty}^{\infty}\int_{-\infty}^{\infty}\Phi_{mn}(\lambda,\mu)\Phi_{pq}(-\lambda,-\mu)\mathrm{d}\lambda\mathrm{d}\mu = \frac{ab}{4}\delta_{mp}\delta_{nq}. \tag{3.30}$$

Hence, coupled equation can be written as

$$\frac{1}{2i\omega}\sum_{m,n}\sum_{p,q} B_{mn}K_{mn}\overline{\Theta}_{mnpq} - \frac{ab}{4}\sum_{m,n} B_{mn} = -\frac{\tilde{F}}{4\pi}\sum_{p,q}\gamma_{pq}\left(x_0,y_0\right), \tag{3.31}$$

where

$$\gamma_{pq}\left(x_0,y_0\right) = \int_{-\infty}^{\infty}\int_{-\infty}^{\infty}\frac{\Phi_{pq}(-\lambda,-\mu)}{Z_a(\lambda,\mu)}\mathrm{e}^{\mathrm{i}\lambda x_0+\mathrm{i}\mu y_0}\mathrm{d}\lambda\mathrm{d}\mu. \tag{3.32}$$

In the matrix form Eq. 3.31 becomes

$$\boxed{\frac{1}{2i\omega}K_{mn}\left[\overline{\Theta}_{mn,pq}\right]^T\left\{B_{mn}\right\} - \frac{ab}{4}\left\{B_{mn}\right\} = -\frac{\tilde{F}}{4\pi}\left\{\gamma_{\mathrm{pq}}\left(x_0,y_0\right)\right\} \qquad (3.33)}$$

3.4 Conclusions

In this chapter, we have introduced the pressure field generated by the panel, excited by a point harmonic force in the Fourier domain. We have also discussed the formulation of the coupled equation and presented it in the matrix form. Coupled equation contains coupling coefficient ($\overline{\Theta}_{mnpq}$), which arises due to the heavy fluid loading. It signifies, how does one mode is affected by the other mode due to coupling. Coupling coefficient decreases the vibration amplitude of the panels. In the next chapter, coupling coefficient is discussed in details along with derivation of the analytical expression from it for various modes of plate radiation.

Chapter 4

Closed form expressions for modal coupling coefficient

4.1 Introduction

In the fully coupled formulation, *in vacou* modes are coupled due to the heavy fluid loading. The fluid loading effect is entirely captured by the modal coupling coefficient (CC) $\overline{\Theta}_{mnpq}$.

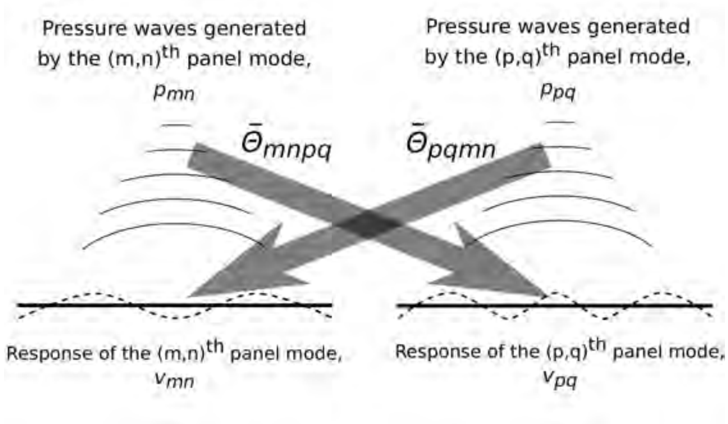

Fig. 4.1 Coupling Coefficient

Coupling coefficient signifies the effect of vibration of $(m, n)^{th}$ mode of the panel on $(p, q)^{th}$ mode. Being a complex quantity its real part is termed as radiation CC and imaginary part as inertia CC. Real part represents radiation loading by surrounding acoustic medium to the panel vibration while imaginary part signifies the virtual mass to be added on the panel. In this chapter, our intention is to analyze coupling coefficient and discuss the methods used for obtaining the analytical expressions for various modes of panel radiation from it.

4.2 Modal coupling coefficient

Mathematically coupling coefficient is given as (Eq. (3.28))

$$\overline{\Theta}_{mnpq} = \int_{-\infty}^{\infty}\int_{-\infty}^{\infty} \frac{\Phi_{mn}(\lambda,\mu)\Phi_{pq}(-\lambda,-\mu)}{Z_a(\lambda,\mu)} \mathrm{d}\lambda \mathrm{d}\mu \tag{4.1}$$

where $\Phi_{mn}(\lambda,\mu)$ and $\Phi_{pq}(-\lambda,-\mu)$ are [12]

$$\begin{aligned}\Phi_{mn}(\lambda,\mu) = -\frac{ab}{8\pi}&\left\{e^{im\pi/2} sinc\left[\frac{(\lambda+m\pi/a)a}{2}\right] - e^{-im\pi/2} sinc\left[\frac{(\lambda-m\pi/a)a}{2}\right]\right\}\\ &\times\left\{e^{in\pi/2} sinc\left[\frac{(\mu+n\pi/b)b}{2}\right] - e^{-in\pi/2} sinc\left[\frac{(\mu-m\pi/b)b}{2}\right]\right\}\end{aligned} \tag{4.2}$$

Value of $Z_a(\lambda,\mu)$ is given in the Eq. (3.14). It can be deduced that the numerator, $\Phi_{mn}(\lambda,\mu)\,\Phi_{pq}(-\lambda,-\mu)$ has a multiplying factor in λ of the form $1 + (-1)^{m+p} - (-1)^m\,\mathrm{e}^{\mathrm{i}\lambda a} - (-1)^p\,\mathrm{e}^{-\mathrm{i}\lambda a}$. When $m+p$ is odd this results in $\pm 2\mathrm{i}\sin\lambda a$ and since the rest of the integrand is even in λ, the integral over λ from $-\infty$ to ∞ vanishes. Similar is the case for the integral over μ when $n+q$ is odd. Thus, we can write

$$\bar{\Theta}_{mnpq} = 0, \qquad\qquad \text{if } m+p \text{ or } n+q \text{ is odd}\ .$$

On the other hand, when $m+p$ is even, we get $1+(-1)^{m+p} - (-1)^m\,\mathrm{e}^{\mathrm{i}\lambda a} - (-1)^p\,\mathrm{e}^{-\mathrm{i}\lambda a} = 2\,[1-(-1)^m\cos\lambda a]$. Similarly, when $n+q$ is even, $1+(-1)^{n+q} - (-1)^n\,\mathrm{e}^{\mathrm{i}\mu b} - (-1)^q\,\mathrm{e}^{-\mathrm{i}\mu b} = 2\,[1-(-1)^n\cos\mu b]$. Thus, we see that $\bar{\Theta}_{mnpq}$ is non-zero only when $m+p$ and $n+q$ are even, i.e., m and p and n and q have the same parity (either both odd or both even) [6]. Hence, each mode is coupled to at most only one quarter of all the other modes. Therefore, the nonzero components of $\bar{\Theta}_{mnpq}$ are given by (when $m+p$ and $n+q$ are even)

$$\bar{\Theta}_{mnpq} = \frac{4\,k_m\,k_n\,k_p\,k_q}{\rho_0 ck\,(2\pi)^2}\, I^{mnpq}, \tag{4.3}$$

where

$$I^{mnpq} = \int_{-\infty}^{\infty}\int_{-\infty}^{\infty} \frac{[1-(-1)^m \cos\lambda a]\,[1-(-1)^n \cos\mu b]\,(k^2-\lambda^2-\mu^2)^{\frac{1}{2}}}{(\lambda^2-k_m^2)\left(\lambda^2-k_p^2\right)(\mu^2-k_n^2)\left(\mu^2-k_q^2\right)}\,\mathrm{d}\lambda\,\mathrm{d}\mu. \quad (4.4)$$

In the equation above, we denote the integral over λ as

$$I_1^{mp}(\mu) = \int_{-\infty}^{\infty} \frac{[1-(-1)^m \cos\lambda a]\,(k^2-\lambda^2-\mu^2)^{\frac{1}{2}}}{(\lambda^2-k_m^2)\left(\lambda^2-k_p^2\right)}\,\mathrm{d}\lambda, \quad (4.5)$$

and use the fact that for an even function $f(\lambda)$

$$\int_{-\infty}^{\infty} f(\lambda)\cos\lambda a\,\mathrm{d}\lambda = \int_{-\infty}^{\infty} f(\lambda)\,\mathrm{e}^{\mathrm{i}\lambda a}\,\mathrm{d}\lambda.$$

Thus

$$I_1^{mp}(\mu) = \int_{-\infty}^{\infty} \frac{\left[1-(-1)^m\,\mathrm{e}^{\mathrm{i}\lambda a}\right]\,(k^2-\lambda^2-\mu^2)^{\frac{1}{2}}}{(\lambda^2-k_m^2)\left(\lambda^2-k_p^2\right)}\,\mathrm{d}\lambda. \quad (4.6)$$

4.3 Branch points and branch cuts

The integrand of $I_1^{mp}(\mu)$ has square root branch points at

$$\lambda_{1,2} = \pm\left(k^2-\mu^2\right)^{\frac{1}{2}}.$$

Depending on the value of μ and hence the location of the branch points $\lambda_{1,2}$, $I_1^{mp}(\mu)$ has to be evaluated differently - **Case 1**: when $|\mu| < k$; $\lambda_{1,2} = \pm(k^2-\mu^2)^{1/2}$, i.e., the branch points lie on the positive and the negative real axis and **Case 2**: when $|\mu| > k$; $\lambda_{1,2} = \pm\mathrm{i}(\mu^2-k^2)^{1/2}$, i.e., the branch points lie on the positive and the negative imaginary axis.

Consider the first case in which $\lambda_{1,2}$ lie on the real axis, i.e.,

$$\lambda_1 = (k^2-\mu^2)^{\frac{1}{2}} \qquad \text{and} \qquad \lambda_2 = -\lambda_1.$$

For $z > 0$, the radiated pressure wave has the form $\mathrm{e}^{\mathrm{i}\xi z-\mathrm{i}\omega t}$ with $\xi = (k^2-\lambda^2-\mu^2)^{\frac{1}{2}} = (\lambda_1^2-\lambda^2)^{\frac{1}{2}}$. We know that for large values of λ, a growing wave is physically inadmissible and hence ξ must be positive imaginary.

$$\xi = \mathrm{i}(\lambda^2 - \lambda_1^2)^{\frac{1}{2}} \qquad \text{for } |\lambda| > \lambda_1.$$

Thus, it is necessary that we choose a feasible definition for ξ so that a growing wave solution never occurs. We will now select an appropriate branch cut and definition for the function $(k^2 - \lambda^2 - \mu^2)^{\frac{1}{2}}$ by looking at it as a product of square roots, i.e.,

$$\left(\lambda_1^2 - \lambda^2\right)^{1/2} = (\lambda_1 - \lambda)^{1/2} (\lambda_1 + \lambda)^{1/2} = |\lambda_1 - \lambda|^{1/2} \, \mathrm{e}^{\mathrm{i}\gamma/2} \, |\lambda_1 + \lambda|^{1/2} \, \mathrm{e}^{\mathrm{i}\theta/2} \tag{4.7}$$

The complex functions $(\lambda_1 - \lambda)$ and $(\lambda_1 + \lambda)$ are shown in Figs. 4.2(a) and 4.2(b), respectively.

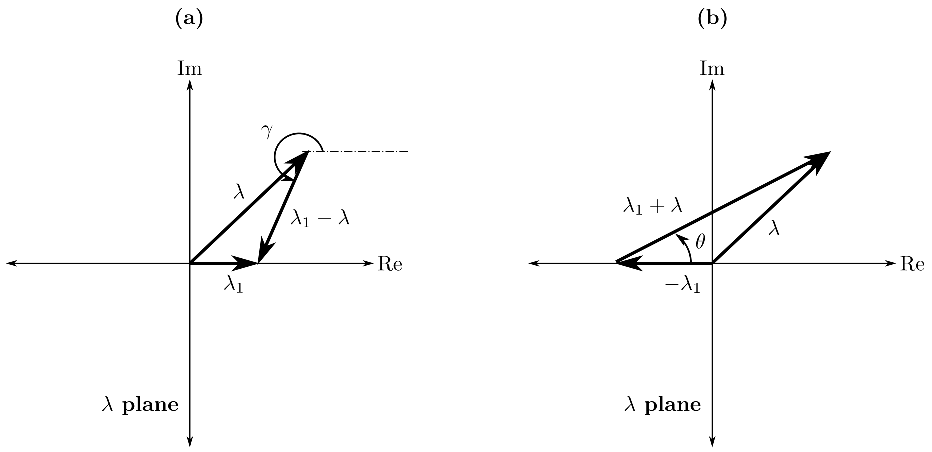

Fig. 4.2 Vectors of $\lambda_1 - \lambda$ and $\lambda_1 + \lambda$ (case 1) in the complex λ plane.

From Fig. 4.2(a), as γ varies from 0 to 2π, the resulting branch cut of $(\lambda_1 - \lambda)^{1/2}$ runs along the real axis from λ_1 to $-\infty$ (see Fig. 4.3(a)). We may now select the following function definition for $(\lambda_1 - \lambda)^{1/2}$ so that the branch cut modifies to an 'L' shaped one as shown Fig. 4.3(b):

$$(\lambda_1 - \lambda)^{1/2} = \begin{cases} |\lambda_1 - \lambda|^{1/2} \, \mathrm{e}^{\mathrm{i}\gamma/2} & \text{for } \mathrm{Re}(\lambda) > 0 \\ -\,|\lambda_1 - \lambda|^{1/2} \, \mathrm{e}^{\mathrm{i}\gamma/2} & \text{for } \mathrm{Re}(\lambda) < 0 \text{ and } \mathrm{Im}(\lambda) > 0 \\ |\lambda_1 - \lambda|^{1/2} \, \mathrm{e}^{\mathrm{i}\gamma/2} & \text{for } \mathrm{Re}(\lambda) < 0 \text{ and } \mathrm{Im}(\lambda) < 0 \end{cases} \tag{4.8}$$

It will be described later how the above modification of branch cut (and the one which will be explained next) prevent the function $(\lambda_1^2 - \lambda^2)^{1/2}$ from assuming any negative imaginary values for $|\mathrm{Re}(\lambda)| > \lambda_1$.

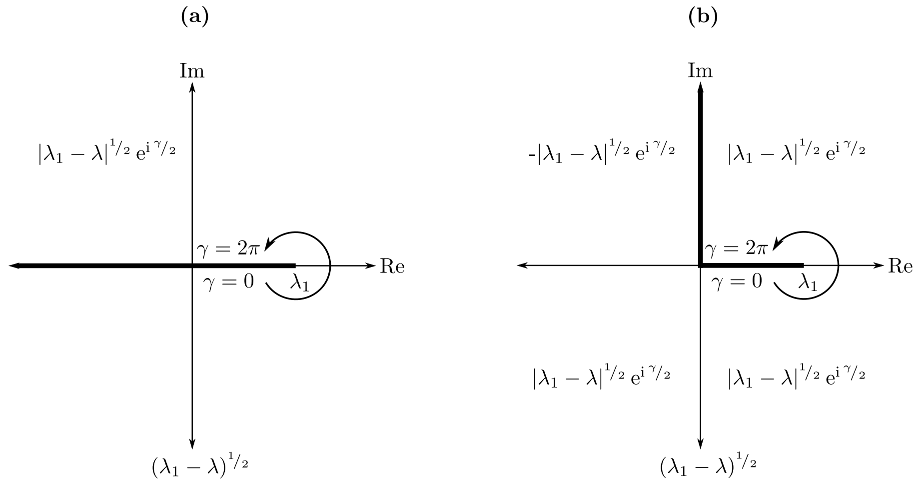

Fig. 4.3 (a) Initial and (b) modified branch cuts of $(\lambda_1 - \lambda)^{1/2}$ (case 1) in the complex λ plane.

Now assume that θ, the argument of $(\lambda_1 + \lambda)^{1/2}$, varies from 0 to 2π. The resulting branch cut of $(\lambda_1 + \lambda)^{1/2}$ extends from $-\lambda_1$ to ∞ along the real axis, as shown in Fig. 4.4(a). It is then modified to an 'L' shaped one by choosing the following function definition for $(\lambda_1 + \lambda)^{1/2}$:

$$(\lambda_1 + \lambda)^{1/2} = \begin{cases} |\lambda_1 + \lambda|^{1/2}\, e^{i\theta/2} & \text{for } \operatorname{Re}(\lambda) < 0 \\ -\,|\lambda_1 + \lambda|^{1/2}\, e^{i\theta/2} & \text{for } \operatorname{Re}(\lambda) > 0 \text{ and } \operatorname{Im}(\lambda) < 0 \\ |\lambda_1 + \lambda|^{1/2}\, e^{i\theta/2} & \text{for } \operatorname{Re}(\lambda) > 0 \text{ and } \operatorname{Im}(\lambda) > 0 \end{cases} \tag{4.9}$$

The modified branch cut is shown in Fig. 4.4(b).

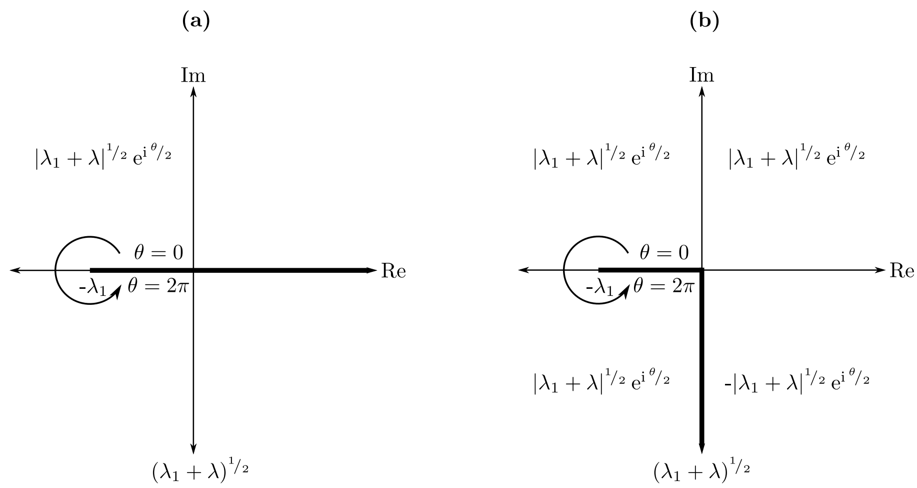

Fig. 4.4 (a) Initial and (b) modified branch cuts of $(\lambda_1 + \lambda)^{\frac{1}{2}}$ (case 1) in the complex λ plane.

Combining the definitions of $(\lambda_1 - \lambda)^{\frac{1}{2}}$ (Eq. (4.9)) and $(\lambda_1 + \lambda)^{\frac{1}{2}}$ (Eq. (4.9)), $(\lambda_1^2 - \lambda^2)^{\frac{1}{2}}$ can be defined as

$$\left(\lambda_1^2 - \lambda^2\right)^{1/2} = \begin{cases} |\lambda_1 - \lambda|^{1/2}\,|\lambda_1 + \lambda|^{1/2}\,\mathrm{e}^{\mathrm{i}(\gamma+\theta)/2} & \text{for } \operatorname{Re}(\lambda) > 0 \text{ and } \operatorname{Im}(\lambda) > 0 \\ -\,|\lambda_1 - \lambda|^{1/2}\,|\lambda_1 + \lambda|^{1/2}\,\mathrm{e}^{\mathrm{i}(\gamma+\theta)/2} & \text{for } \operatorname{Re}(\lambda) < 0 \text{ and } \operatorname{Im}(\lambda) > 0 \\ |\lambda_1 - \lambda|^{1/2}\,|\lambda_1 + \lambda|^{1/2}\,\mathrm{e}^{\mathrm{i}(\gamma+\theta)/2} & \text{for } \operatorname{Re}(\lambda) < 0 \text{ and } \operatorname{Im}(\lambda) < 0 \\ -\,|\lambda_1 - \lambda|^{1/2}\,|\lambda_1 + \lambda|^{1/2}\,\mathrm{e}^{\mathrm{i}(\gamma+\theta)/2} & \text{for } \operatorname{Re}(\lambda) > 0 \text{ and } \operatorname{Im}(\lambda) < 0 \end{cases} \tag{4.10}$$

The arguments γ and θ varies from 0 to 2π. The resulting branch cut of $(\lambda_1^2 - \lambda^2)^{\frac{1}{2}}$ is depicted in Fig. 4.5.

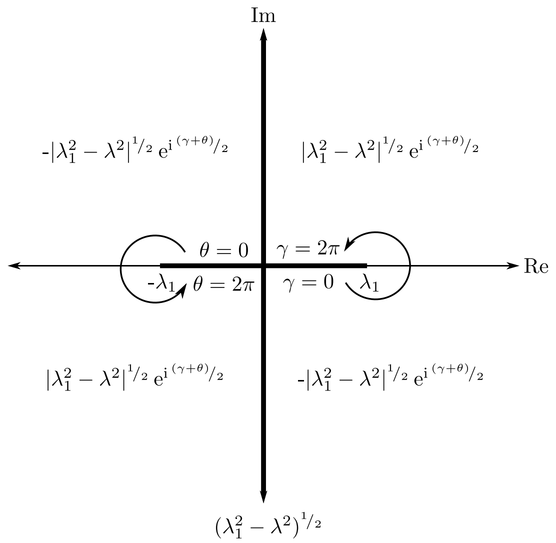

Fig. 4.5 Branch cut of $(\lambda_1^2 - \lambda^2)^{1/2}$ (case 1) in the complex λ plane.

Fig. 4.6 depicts the values of arguments γ and θ along the real axis when $|\operatorname{Re}(\lambda)| > \lambda_1$. It can be found that for all the four cases, as shown in the figure, $(\lambda_1^2 - \lambda^2)^{\frac{1}{2}} = \mathrm{i}\,|\lambda_1^2 - \lambda^2|^{\frac{1}{2}}$. Hence, the selected definition of $(\lambda_1^2 - \lambda^2)^{\frac{1}{2}}$ and the associated branch cut result in an evanescent wave in the z direction for $|\operatorname{Re}(\lambda)| > \lambda_1$.

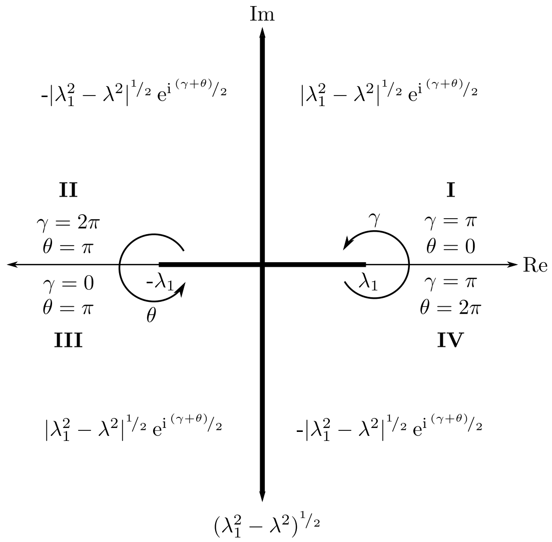

Fig. 4.6 Argument values of $(\lambda_1^2 - \lambda^2)^{\frac{1}{2}}$ along the real axis when $|\mathrm{Re}(\lambda)| > \lambda_1$ (case 1).

Let us now consider the case 2 in which the branch points $\lambda_{1,2}$ lie on the imaginary axis of the complex λ plane.

$$\lambda_1 = \mathrm{i}(\mu^2 - k^2)^{\frac{1}{2}} \qquad \text{and} \qquad \lambda_2 = -\lambda_1.$$

Again, $\xi = (k^2 - \lambda^2 - \mu^2)^{\frac{1}{2}}$ is the z wave number. For $z > 0$ and $|\mathrm{Im}(\lambda)| < \mathrm{Im}(\lambda_1)$, ξ must be positive imaginary and thus avoid z directional growing waves,

$$\xi = \mathrm{i}(\lambda_1^{'2} - \lambda^{'2})^{\frac{1}{2}} \qquad \text{for } |\lambda^{'}| < \lambda_1^{'}.$$

Here the primed variables denote the imaginary part of the respective unprimed quantities. We will now select an appropriate branch cut and definition for the function $(k^2 - \lambda^2 - \mu^2)^{\frac{1}{2}}$ which satisfies the above condition.

As before, we have

$$(\lambda_1^2 - \lambda^2)^{\frac{1}{2}} = (\lambda_1 - \lambda)^{\frac{1}{2}}\,(\lambda_1 + \lambda)^{\frac{1}{2}} = |\lambda_1 - \lambda|^{\frac{1}{2}}\ e^{\,\mathrm{i}\frac{\gamma}{2}}\ |\lambda_1 + \lambda|^{\frac{1}{2}}\ e^{\,\mathrm{i}\frac{\theta}{2}}.$$

The complex functions $(\lambda_1 - \lambda)$ and $(\lambda_1 + \lambda)$ are depicted in Fig. 4.7.

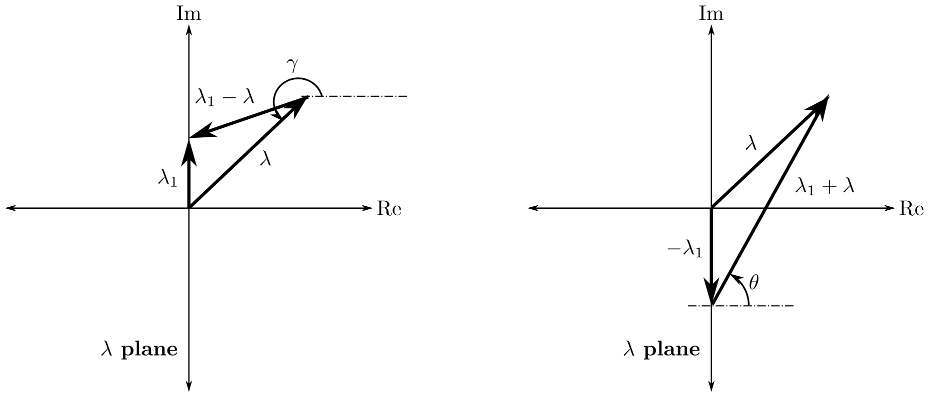

Fig. 4.7 Illustrations of $\lambda_1 - \lambda$ and $\lambda_1 + \lambda$ (case 2) in the complex λ plane.

As γ varies from $-\frac{\pi}{2}$ to $\frac{3\pi}{2}$, the resulting branch cut of $(\lambda_1 - \lambda)^{\frac{1}{2}}$ is along the imaginary axis from λ_1 to ∞, as shown in Fig. 4.8(a). Also, as θ varies from $-\frac{\pi}{2}$ to $\frac{3\pi}{2}$, the branch cut of $(\lambda_1 + \lambda)^{\frac{1}{2}}$ is along the imaginary axis from $-\lambda_1$ to $-\infty$, as shown in Fig. 4.8(b). Thus, we have

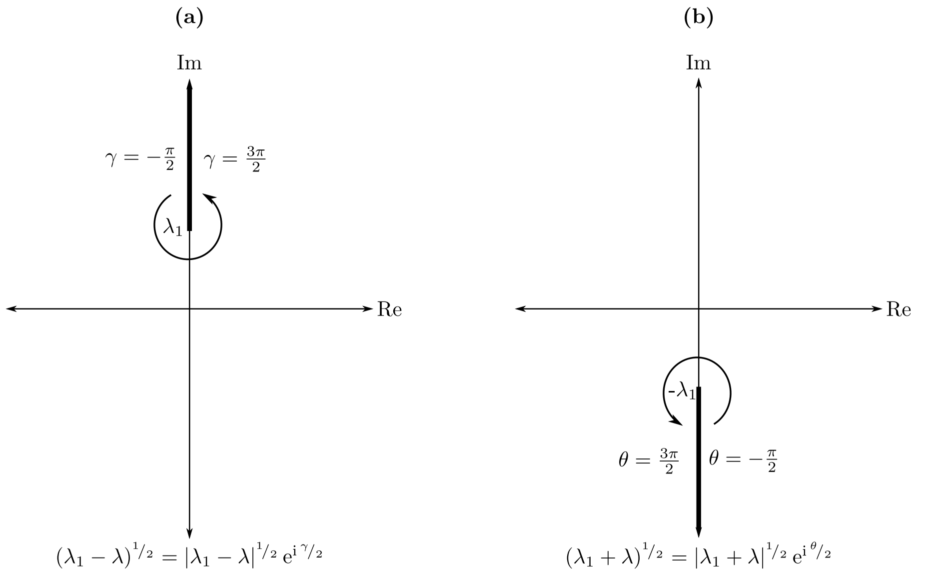

Fig. 4.8 Branch cuts of (a) $(\lambda_1 - \lambda\mathrm{i})$ and (b) $(\lambda_1 + \lambda\mathrm{i})$ for case 2 in the complex λ plane.

$$(\lambda_1^2 - \lambda^2)^{\frac{1}{2}} = \left|\lambda_1^2 - \lambda^2\right|^{\frac{1}{2}} e^{\mathrm{i}\,\frac{(\gamma+\theta)}{2}}, \tag{4.11}$$

where γ and θ vary from $-\frac{\pi}{2}$ to $\frac{3\pi}{2}$. The resulting branch cut is shown in Fig. 4.9. It can be seen that for $|\mathrm{Im}(\lambda)| < \lambda_1^{'}$, along the imaginary axis, the argument values are $\gamma = \frac{\pi}{2}$ and $\theta = \frac{\pi}{2}$ and hence $(\lambda_1^2 - \lambda^2)^{\frac{1}{2}} = \mathrm{i}\;|\lambda_1^2 - \lambda^2|^{\frac{1}{2}}$. Thus, for case 2, by choosing the above definition of $(\lambda_1^2 - \lambda^2)^{\frac{1}{2}}$ we ensure an evanescent wave in the z direction when $|\mathrm{Im}(\lambda)| < \lambda_1'$.

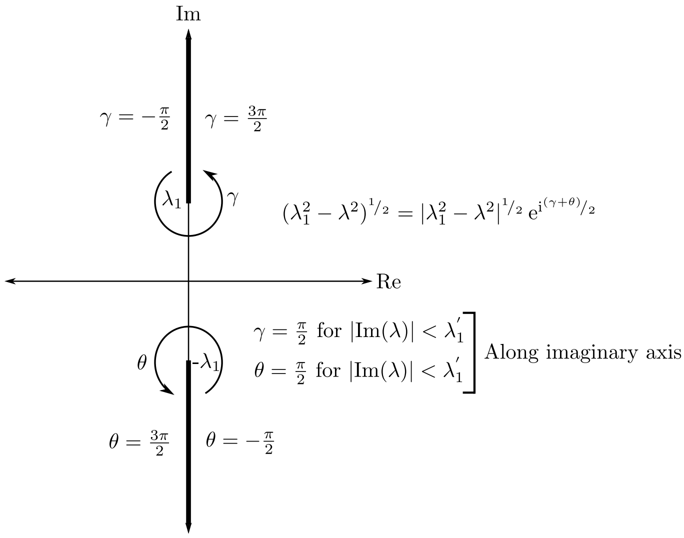

Fig. 4.9 Branch cut of $(\lambda_1^2 - \lambda^2)^{\frac{1}{2}}$ (case 2) as illustrated in the complex λ plane.

4.3.1 Integration contours for $I_1^{mp}(\mu)$ ($k_m, k_p > k$ and $m \neq p$)

The integral $I_1^{mp}(\mu)$, as defined in Eq. (4.6), can now be evaluated using Cauchy's theorem [1] along a contour in the complex λ plane. The contour is different for each of the cases as described before [15]. We consider a scenario of $k_m, k_p > k$, $m + p$ even and $m \neq p$.

I Case 1 ($|\mu| < k$)

The poles, branch points, branch cuts and the integration contour for case 1 ($|\mu| < k$) are depicted in Fig. 4.10.

Using Cauchy's theorem we get

$$\begin{aligned}\mathrm{P}\left[I_1^{mp}(\mu)\right] = I_1^{mp}(\mu : |\mu| < k) = \pi\mathrm{i}\left[\mathrm{Res}(k_m) + \mathrm{Res}(k_p) + \mathrm{Res}(-k_m) + \mathrm{Res}(-k_p)\right] \\ - (\Gamma_1 + \Gamma_2 + \Gamma_3 + \Gamma_4),\end{aligned}$$

where P[∗] denotes the principal value of the integral and Res(∗) denotes the residue of the integrand at the specified poles. The integrals $\Gamma_1, \Gamma_2, \Gamma_3$ and Γ_4 are derived in

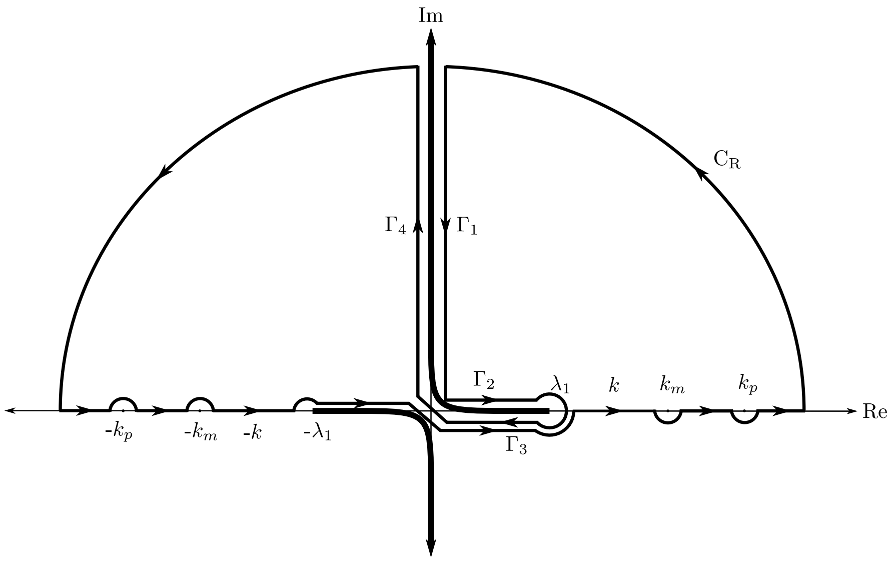

Fig. 4.10 Integration contour of $I_1^{mp}(\mu)$ for case 1 ($|\mu| < k$) when $k_m, k_p > k$ and $k_m \neq k_p$.

detail in Appendix A and the final forms are given below:

$$\begin{aligned} \Gamma_1 &= \mathrm{i} \int_0^\infty \frac{\left[1-(-1)^m\ \mathrm{e}^{-ay}\right]\ |\lambda_1^2+y^2|^{\frac{1}{2}}}{\left(y^2+k_m^2\right)\left(y^2+k_p^2\right)}\,\mathrm{d}y, \\ \Gamma_2 &= -\int_0^{\lambda_1} \frac{\left[1-(-1)^m\ e^{iax}\right]\ |\lambda_1^2-x^2|^{\frac{1}{2}}}{\left(x^2-k_m^2\right)\left(x^2-k_p^2\right)}\,\mathrm{d}x, \\ \Gamma_3 &= -\int_0^{\lambda_1} \frac{\left[1-(-1)^m\ e^{iax}\right]\ |\lambda_1^2-x^2|^{\frac{1}{2}}}{\left(x^2-k_m^2\right)\left(x^2-k_p^2\right)}\,\mathrm{d}x \\ \text{and}\quad \Gamma_4 &= \mathrm{i} \int_0^\infty \frac{\left[1-(-1)^m\ \mathrm{e}^{-ay}\right]\ |\lambda_1^2+y^2|^{\frac{1}{2}}}{\left(y^2+k_m^2\right)\left(y^2+k_p^2\right)}\,\mathrm{d}y. \end{aligned} \tag{4.12}$$

It is shown in the Appendix A that the residues at simple poles $k_m, k_p, -k_m$ and $-k_p$ identically go to zero, i.e.,

$$\mathrm{Res}(k_m) = \mathrm{Res}(k_p) = \mathrm{Res}(-k_m) = \mathrm{Res}(-k_p) = 0. \tag{4.13}$$

Thus,

$$I_1^{mp}(\mu : |\mu| < k) = -(\Gamma_1 + \Gamma_2 + \Gamma_3 + \Gamma_4).$$

Substituting for $\Gamma_1, \Gamma_2, \Gamma_3$ and Γ_4 and grouping the real and imaginary terms we get

$$I_1^{mp}(\mu : |\mu| < k) = 2 \int_0^{\lambda_1} \frac{[1-(-1)^m \cos ax]\, |\lambda_1^2 - x^2|^{\frac{1}{2}}}{(x^2-k_m^2)\left(x^2-k_p^2\right)}\, \mathrm{d}x$$
$$- 2\,\mathrm{i} \left[\int_0^{\lambda_1} \frac{(-1)^m \sin ax \; |\lambda_1^2 - x^2|^{\frac{1}{2}}}{(x^2-k_m^2)\left(x^2-k_p^2\right)}\, \mathrm{d}x + \int_0^{\infty} \frac{[1-(-1)^m \,\mathrm{e}^{-ay}]\, |\lambda_1^2 + y^2|^{\frac{1}{2}}}{(y^2+k_m^2)\left(y^2+k_p^2\right)}\, \mathrm{d}y \right]. \quad (4.14)$$

II Case 2 ($|\mu| > k$)

The poles, branch points, branch cuts and the integration contour for case 2 ($|\mu| > k$) are shown in Fig. 4.11.

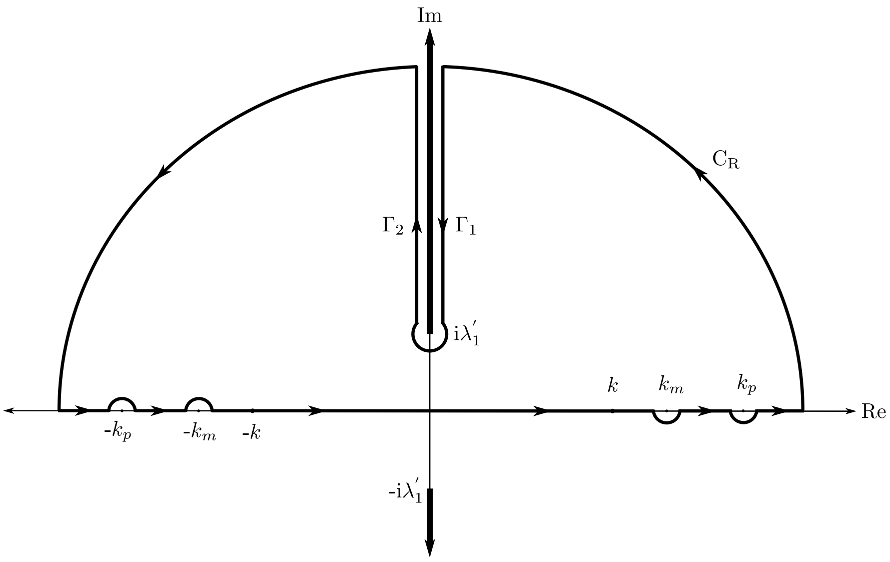

Fig. 4.11 Integration contour of $I_1^{mp}(\mu)$ for case 2 ($|\mu| > k$) when $k_m, k_p > k$ and $k_m \neq k_p$.

Now, using Cauchy's theorem we get

$$\mathrm{P}\left[I_1^{mp}(\mu)\right] = I_1^{mp}(\mu : |\mu| > k) = \pi\mathrm{i}\left[\mathrm{Res}(k_m) + \mathrm{Res}(k_p) + \mathrm{Res}(-k_m) + \mathrm{Res}(-k_p)\right] - (\Gamma_1 + \Gamma_2),$$

where P[∗] denotes the principal value of the integral and Res(∗) denotes the residue of the integrand at the specified poles. The integrals Γ_1 and Γ_2 are different from those in case 1. They are derived in detail in Appendix B and the final forms are given below.

$$\Gamma_1 = \Gamma_2 = \mathrm{i} \int\limits_{\lambda_1'}^{\infty} \frac{\left[1-(-1)^m\ \mathrm{e}^{-ay}\right] \left|\lambda_1'^2 - y^2\right| \frac{1}{2}}{\left(y^2+k_m^2\right)\left(y^2+k_p^2\right)}\,\mathrm{d}y. \tag{4.15}$$

The residues are also derived in Appendix B and are identically zero, i.e.,

$$\mathrm{Res}(k_m) = \mathrm{Res}(k_p) = \mathrm{Res}(-k_m) = \mathrm{Res}(-k_p) = 0.$$

We now have

$$I_1^{mp}(\mu : |\mu| > k) = -(\Gamma_1 + \Gamma_2).$$

Substituting for Γ_1 and Γ_2 we get

$$I_1^{mp}(\mu : |\mu| > k) = -2\,\mathrm{i} \int\limits_{\lambda_1'}^{\infty} \frac{\left[1-(-1)^m\ \mathrm{e}^{-ay}\right] \left|\lambda_1'^2 - y^2\right|^{\frac{1}{2}}}{\left(y^2+k_m^2\right)\left(y^2+k_p^2\right)}\,\mathrm{d}y. \tag{4.16}$$

Having obtained $I_1^{mp}(\mu)$ for $|\mu| < k$ and $|\mu| > k$, the I^{mnpq} integral (Eq. (4.4)) simplifies to

$$\begin{aligned} I^{mnpq} = 2 &\int\limits_0^k \frac{\left[1-(-1)^n \cos\mu b\right]}{\left(\mu^2-k_n^2\right)\left(\mu^2-k_q^2\right)}\, I_1^{mp}(\mu : |\mu| < k)\,\mathrm{d}\mu \\ &+ 2\int\limits_k^{\infty} \frac{\left[1-(-1)^n \cos\mu b\right]}{\left(\mu^2-k_n^2\right)\left(\mu^2-k_q^2\right)}\, I_1^{mp}(\mu : |\mu| > k)\,\mathrm{d}\mu, \end{aligned} \tag{4.17}$$

where $I_1^{mp}(\mu : |\mu| < k)$ and $I_1^{mp}(\mu : |\mu| > k)$ can be evaluated using Eqs. (4.14) and (4.16), respectively. This equation, however, can be used as a general expression for evaluating the coupling coefficients for the remaining types of modal interactions as well.

4.4 Derivation of the closed forms for I^{mnpq}

The coupling coefficient $\bar{\Theta}_{mnpq}$ (Eq. (4.1)) quantifies the interaction between the panel modes ($(m,n)^{\mathrm{th}}$ mode with $(p,q)^{\mathrm{th}}$ mode) due to the fluid loading. In this study, we find approximate closed form expressions for $\bar{\Theta}_{mnpq}$ based on the type of interacting modes as listed in Table 2.1. It is readily known that there can be as many as 25 types of interactions. However, as the coupling coefficients are commutative (see Eq. (4.1)), it is only required to find the approximate expressions for 15 types of interactions: 1) corner - corner, 2) corner - X edge, 3) corner - Y edge, 4) corner - XY edge, 5) corner - AF, 6) X edge - X edge, 7) X edge - Y edge, 8) X edge - XY edge, 9) X edge - AF, 10) Y edge - Y edge, 11) Y edge - XY edge, 12) Y edge - AF, 13) XY edge - XY edge, 14) XY edge - AF and 15) AF - AF. We start by finding the closed form for the Y edge - Y edge coupling coefficient, which is the simplest of all. While finding the closed form expressions, we have considered only the dominant terms (or contributions). Approximations relevant to each of the cases are made at appropriate places in the derivation.

4.4.1 Y edge - Y edge modes ($k_m, k_p > k$ and $k_n, k_q < k$)

The derivation of I^{mnpq} for the Y edge - Y edge case is outlined in Fig. 4.12 as a flow chart. We use Eq. (4.17) to evaluate I^{mnpq}, in which the inner integrals $I_1^{mp}(\mu : |\mu| < k)$ and $I_1^{mp}(\mu : |\mu| > k)$ are evaluated using Eqs. (4.14) and (4.16), respectively. We consider two cases: 1) $k_m \neq k_p$ and $k_n = k_q$ and 2) $k_m = k_p$ and $k_n = k_q$.

I $\quad k_m \neq k_p$ and $k_n = k_q$

We have the following approximation by Kraichnan [10, 6, 15] (see Appendix C)

$$\left.\frac{[1-(-1)^n \cos \mu b]}{\left(\mu^2-k_n^2\right)\left(\mu^2-k_q^2\right)}\right|_{n=q} \approx \frac{\pi b}{4k_n^2}\,\delta(\mu-k_n). \tag{4.18}$$

Substituting this into Eq. (4.17) and knowing that $k_n < k$ we get

$$I^{mnpq} \approx \frac{\pi b}{2k_n^2}\, I_1^{mp}(k_n : k_n < k), \tag{4.19}$$

where $I_1^{mp}(k_n : k_n < k)$ can be evaluated using Eq. (4.14). The detailed derivation of I^{mnpq} when $k_m \neq k_p$ and $k_n = k_q$ is given in Appendix D.1. The result is given in the box below.

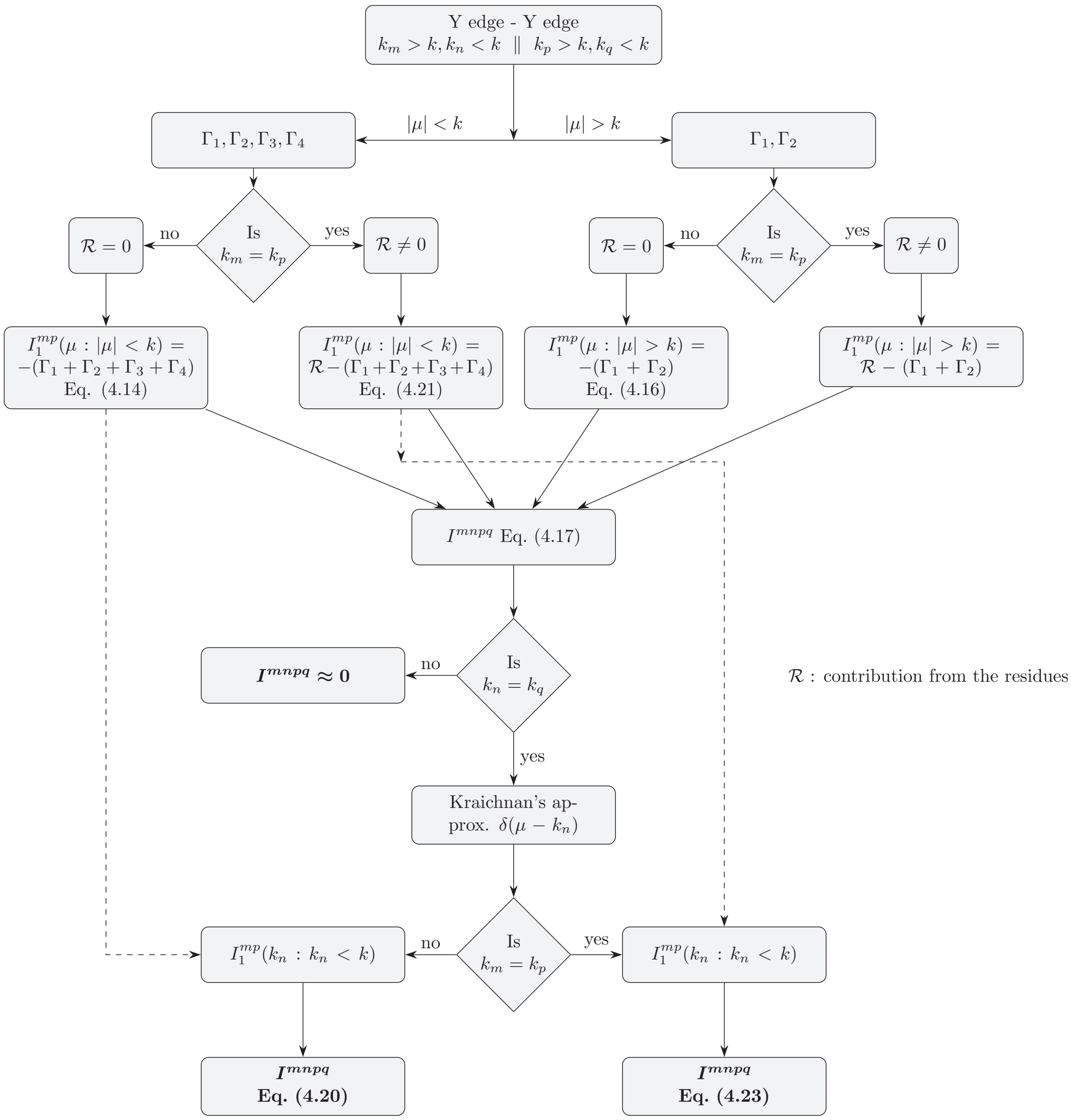

Fig. 4.12 A flow chart depicting the derivation of I^{mnpq} for the Y edge - Y dege interaction.

$$I^{mnpq} = I_R^{mnpq} + \mathrm{i}\, I_\chi^{mnpq}, \tag{4.20}$$

where the real part of I^{mnpq} is given by

$$I_R^{mnpq} \approx \frac{\pi^2 b}{2k_n^2}\left[\frac{k_p\sqrt{k_m^2-\lambda_1^2}-k_m\sqrt{k_p^2-\lambda_1^2}}{k_m^3 k_p - k_m k_p^3} - \frac{\lambda_1(-1)^m \mathrm{J}_1\left(a\lambda_1\right)}{a\left(\lambda_1^2-k_m^2\right)\left(\lambda_1^2-k_p^2\right)}\right]\delta_{nq}$$

and the imaginary part of I^{mnpq} is given by

$$I_\chi^{mnpq} \approx -\frac{\pi b}{k_n^2}(A+B+C)\,\delta_{nq}$$

with

$$A = \frac{\pi\lambda_1(-1)^m \mathrm{H}_1\left(a\lambda_1\right)}{2a\left(\lambda_1^2-k_m^2\right)\left(\lambda_1^2-k_p^2\right)},$$

$$B = \frac{2k\sqrt{2k^2-k_n^2}+\left(k^2-k_n^2\right)\log\left(\frac{\left(\sqrt{2k^2-k_n^2}+k\right)^2}{k^2-k_n^2}\right)}{4k_m^2 k_p^2} + \frac{\log\left(\frac{k^2+k_p^2}{k^2+k_m^2}\right)}{2\left(k_p^2-k_m^2\right)}$$

and $$C = \frac{(-1)^{m+1}}{12ak_m^2k_p^2}\left\{2\sqrt{\frac{1}{a^2}+k^2-k_n^2}-\left(k^2-k_n^2\right)\right.$$
$$\left.\times\left[-4a^2\sqrt{k^2-k_n^2}+4a^2\sqrt{\frac{1}{a^2}+k^2-k_n^2}-3a\log\left(\frac{\left(\sqrt{\frac{1}{a^2}+k^2-k_n^2}+\frac{1}{a}\right)^2}{k^2-k_n^2}\right)\right]\right\}.$$

II $\quad k_m = k_p$ **and** $k_n = k_q$

In this case, the poles of the integrand of $I_1^{mp}(\mu)$ (Eq. (4.6)) are at $\lambda = \pm k_m$ and are of multiplicity two. The residues at the poles when $k_m = k_p$ are evaluated in the Appendix A and are given below.

$$\mathrm{Res}(-k_m) = \mathrm{Res}(k_m) = \frac{a\,\left|\lambda_1^2-k_m^2\right|^{\frac{1}{2}}}{4\,k_m^2}.$$

Thus, for case 1, the contour integration around the branch cut as shown in Fig. 4.10 (note that for this case $k_m = k_p$ in the figure) results in

$$\mathrm{P}\left[I_1^{mp}(\mu)\right] = I_1^{mp}(\mu : |\mu| < k) = \pi\mathrm{i}\left[\mathrm{Res}(k_m)+\mathrm{Res}(-k_m)\right]-\left(\Gamma_1+\Gamma_2+\Gamma_3+\Gamma_4\right).$$

Substituting for the residues and the Γ_i's from Eq. (4.12) we obtain

$$
\begin{aligned}
I_1^{mp}(\mu : |\mu| < k) = 2 \int_0^{\lambda_1} & \frac{[1-(-1)^m \cos ax]\, |\lambda_1^2 - x^2|^{\frac{1}{2}}}{(x^2-k_m^2)^2} \,\mathrm{d}x \\
& - 2\,\mathrm{i} \left[\frac{-\pi a\, |\lambda_1^2 - k_m^2|^{\frac{1}{2}}}{4\,k_m^2} + \int_0^{\lambda_1} \frac{(-1)^m \sin ax\, |\lambda_1^2 - x^2|^{\frac{1}{2}}}{(x^2-k_m^2)^2} \,\mathrm{d}x \right. \\
& \left. + \int_0^{\infty} \frac{[1-(-1)^m\, \mathrm{e}^{-ay}]\, |\lambda_1^2 + y^2|^{\frac{1}{2}}}{(y^2+k_m^2)^2} \,\mathrm{d}y \right].
\end{aligned} \tag{4.21}
$$

Using Kraichnan's assumption (Eq. (4.18)) and knowing that $k_n < k$ we get

$$
I^{mnpq} \approx \frac{\pi b}{2k_n^2}\, I_1^{mp}(k_n : k_n < k), \tag{4.22}
$$

where $I_1^{mp}(k_n : k_n < k)$ is evaluated using Eq. (4.21). Detailed derivation of I^{mnpq} when $k_m = k_p$ and $k_n = k_q$ is given in Appendix D.1. The result is summarized below.

$$
I^{mnpq} = I_R^{mnpq} + \mathrm{i}\, I_\chi^{mnpq}, \tag{4.23}
$$

where the real part of I^{mnpq} is given by

$$
I_R^{mnpq} \approx \frac{\pi^2 b}{2k_n^2} \left[\frac{\lambda_1^2}{2k_m^3 \sqrt{k_m^2 - \lambda_1^2}} - \frac{\lambda_1(-1)^m J_1(a\lambda_1)}{a\,(k_m^2 - \lambda_1^2)^2} \right] \delta_{mp}\, \delta_{nq}
$$

and the imaginary part of I^{mnpq} is given by

$$
I_\chi^{mnpq} \approx \left[-\frac{\pi b}{k_n^2}(A + B + C) + D \right] \delta_{mp}\, \delta_{nq}
$$

with

$$
A = \frac{\pi \lambda_1 (-1)^m \mathrm{H}_1(a\lambda_1)}{2a\,(\lambda_1^2 - k_m^2)^2},
$$

$$
B = \frac{2k\sqrt{2k^2 - k_n^2} + (k^2 - k_n^2)\log\left(\frac{\left(\sqrt{2k^2 - k_n^2} + k\right)^2}{k^2 - k_n^2} \right)}{4k_m^4} + \frac{1}{2\,(k^2 + k_m^2)},
$$

$$C = \frac{(-1)^{m+1}}{12ak_m^4}\left\{2\sqrt{\frac{1}{a^2}+k^2-k_n^2}-\left(k^2-k_n^2\right)\right.$$
$$\left.\times\left[-4a^2\sqrt{k^2-k_n^2}+4a^2\sqrt{\frac{1}{a^2}+k^2-k_n^2}-3a\log\left(\frac{\left(\sqrt{\frac{1}{a^2}+k^2-k_n^2}+\frac{1}{a}\right)^2}{k^2-k_n^2}\right)\right]\right\}$$

$$\text{and } D = \frac{\pi^2 ab\sqrt{k_m^2-\lambda_1^2}}{4k_m^2k_n^2}.$$

For all the cases when $k_n \neq k_q$, it is assumed that $I^{mnpq} \approx 0$ (see Appendix C).

4.4.2 X edge - X edge modes ($k_m, k_p < k$ and $k_n, k_q > k$)

For the two instances, when $k_m = k_p < k$ and $k_n \neq k_q > k$ and when $k_m = k_p < k$ and $k_n = k_q > k$, the integral I^{mnpq} can be obtained from Eqs. (4.20) and (4.23), respectively, with the transformation rule

$$m \leftrightarrow n, p \leftrightarrow q \text{ and } a \leftrightarrow b.$$

And for all the cases, when $k_m \neq k_p$, we assume that $I^{mnpq} \approx 0$.

4.4.3 Corner - corner modes ($k_m, k_n, k_p, k_q > k$)

The derivation of I^{mnpq} for the corner - corner interaction is outlined in Fig. 4.17. The integral I^{mnpq} can be evaluated using Eq. (4.17)

$$I^{mnpq} = 2\int_0^k \frac{[1-(-1)^n\cos\mu b]}{\left(\mu^2-k_n^2\right)\left(\mu^2-k_q^2\right)} I_1^{mp}(\mu : |\mu| < k)\,\mathrm{d}\mu$$
$$+ 2\int_k^\infty \frac{[1-(-1)^n\cos\mu b]}{\left(\mu^2-k_n^2\right)\left(\mu^2-k_q^2\right)} I_1^{mp}(\mu : |\mu| > k)\,\mathrm{d}\mu,$$

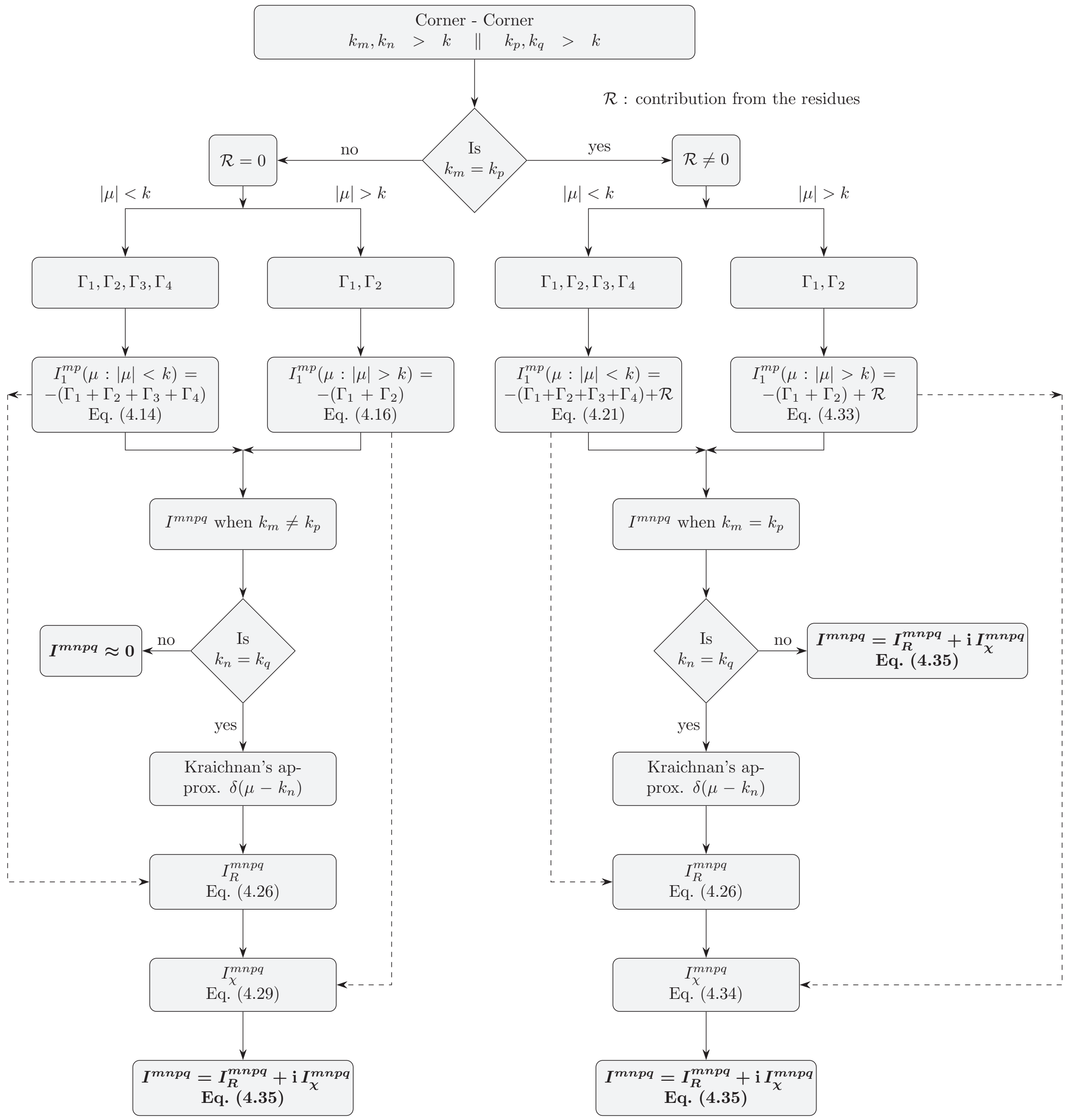

Fig. 4.13 A flow chart depicting the derivation of I^{mnpq} for the corner - corner interaction.

where $I_1^{mp}(\mu : |\mu| < k)$ is evaluated using Eq. (4.14)

$$I_1^{mp}(\mu : |\mu| < k) = 2 \int_0^{\lambda_1} \frac{[1 - (-1)^m \cos ax] \, |\lambda_1^2 - x^2|^{\frac{1}{2}}}{(x^2 - k_m^2)\,\left(x^2 - k_p^2\right)} \, \mathrm{d}x$$

$$- 2\,\mathrm{i} \left[\int_0^{\lambda_1} \frac{(-1)^m \sin ax \, |\lambda_1^2 - x^2|^{\frac{1}{2}}}{(x^2 - k_m^2)\,\left(x^2 - k_p^2\right)} \, \mathrm{d}x + \int_0^{\infty} \frac{[1 - (-1)^m \, \mathrm{e}^{-ay}] \, |\lambda_1^2 + y^2|^{\frac{1}{2}}}{(y^2 + k_m^2)\,\left(y^2 + k_p^2\right)} \, \mathrm{d}y \right].$$

As $k_m, k_p > \lambda_1$ ($\lambda_1^2 = k^2 - \mu^2$), there exist no regular singularities in the above integrals. The term $I_1^{mp}(\mu : |\mu| > k)$ in Eq. (4.17) can be evaluated using Eq. (4.16)

$$I_1^{mp}(\mu : |\mu| > k) = -2\,\mathrm{i} \int\limits_{\lambda_1'}^{\infty} \frac{\left[1 - (-1)^m\ \mathrm{e}^{-ay}\right] \left|{\lambda_1'}^2 - y^2\right|^{\frac{1}{2}}}{\left(y^2 + k_m^2\right)\left(y^2 + k_p^2\right)}\,\mathrm{d}y,$$

where ${\lambda_1'}^2 = \mu^2 - k^2$.

(a) $\boldsymbol{k_m \neq k_p}$ and $\boldsymbol{k_n = k_q}$

Assume that $k_m \neq k_p > k$, and $k_n = k_q > k$. Substituting the Kraichnan's approximation (Eq. (4.18)) into Eq. (4.17) and knowing that $k_n > k$ we get

$$I^{mnpq} \approx \frac{\pi b}{2k_n^2}\, I_1^{mp}\left(k_n : k_n > k\right), \tag{4.24}$$

where $I_1^{mp}\left(k_n : k_n > k\right)$ can be evaluated using Eq. (4.16) by substituting $\mu = k_n$, which is purely an imaginary quantity. However, for the corner - corner type of interaction, there must exist a real term, although small, associated with the radiation coupling in addition to the inertial coupling part (imaginary term) in the modal coupling coefficient [6, 15]. Here, the real part of I^{mnpq} can be evaluated using

$$I_R^{mnpq} = 2\int\limits_0^k \frac{\left[1 - (-1)^n \cos\mu b\right]}{\left(\mu^2 - k_n^2\right)\left(\mu^2 - k_q^2\right)}\,\mathrm{Re}\left[I_1^{mp}(\mu : |\mu| < k)\right]\,\mathrm{d}\mu. \tag{4.25}$$

From Eq. (4.14)

$$\mathrm{Re}\left[I_1^{mp}(\mu : |\mu| < k)\right] = 2\int\limits_0^{\lambda_1} \frac{\left[1 - (-1)^m\ \cos ax\right]\,|\lambda_1^2 - x^2|^{\frac{1}{2}}}{\left(x^2 - k_m^2\right)\left(x^2 - k_p^2\right)}\,\mathrm{d}x.$$

Therefore, by the approximation $\left(x^2 - k_m^2\right)\left(x^2 - k_p^2\right)\left(\mu^2 - k_n^2\right)\left(\mu^2 - k_q^2\right) \approx k_m^2\, k_n^2\, k_p^2\, k_q^2$ we get

$$I_R^{mnpq} \approx \frac{4}{k_m^2\, k_n^2\, k_p^2\, k_q^2} \int\limits_0^k \int\limits_0^{\sqrt{k^2-\mu^2}} \left[1 - (-1)^m \cos xa\right]\left[1 - (-1)^n \cos\mu b\right] \sqrt{k^2 - \mu^2 - x^2}\,\mathrm{d}x\,\mathrm{d}\mu.$$

After a few simplifications [15, 6],

$$I_R^{mnpq} \approx \frac{4}{k_m^2\, k_n^2\, k_p^2\, k_q^2} \left[\frac{\pi(-1)^m (ak\cos(ak) - \sin(ak))}{2a^3} + \frac{\pi(-1)^n (bk\cos(bk) - \sin(bk))}{2b^3} \right.$$
$$\left. + \frac{\pi(-1)^{m+n} \left(k\sqrt{a^2+b^2}\cos\left(k\sqrt{a^2+b^2}\right) - \sin\left(k\sqrt{a^2+b^2}\right)\right)}{2\left(a^2+b^2\right)^{3/2}} + \frac{\pi k^3}{6} \right]. \quad (4.26)$$

Now, the imaginary part of I^{mnpq} when $k_n = k_q$ and $k_m \neq k_p$ is given by Eq. (4.24)

$$I_\chi^{mnpq} \approx \frac{\pi b}{2k_n^2} \operatorname{Im}\left[I_1^{mp}\left(k_n : k_n > k\right)\right]. \quad (4.27)$$

As mentioned earlier, $I_1^{mp}\left(k_n : k_n > k\right)$ is purely an imaginary quantity (see Eq. (4.16)). A detailed derivation of $I_1^{mp}\left(k_n : k_n > k\right)$ is given in Appendix D.2 and the result is given below.

$$I_1^{mp}(k_n : k_n > k) \approx -\frac{\mathrm{i}\log\left(\frac{k^2+k_m^2}{k^2+k_p^2}\right)}{k_m^2 - k_p^2}\, \delta_{nq}. \quad (4.28)$$

Substituting this into Eq. (4.27) we get

$$I_\chi^{mnpq} \approx -\frac{\pi b \log\left(\frac{k^2+k_m^2}{k^2+k_p^2}\right)}{2k_n^2\left(k_m^2 - k_p^2\right)}\, \delta_{nq}. \quad (4.29)$$

(b) $\boldsymbol{k_m = k_p}$ and $\boldsymbol{k_n \neq k_q}$

The real part of I^{mnpq} can be obtained from Eq. (4.26) using the transformation rule $m \leftrightarrow n$, $p \leftrightarrow q$ and $a \leftrightarrow b$. The imaginary part of I^{mnpq} can be obtained from

$$I_\chi^{mnpq} \approx \frac{\pi a}{2k_m^2} \operatorname{Im}\left[I_1^{nq}\left(k_m : k_m > k\right)\right]. \quad (4.30)$$

Using the transformation rule $m \leftrightarrow n$, $p \leftrightarrow q$ and $a \leftrightarrow b$ in Eq. (4.29) we get

$$I_\chi^{mnpq} \approx -\frac{\pi a \log\left(\frac{k^2+k_n^2}{k^2+k_q^2}\right)}{2k_m^2\left(k_n^2 - k_q^2\right)}\, \delta_{mp}. \quad (4.31)$$

(c) $\boldsymbol{k_m = k_p}$ and $\boldsymbol{k_n = k_q}$

The real part of I^{mnpq} can be evaluated using Eq. (4.25). When $k_m = k_p$ we have to include the contribution from the residues at $\pm k_m$ in the integral $I_1^{mp}(\mu : |\mu| < k)$. The resulting expression for $I_1^{mp}(\mu : |\mu| < k)$ is the same as given in Eq. (4.21). It can be seen that the contribution from the residues is purely imaginary. Hence, the residues do not contribute to the real part of I^{mnpq}. Therefore, the Eq. (4.26) for I_R^{mnpq} is still valid when $k_m = k_p$ and $k_n = k_q$.

When $k_m = k_p$ and $k_n = k_q$, either Eq. (4.27) or Eq. (4.30) can be used to evaluate I_χ^{mnpq}. Consider Eq. (4.27). When $k_m = k_p$, the integral $I_1^{mp}(k_n : k_n > k)$, given by Eq. (4.16), has to be modified to account for the poles of multiplicity two at $\pm k_m$. For the case 2 ($|\mu| > k$), the residues at the poles are (see Appendix B)

$$\mathrm{Res}(-k_m) = \mathrm{Res}(k_m) = \frac{a\,|\lambda_1^2 - k_m^2|^{\frac{1}{2}}}{4\,k_m^2},$$

where $\lambda_1 = \mathrm{i}\lambda_1' = \mathrm{i}\,|\mu^2 - k^2|^{\frac{1}{2}}$. Thus, the contour integration around the branch cut, as shown in Fig. 4.11 (note that for this case $k_m = k_p$ in the figure), results in

$$\mathrm{P}\left[I_1^{mp}(\mu)\right] = I_1^{mp}(\mu : |\mu| > k) = \pi\mathrm{i}\left[\mathrm{Res}(k_m) + \mathrm{Res}(-k_m)\right] - (\Gamma_1 + \Gamma_2).$$

Substituting for the residues and the Γ_i's from Eq. (4.15) we obtain

$$I_1^{mp}(\mu : |\mu| > k) = -2\,\mathrm{i}\left[\frac{-\pi a\,|\lambda_1^2 - k_m^2|^{\frac{1}{2}}}{4\,k_m^2} + \int_{\lambda_1'}^{\infty} \frac{\left[1 - (-1)^m\ \mathrm{e}^{-ay}\right]\left|\lambda_1'^2 - y^2\right|^{\frac{1}{2}}}{\left(y^2 + k_m^2\right)^2}\,\mathrm{d}y\right]\delta_{mp}. \tag{4.32}$$

We obtain (see Appendix D.2)

$$I_1^{mp}(k_n : k_n > k) \approx \mathrm{i}\left[\frac{\pi a\ |k_m^2 + k_n^2 - k^2|^{\frac{1}{2}}}{2\,k_m^2} - \frac{1}{(k^2 + k_m^2)}\right]\delta_{mp}. \tag{4.33}$$

Substituting the above equation into Eq. (4.27) we get

$$I_\chi^{mnpq} \approx \left[\frac{\pi^2 ab\ |k_m^2 + k_n^2 - k^2|^{\frac{1}{2}}}{4\,k_m^2\,k_n^2} - \frac{\pi b}{2\,k_n^2\,(k^2 + k_m^2)}\right]\delta_{mp}\,\delta_{nq}.$$

However, it is found that the above expression is a poor approximation when $k_m = k_p$ and $k_n = k_q$. A correction term $-\frac{\pi b}{2\,k_n^2(k^2+k_m^2)}$, similar to the second term inside the square bracket, is added to the above expression. Thus, for $k_m = k_p$ and $k_n = k_q$, the imaginary part of I^{mnpq} is given by

$$I_\chi^{mnpq} \approx \left[\frac{\pi^2 ab\ |k_m^2 + k_n^2 - k^2|^{\frac{1}{2}}}{4\,k_m^2\,k_n^2} - \frac{\pi a}{2\,k_m^2\,(k^2 + k_n^2)} - \frac{\pi b}{2\,k_n^2\,(k^2 + k_m^2)}\right]\delta_{mp}\,\delta_{nq}. \tag{4.34}$$

Summarizing, using Eqs. (4.26), (4.29), (4.31) and (4.34),

$$I^{mnpq} = I_R^{mnpq} + \mathrm{i}\, I_\chi^{mnpq}, \tag{4.35}$$

where

$$I_R^{mnpq} \approx \frac{4}{k_m^2\, k_n^2\, k_p^2\, k_q^2} \left[\frac{\pi k^3}{6} + \frac{\pi(-1)^m (ak\cos(ak) - \sin(ak))}{2a^3} + \frac{\pi(-1)^n (bk\cos(bk) - \sin(bk))}{2b^3} \right.$$
$$\left. + \frac{\pi(-1)^{m+n} \left(k\sqrt{a^2+b^2} \cos\left(k\sqrt{a^2+b^2}\right) - \sin\left(k\sqrt{a^2+b^2}\right)\right)}{2\left(a^2+b^2\right)^{3/2}} \right]$$

and

$$I_\chi^{mnpq} \approx A\,\delta_{mp} + B\,\delta_{nq} - (A+B)\,\delta_{mp}\,\delta_{nq} + C\,\delta_{mp}\,\delta_{nq}$$

with

$$A = -\frac{\pi a \log\left(\frac{k^2+k_n^2}{k^2+k_q^2}\right)}{2k_m^2\left(k_n^2 - k_q^2\right)},$$

$$B = -\frac{\pi b \log\left(\frac{k^2+k_m^2}{k^2+k_p^2}\right)}{2k_n^2\left(k_m^2 - k_p^2\right)}$$

and

$$C = \frac{\pi^2 ab\, |k_m^2 + k_n^2 - k^2|^{\frac{1}{2}}}{4\, k_m^2\, k_n^2} - \frac{\pi a}{2\, k_m^2\, (k^2 + k_n^2)} - \frac{\pi b}{2\, k_n^2\, (k^2 + k_m^2)}.$$

4.5 Conclusions

A two-way coupled formulation in the wave number domain is presented to study the sound radiation from a finite panel set in a baffle. The formulation is general and assumes arbitrary fluid loading on the panel. The fluid loading leads to a complex modal coupling coefficient in the coupled equation of motion. The modal coupling coefficient, defined in integral form, is different from that defined by Davies [6] and Pope [15] - the square root function now appears in the numerator of the integrand. The real part of the coupling coefficient acts as the radiation damping and the imaginary part offers virtual mass addition to the structure. Individual approximate expressions in closed form are obtained for the modal coupling coefficient based on the panel modal wavenumbers. With known analytical expression of the coupling coefficient, in the next chapter we will derive the coupled equation which uses coupling coefficient.

Chapter 5

Modal analysis of fluid loaded panel

5.1 Introduction

Modal parameters of a vibrating system consists of, natural frequency, mode shape and damping. In this chapter our focus is to estimate the natural frequencies and mode shapes of a heavy fluid loaded panel. Material damping is neglected (η) in the investigation. Coupled equation of motion (Eq. 3.33) is

$$\frac{1}{2i\omega}K_{mn}\left[\overline{\Theta}_{mn,pq}\right]^T\{B_{mn}\}-\frac{ab}{4}\{B_{mn}\}=-\frac{\tilde{F}}{4\pi}\{\gamma_{\mathrm{pq}}(x_0,y_0)\}. \tag{5.1}$$

For modal parameter estimation, free vibration analysis is done. Hence, Eq.(5.1) for free vibration can be written as

$$\frac{1}{2i\omega}K_{mn}\left[\overline{\Theta}_{mn,pq}\right]^T\{B_{mn}\}-\frac{ab}{4}\{B_{mn}\}=\{0\}, \tag{5.2}$$

on further simplification

$$\left(\frac{1}{2i\omega}K_{mn}\left[\overline{\Theta}_{mn,pq}\right]^T-\frac{ab}{4}[I]\right)\{B_{mn}\}=\{0\}. \tag{5.3}$$

Above equation represents the eigen value problem where, coefficients of B_{mn} is a square matrix. The frequencies at which determinant of the matrix vanishes gives coupled natural frequency. The results are evaluated using the following property of the plate and acoustic medium.

Panel dimensions	$a = 0.455$ m, $b = 0.546$ m and $h = 0.003$ m
Panel material properties (steel)	$E = 210$ GPa, $\rho_p = 7850$ kg/m^3, $\nu = 0.3$
Properties of the acoustic medium (water)	$\rho_0 = 998.2$ kg/m^3 and $c = 1481$ m/s

Table 5.1 The panel dimensions and material properties considered for the validation case.

5.2 The eigenvalue problem and natural frequencies

In this section, we intend to evaluate the coupled natural frequency using Eq. (5.3). As stated in the previous section, the coefficient of B$_{mn}$ is a square matrix. Size of the matrix depends upon the number of resonance frequencies to be evaluated. For simplification, we start with lower modes frequencies (i.e. first four modes). However, similar approach can be used for estimating the higher modes frequencies as well. For the first four modes, the coupled equation (Eq. 5.3) becomes

$$\left(\frac{1}{2i\omega}\begin{bmatrix} K_{11}\overline{\Theta}_{11,11} & K_{12}\overline{\Theta}_{12,11} & K_{21}\overline{\Theta}_{21,11} & K_{22}\overline{\Theta}_{22,11} \\ K_{11}\overline{\Theta}_{11,12} & K_{12}\overline{\Theta}_{12,12} & K_{21}\overline{\Theta}_{21,12} & K_{22}\overline{\Theta}_{22,12} \\ K_{11}\overline{\Theta}_{11,21} & K_{12}\overline{\Theta}_{12,21} & K_{21}\overline{\Theta}_{21,21} & K_{22}\overline{\Theta}_{22,21} \\ K_{11}\overline{\Theta}_{11,22} & K_{12}\overline{\Theta}_{12,22} & K_{21}\overline{\Theta}_{21,22} & K_{22}\overline{\Theta}_{22,22} \end{bmatrix} - \frac{ab}{4}\begin{bmatrix} 1 & 0 & 0 & 0 \\ 0 & 1 & 0 & 0 \\ 0 & 0 & 1 & 0 \\ 0 & 0 & 0 & 1 \end{bmatrix}\right)\begin{bmatrix} B_{11} \\ B_{12} \\ B_{21} \\ B_{22} \end{bmatrix} = \begin{bmatrix} 0 \\ 0 \\ 0 \\ 0 \end{bmatrix},$$

on simplification

$$\left(\frac{1}{2\mathrm{i}\omega}\begin{bmatrix} K_{11}\overline{\Theta}_{11,11} - 2\mathrm{i}\omega ab/4 & K_{12}\overline{\Theta}_{12,11} & K_{21}\overline{\Theta}_{21,11} & K_{22}\overline{\Theta}_{22,11} \\ K_{11}\overline{\Theta}_{11,12} & K_{12}\overline{\Theta}_{12,12} - 2\mathrm{i}\omega ab/4 & K_{21}\overline{\Theta}_{21,12} & K_{22}\overline{\Theta}_{22,12} \\ K_{11}\overline{\Theta}_{11,21} & K_{12}\overline{\Theta}_{12,21} & K_{21}\overline{\Theta}_{21,21} - 2\mathrm{i}\omega ab/4 & K_{22}\overline{\Theta}_{22,21} \\ K_{11}\overline{\Theta}_{11,22} & K_{12}\overline{\Theta}_{12,22} & K_{21}\overline{\Theta}_{21,22} & K_{22}\overline{\Theta}_{22,22} - 2\mathrm{i}\omega ab/4 \end{bmatrix}\right)\begin{bmatrix} B_{11} \\ B_{12} \\ B_{21} \\ B_{22} \end{bmatrix} = \begin{bmatrix} 0 \\ 0 \\ 0 \\ 0 \end{bmatrix}.$$

Each term of the coupled matrix contains coupling coefficient ($\overline{\Theta}_{mn,pq}$). Using the fact that $\overline{\Theta}_{mn,pq}$=0, when m $\neq$ p or n $\neq$ q [6, 15], the coupled equation modifies to

$$\left(\frac{1}{2i\omega}\begin{bmatrix} K_{11}\overline{\Theta}_{11,11}-X & 0 & 0 & 0 \\ 0 & K_{12}\overline{\Theta}_{12,12}-X & 0 & 0 \\ 0 & 0 & K_{21}\overline{\Theta}_{21,21}-X & 0 \\ 0 & 0 & 0 & K_{22}\overline{\Theta}_{22,22}-X \end{bmatrix}\right)\begin{bmatrix} B_{11} \\ B_{12} \\ B_{21} \\ B_{22} \end{bmatrix} = \begin{bmatrix} 0 \\ 0 \\ 0 \\ 0 \end{bmatrix} \quad (5.4)$$

Where, $X = 2\mathrm{i}\omega ab/4$. From Eq.(5.4), characteristic equations are

$$1/(2\mathrm{i}\omega)\left(\left[D(1-\mathrm{i}\eta)\left((\pi/a)^2+(\pi/b)^2\right)^2-m_p\omega^2\right]\overline{\Theta}_{11,11}-2\mathrm{i}\omega ab/4\right)B_{11}=0, \quad (5.5)$$

$$1/(2\mathrm{i}\omega)\left(\left[D(1-\mathrm{i}\eta)\left((\pi/a)^2+(2\pi/b)^2\right)^2-m_p\omega^2\right]\overline{\Theta}_{12,12}-2\mathrm{i}\omega ab/4\right)B_{12}=0, \quad (5.6)$$

$$1/(2\mathrm{i}\omega)\left(\left[D(1-\mathrm{i}\eta)\left((2\pi/a)^2+(\pi/b)^2\right)^2-m_p\omega^2\right]\overline{\Theta}_{21,21}-2\mathrm{i}\omega ab/4\right)B_{21}=0, \quad (5.7)$$

$$1/(2\mathrm{i}\omega)\left(\left[D(1-\mathrm{i}\eta)\left((2\pi/a)^2+(2\pi/b)^2\right)^2-m_p\omega^2\right]\overline{\Theta}_{22,22}-2\mathrm{i}\omega ab/4\right)B_{22}=0. \quad (5.8)$$

Since, the selected modes are lower modes (corner mode [13]), the corner modes analytical expressions of the coupling coefficient (Eq. 4.35) are used in the above equations. Corresponding modes natural frequencies can be found by either solving Eqs. (5.5), (5.6), (5.7), (5.8) independently or by finding the zero crossing of the coupled matrix determinant(Eq. 5.4).

Determinant of the coupled matrix turns out to be a complex number. Hence, question arises is it the real or the imaginary term which gives natural frequency?. The real term of the coupling coefficient is related to the radiation damping on the panel response and imaginary term to the virtual mass addition on the panel [6] . Hence, it is the imaginary term of the matrix determinant which gives natural frequency (without 1/(2 i ω)). This is further verified by varying the material damping (η) and knowing that, there should not by considerable change in the frequency when η is varied. The results are compared with the frequency obtained by zero crossing of the real and imaginary term of determinant (with 1/(2 i ω)) when η =0.01 (Table 5.2).

Frequency when η =0.01			Real freq and imaginary zero crossing frequency when η is varied			
Real freq. (Hz)	Imag freq. (Hz)	Different η	Real freq. (Hz)	Diff. (%)	Imag. freq(Hz)	Diff. (%)
		0.10	10.85	-0.36	9.42	-1.46
10.89	9.56	0.15	10.82	-0.64	9.20	-3.76
		0.20	10.76	-1.19	8.84	-7.53

Table 5.2 Variation of natural frequency with material damping variation.

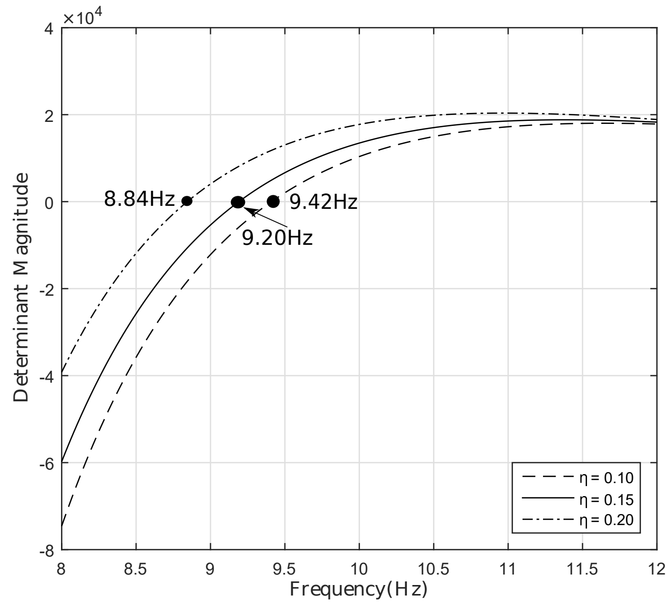

Fig. 5.1 Imaginary term plot of coupled Eq. (5.4) for different η.

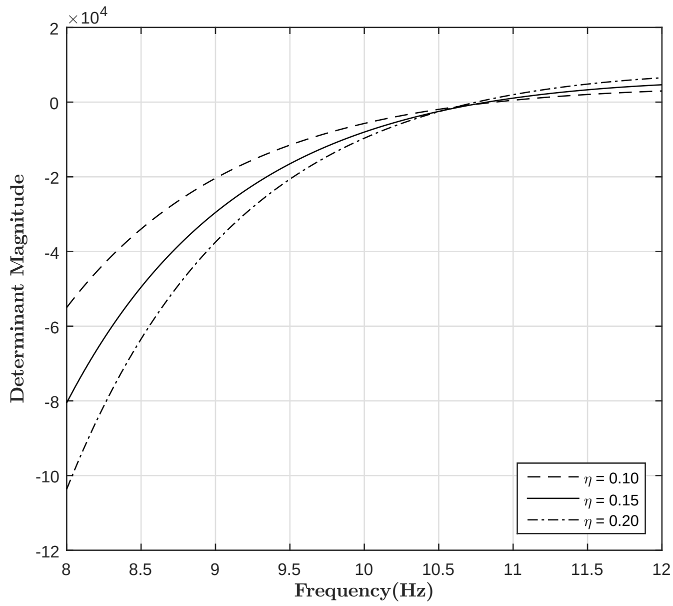

Fig. 5.2 Real term plot of coupled Eq. (5.4) for different η.

Results in the Table (5.2) shows that, with variation in the material damping, minor changes in the frequencies obtained from the zero crossing of the real term is observed. However, considerable changes in the frequencies obtained from imaginary term is reported. Hence, we can say that, it is the real term of the coupled equation which gives natural frequencies. Real and imaginary terms are plotted (Figs. (5.1), (5.2)) showing the frequencies obtained from zero crossing, when material damping is varied.

5.3 Validation of the coupled equation

In this section, we intend to validate the coupled equation by finding the uncoupled frequency from it as a special case. In the last part of section, uncoupled and coupled frequencies will be compared with the frequencies obtained from the closed form expressions of the uncoupled equation and simulation. From Eq. (5.5)

$$\frac{1}{2\mathrm{i}\omega}\left(\left[D(1-\mathrm{i}\eta)\left((\pi/a)^2+(\pi/b)^2\right)^2-m_p\omega^2\right]\overline{\Theta}_{11,11}-2\mathrm{i}\omega ab/4\right)=0, \tag{5.9}$$

Lets

$$\overline{\Theta}_{11,11}=\frac{\Theta^{'}_{11,11}}{\rho_0}, \tag{5.10}$$

Hence,

$$\left[D(1-\mathrm{i}\eta)\left((\pi/a)^2+(\pi/b)^2\right)^2-m_p\omega^2\right]\frac{\Theta^{'}_{11,11}}{\rho_0}-2\mathrm{i}\omega ab/4=0. \tag{5.11}$$

On further simplification

$$\rho_p\left[\frac{D(1-\mathrm{i}\eta)\left((\pi/a)^2+(\pi/b)^2\right)^2}{\rho_p}-h\omega^2\right]\frac{\overline{\Theta}^{'}_{11,11}}{\rho_0}-\frac{2\mathrm{i}\omega ab}{4}=0, \tag{5.12}$$

$$\left[\frac{D(1-\mathrm{i}\eta)\left((\pi/a)^2+(\pi/b)^2\right)^2}{\rho_p}-h\omega^2\right]\overline{\Theta}^{'}_{11,11}-2\mathrm{i}\omega\frac{\rho_0}{\rho_p}\frac{ab}{4}=0. \tag{5.13}$$

For a light fluid loading (uncoupled case), fluid density (ρ_0) is assumed to be very less compared to material density (ρ_p). Hence,

$$\left[D(1-\mathrm{i}\eta)\left((\pi/a)^2+(\pi/b)^2\right)^2-m_p\omega^2\right]\overline{\Theta}^{'}_{11,11}=0. \tag{5.14}$$

Which on simplification gives the closed form expression for the first uncoupled natural frequency of a plate

$$\omega_{11}=\left(\frac{D(1-\mathrm{i}\eta)}{m_p}\right)^{0.5}\left[\left(\frac{\pi}{a}\right)^2+\left(\frac{\pi}{b}\right)^2\right]^2. \tag{5.15}$$

Uncoupled frequency obtained from the coupled equation is plotted in Fig. (5.3) and results are compared with the frequencies obtained from LMS virtual lab simulation (Table 5.3).

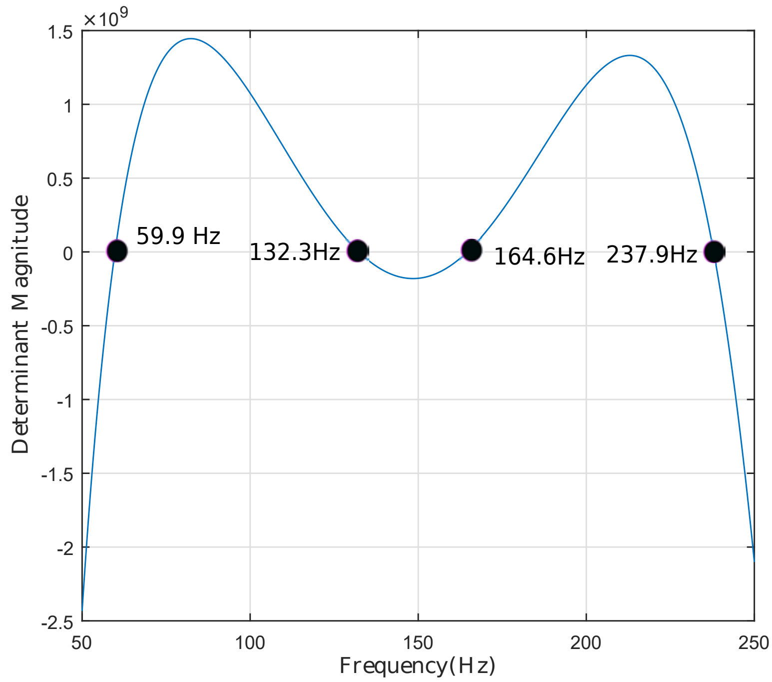

Fig. 5.3 Plot of uncoupled frequencies obtained from the coupled equation.

Mode No.	LMS frequency (Hz)	Present study (Hz)	Difference # (%)
1,1	60.06	59.9	-0.27
1,2	133.9	132.3	-1.19
2,1	166.39	164.6	-1.07
2,2	240.23	237.9	-0.97

Table 5.3 Uncoupled natural frequency comparison (LMS vs Coupled equation).

Result shows a close match between the frequencies. Comparison of the coupled frequencies obtained from the determinant of Eq. (5.4) with the frequencies obtained from LMS virtual lab simulation and the mean quadratic velocity (MQV) [12] is listed in Table (5.4).

Mode No.	LMS Frequency (Hz)	MQV (Hz)	Present study (Hz)	Difference # (%)
1,1	10.29	9.69	9.57	-6.99
1,2	28.94	28.15	27.50	-4.97
2,1	37.88	37.01	36.41	-3.88
2,2	60.35	58.93	58.27	-3.44

Table 5.4 Comparison of coupled natural frequency.

Though, some difference in results between the LMS evaluated frequencies and present study is observed, it is not very significant. The results closely matches with the frequency obtained from mean quadratic velocity.

5.4 Modal coefficients

After finding the coupled resonance frequency, in this section we focus on evaluating the modal coefficients i.e. B_{mn} at different natural frequencies. Firstly, evaluation of modal coefficient is done for the first six modes which will later be validated for the first nine modes. Coupled equation for the first six modes is

$$\left(\frac{1}{2i\omega}\begin{bmatrix} X_1 & K_{12}\overline{\Theta}_{12,11} & K_{13}\overline{\Theta}_{13,11} & K_{21}\overline{\Theta}_{21,11} & K_{22}\overline{\Theta}_{22,11} & K_{31}\overline{\Theta}_{31,11} \\ K_{11}\overline{\Theta}_{11,12} & X_2 & K_{13}\overline{\Theta}_{13,12} & K_{21}\overline{\Theta}_{21,12} & K_{22}\overline{\Theta}_{22,12} & K_{31}\overline{\Theta}_{31,12} \\ K_{11}\overline{\Theta}_{11,13} & K_{12}\overline{\Theta}_{12,13} & X_3 & K_{21}\overline{\Theta}_{21,13} & K_{22}\overline{\Theta}_{22,13} & K_{31}\overline{\Theta}_{31,13} \\ K_{11}\overline{\Theta}_{11,21} & K_{12}\overline{\Theta}_{12,21} & K_{13}\overline{\Theta}_{13,21} & X_4 & K_{22}\overline{\Theta}_{22,21} & K_{31}\overline{\Theta}_{31,21} \\ K_{11}\overline{\Theta}_{11,22} & K_{12}\overline{\Theta}_{12,22} & K_{13}\overline{\Theta}_{13,22} & K_{21}\overline{\Theta}_{21,22} & X_5 & K_{31}\overline{\Theta}_{31,22} \\ K_{11}\overline{\Theta}_{11,31} & K_{12}\overline{\Theta}_{12,31} & K_{13}\overline{\Theta}_{13,31} & K_{21}\overline{\Theta}_{21,31} & K_{22}\overline{\Theta}_{22,31} & X_6 \end{bmatrix}\right)\begin{bmatrix} B_{11} \\ B_{12} \\ B_{13} \\ B_{21} \\ B_{22} \\ B_{31} \end{bmatrix} = \begin{bmatrix} 0 \\ 0 \\ 0 \\ 0 \\ 0 \\ 0 \end{bmatrix}.$$

Here the diagonal term are abbreviated as
$X_1 = K_{11}\overline{\Theta}_{11,11} - 2i\omega ab/4$, $X_2 = K_{12}\overline{\Theta}_{12,12} - 2i\omega ab/4$, $X_3 = K_{13}\overline{\Theta}_{13,13} - 2i\omega ab/4$, $X_4 = K_{21}\overline{\Theta}_{21,21} - 2i\omega ab/4$, $X_5 = K_{22}\overline{\Theta}_{22,22} - 2i\omega ab/4$, and $X_6 = K_{31}\overline{\Theta}_{31,31} - 2i\omega ab/4$.

Coupled natural frequencies obtained for these modes are

Mode No.	LMS Frequency (Hz)	Present study (Hz)	Difference (%)
1,1	10.29	9.48	-7.87
1,2	28.94	27.50	-5.49
2,1	37.88	36.40	-4.09
2,2	60.35	58.27	-3.43
1,3	65.71	63.49	-3.37
3,1	93.95	91.77	-2.31

Table 5.5 First six modes coupled natural frequencies (Hz).

Modal coefficients are computed at the first and third natural frequency i.e., 9.48 Hz and 36.40 Hz by assuming $B_{11} = 1$ and $B_{13} = 1$ respectively.

First Modeshape (B_{11})		Third Modeshape (B_{13})	
Modal coefficients	Magnitude (B_{11}=1)	Modal coefficients	Magnitude (B_{13}=1)
B_{12}	0.0000 + 0.0000 i	B_{11}	-0.1991+ 0.0022i
B_{13}	0.0031 - 0.0000 i	B_{12}	0.0000 + 0.0000i
B_{21}	0.0000 + 0.0000 i	B_{21}	0.0040 + 0.0000i
B_{22}	0.0000 + 0.0000 i	B_{22}	0.0000 + 0.0000i
B_{31}	0.0000 + 0.0000 i	B_{31}	-0.0003 + 0.0000i

Table 5.6 Modal coefficient at first and third mode shape.

It is observed that the cross modal coefficients are negligible compared to the self modal coefficient. Hence, cross modes coupling is minimal. This validates the Davies statement [6] that the modes in case of heavy fluid loading remains to be *in vacuo* modes. Thus, off diagonal elements of the coupled equation (matrix) which corresponds to the cross mode coupling can be neglected while evaluating the coupled natural frequencies.

The above said statements are further validated considering the first 9 modes natural frequencies. The coupled resonances obtained from the fully populated matrix are listed in the Table 5.7 .

Mode No.	LMS Frequency (Hz)	Present study (Hz)	Difference (%)
1,1	10.29	9.48	-7.87
1,2	28.94	27.35	-5.49
2,1	37.88	36.33	-4.09
2,2	60.35	58.28	-3.43
1,3	65.71	63.49	-3.37
3,1	93.95	91.78	-2.31
2,3	101.30	98.48	-2.78
3,2	120.10	117.30	-2.33
1,4	124.60	121.50	-2.50

Table 5.7 Coupled natural frequencies for the first 9 modes.

Modal coefficients at the first and second natural frequency i.e. 9.48 Hz and 27.35 Hz by assuming $B_{11} = 1$ and $B_{12} = 1$ respectively are computed and reported below

First Modeshape (B_{11})		Second Modeshape (B_{12})	
Modal coefficients	Magnitude (B_{11}=1)	Modal coefficients	Magnitude (B_{12}=1)
B_{12}	-0.0508 + 0.0317 i	B_{11}	0.0000 + 0.0000 i
B_{13}	0.0032 - 0.0000 i	B_{13}	0.0000 + 0.0000 i
B_{14}	-0.0009 + 0.0006 i	B_{14}	0.0178 + 0.0000 i
B_{21}	0.0000 + 0.0000 i	B_{21}	0.0178 + 0.0000 i
B_{22}	0.0000 + 0.0000 i	B_{22}	0.0000 + 0.0000 i
B_{23}	0.0000 + 0.0000 i	B_{23}	0.0000 + 0.0000 i
B_{31}	0.0000 - 0.0000 i	B_{31}	0.0000 + 0.0000 i
B_{32}	-0.0004 + 0.0003 i	B_{32}	0.0086 + 0.0000 i

Table 5.8 Modal coefficient at first and second mode shape (9 × 9).

From the results of Table (5.6) and (5.8) we can conclude that, considering the diagonal term alone while evaluating the natural frequencies from the coupled equation may not give any significant difference with the frequencies computed from the fully populated matrix.

This conclusion is further validated, considering two cases i.e. first six and nine modes and evaluating the frequencies. Results are compared for the frequencies obtained from the fully populated coupled matrix and the matrix with only diagonal elements.

		Present study from the coupled matrix		
Mode no.	LMS frequency (Hz)	Fully populated matrix (Hz)	Only diagonal elements (Hz)	Difference (%)
1,1	10.29	9.48	9.57	0.95
1,2	28.94	27.50	27.50	0.00
2,1	37.88	36.40	36.41	0.03
2,2	60.35	58.27	58.27	0.00
1,3	65.71	63.49	63.49	0.00
3,1	93.95	91.77	91.78	0.01

Table 5.9 Coupled frequencies (fully populated vs diagonal) for first 6 modes.

The results show that there is no considerable difference between the frequencies obtained from with and without off diagonal term in the coupled equation. For the first 9 modes, results are listed in the Table (5.10).

		Present study from the coupled matrix		
Mode no.	LMS frequency (Hz)	Fully populated matrix (Hz)	Only diagonal elements (Hz)	Difference (%)
1,1	10.29	9.48	9.57	0.95
1,2	28.94	27.35	27.50	0.55
2,1	37.88	36.33	36.40	0.19
2,2	60.35	58.28	58.27	-0.02
1,3	65.71	63.49	63.49	0.00
3,1	93.95	91.78	91.78	0.00
2,3	101.30	98.48	98.46	-0.02
3,2	120.10	117.30	117.30	0.00
1,4	124.60	121.50	121.50	0.00

Table 5.10 Coupled frequencies (fully populated vs diagonal) for first 9 modes.

From the results of Table (5.9) and (5.10), we conclude that there is no significant difference in the natural frequencies evaluated from the fully populated matrix to the one in which only diagonal elements are present.

As we have to consider only the diagonal terms, we can easily identify the individual natural frequencies without solving the full matrix problem, i.e., each diagonal term in the matrix corresponds to the resonance of a unique mode. Hence, we can take generalized diagonal term and vary the index (m,n) in order to find a particular mode coupled frequency.

5.5 Closed form expression for natural frequency

Generalized diagonal term for the $(\mathrm{m,n})^{th}$ mode is (Eq. 5.4)

$$\frac{1}{2\mathrm{i}\omega}\left[\left[D(1-\mathrm{i}\eta)\left((m\pi/a)^2+(n\pi/b)^2\right)^2-m_p\omega^2\right]\overline{\Theta}_{mn,mn}-2\mathrm{i}\omega ab/4\right]. \tag{5.16}$$

Neglecting material damping (η), the expression for the coupled frequency evaluation is

$$\frac{1}{2\mathrm{i}\omega}\left[\left[D\left((m\pi/a)^2+(n\pi/b)^2\right)^2-m_p\omega^2\right]\overline{\Theta}_{mn,mn}-2\mathrm{i}\omega ab/4\right]=0. \tag{5.17}$$

Eq. (5.17) is complex in nature. The analytical expressions for the coupling coefficient (either corner mode (Eq. 4.35) or edge mode (Eq. 4.23)) are put into above equation and coupled resonance frequencies are evaluated. The contribution of real part of the coupling coefficient in determining natural frequency is negligible. Hence, closed form expression for estimating the coupled resonance frequency is

$$\boxed{\frac{1}{2\omega}\left[\left[D\left((m\pi/a)^2+(n\pi/b)^2\right)^2-m_p\omega^2\right]\mathrm{Imag.}(\overline{\Theta}_{mn,mn})-2\omega ab/4\right]=0. \quad (5.18)}$$

Till now, we have obtained the coupled resonance frequencies of lower modes which are essentially corner modes [6]. These frequencies are obtained from Eq. (5.18) by using the analytical expressions of (corner mode) coupling coefficient. Higher order modes can have edge mode interaction as well. Hence, resonance frequencies for such modes can be evaluated by following the below steps.

- Select the mode $(\mathrm{m,n})^{th}$ whose resonance frequency is to be evaluated. Find the frequency ranges in which this mode is either corner or edge mode interactions.

- Starting with the corner mode interactions, use Eq. (5.18) and plot it in the frequency range in which it is corner mode interactions. The frequency at which zero crossing happens gives coupled resonance frequency. If there is no zero crossing go to next step.
- Use the analytical expression for the edge mode coupling coefficient in Eq. (5.18) and plot it. Zero crossing frequency gives the coupled resonance frequency of that particular mode.

Now, we compare the resonance frequencies evaluated from Eq. (5.18) for higher modes of the plate. Resonance frequencies are evaluated keeping 10000 Hz as upper limit. It is observed that only corner, Y edge and X edge mode type interactions participate while evaluating the coupled resonance. The resonance frequencies are compared with the simulation results. This study is done for two different plate dimensions (h= 0.003m) and results are presented in the following section.

5.5.1 Resonance frequencies for the plate $0.455\mathbf{m} \times 0.546\mathbf{m}$

Corner mode interactions

Mode no.	LMS frequency (Hz)	Present study (Hz)	Difference (%)
2,10	1134.27	1133.95	-0.03
6,10	1750.39	1749.38	-0.06
11,2	2119.74	2118.02	-0.08
7,14	3422.42	3414.24	-0.24
14,4	3904.62	3895.88	-0.22
13,8	4044.49	4035.75	-0.22
9,15	4584.00	4569.64	-0.31

Table 5.11 Comparison of coupled natural frequency for c-c mode interactions (Higher Modes).

Y edge mode interactions

Mode no.	LMS frequency (Hz)	Present study (Hz)	Difference (%)
10,1	1655.30	1654.98	-0.02
11,1	2076.91	2075.33	-0.08
12,1	2553.27	2549.57	-0.14
13,1	3085.36	3079.39	-0.19
13,2	3130.43	3124.36	-0.19
14,1	3674.17	3665.01	-0.25
14,2	3720.26	3710.87	-0.25

Table 5.12 Comparison of frequency for Y-Y edge mode interactions.

X edge mode interactions

Mode no.	LMS frequency (Hz)	Present study (Hz)	Difference (%)
1,12	1664.02	1667.95	0.24
1,13	2012.10	2016.68	0.23
1,14	2398.09	2402.95	0.20
1,15	2822.40	2827.27	0.17
1,17	3788.94	3791.81	0.08
2,17	3855.34	3854.38	0.02
3,17	3966.19	3957.68	-0.21
1,18	4331.12	4330.10	-0.02

Table 5.13 Comparison of frequency for X-X edge mode interactions.

Results from the Table (5.11), (5.12), (5.13) shows that, the coupled resonance frequencies evaluated from (Eq. 5.18) matches very well with the simulated results for a plate under heavy fluid loading. These results are further validated considering a rectangular plate of different dimensions in the following section.

5.5.2 Resonance frequencies for the plate 1.5m × 1.8m

Corner mode interactions

Mode no.	LMS frequency (Hz)	Present study (Hz)	Difference (%)
4,10	74.86	74.43	-0.57
11,6	144.51	144.16	-0.24
6,13	153.68	153.16	-0.33
8,12	166.87	166.32	-0.43
12,6	173.07	172.58	-0.28
11,9	183.58	182.98	-0.32
13,13	331.15	329.27	-0.57

Table 5.14 Comparison of frequencies for C-C mode interactions (Higher modes).

Y edge mode interactions

Mode no.	LMS frequency (Hz)	Present study (Hz)	Difference (%)
11,1	115.27	115.19	-0.07
12,1	142.68	142.58	-0.07
13,1	173.81	173.45	-0.21
14,1	208.51	207.92	-0.28
15,1	246.99	246.10	-0.36
15,2	249.81	248.88	-0.37

Table 5.15 Comparison of coupled natural frequencies for Y-Y edge mode interactions.

X edge mode interactions

Mode No.	LMS frequency (Hz)	Present study (Hz)	Difference (%)
1,13	111.57	111.36	-0.19
1,14	133.79	133.50	-0.22
1,15	158.45	158.05	-0.25
1,16	185.60	185.07	-0.29
1,17	215.33	214.06	-0.59
2,17	219.29	218.55	-0.34

Table 5.16 Comparison of frequencies for X-X edge mode interactions.

The results from the Table (5.14), (5.15), (5.16) are in concurrence with the results obtained in Table (5.11), (5.12), (5.13), hence we conclude that the coupled derived in Eq. (5.18) is reasonably accurate for estimating the coupled resonance frequency.

5.6 Conclusions

In this chapter, we have discussed the formulation of coupled equation in the matrix form. Zero crossing of the real part of determinant of matrix gives resonance frequency. The expression for determining the uncoupled natural frequency is derived from the coupled equation. Uncoupled and coupled frequencies are estimated from the coupled equation and compared with simulation. Close match in the frequencies is observed. It is further observed that, the cross mode coupling is minimal. Hence, diagonal terms alone can be used in the coupled matrix for estimating natural frequency. Further, it is shown that the real term of the coupling coefficient doesn't contribute in frequency estimation.

Within the practical frequency range (10000Hz), it is found that the corner and edge mode interactions are good enough for finding the coupled resonance frequencies, for a given standard size plate. Finally, the closed form of the coupled equation used for resonance frequency estimation is presented and is validated for two different size of plates. The results are compared with simulation and close match is observed between them.

Chapter 6

Conclusions

The main work of this thesis is to evaluate the resonance frequencies and mode shapes of a fluid loaded finite panel set in an infinite baffle. The work is presented in three parts: In first, the discussion on vibration of a fluid loaded panel is done followed by derivation of closed form expressions for the modal coupling coefficient and in the last part, modal analysis of the fluid loaded panel is done where results related to the coupled resonances and mode shapes are presented.

In this chapter, a brief description of the mathematical models developed and the important results obtained in the thesis is summarized. Future work which can be pursuit following this work is also discussed at the last.

6.1 The two-way coupled analysis

In this part of the thesis (chapters 2 and 3), a two-way coupled formulation is presented, which includes the effect of fluid loading on the panel response. The fluid loading invokes a coupling between the *in vacuo* natural modes of the panel. Mathematically this coupling is represented as modal coupling coefficient in the equation of motion.

In chapter 2, mathematical formulation of the radiation and transmission problem is discussed. Brief introduction of the governing differential equations for structures and acoustics is presented. In chapter 3, we developed the fully coupled model for the sound radiation for a flexible panel set in the baffle and excited by a harmonic point force. The coupled equation having coupling coefficient is presented in the matrix form as eigen value problem. The frequency at which real part of the determinant vanishes gives coupled resonance frequency.

6.2 Closed form expressions for the modal coupling coefficient

In this part (chapter 4), approximate expressions for the modal coupling coefficient are obtained based on the associated panel wave numbers using the contour integration technique. The derived expressions for the modal coupling coefficient are valid for the entire frequency range and for any fluid loading conditions; for a given acoustic medium the coupling coefficient is inversely proportional to the density of the medium and the speed of sound in that medium.

The modal coupling coefficient represents the interaction between different *in vacuo* panel modes. It is a complex quantity - the real part represents the radiation damping and acts along with the structural damping, whereas the imaginary part represents the inertia loading on the panel. The combined effect of the radiation and the inertia coupling terms causes a reduction in the panel response from its *in vacuo* values. The inertia coupling term is responsible for decrease in the resonance frequencies of the fluid-loaded panel. It is observed that of the fifteen different modal interactions only two are sufficient for coupled resonance evaluation, namely, corner - corner (C-C) and edge - edge (E-E) mode interactions.

At very low frequencies, the coupling is predominantly due to the interaction between the subsonic modes. The corresponding modal coupling coefficient has a large reactive part (inertia coupling). As the frequency increases, more panel modes become supersonic and the radiation coupling increases with frequency. And at higher frequencies, the radiation coupling dominates over the inertia coupling.

6.3 Modal analysis of fluid loaded panels

In this part of thesis (chapter 5), a two-way coupled formulation is done in the wave number domain and using it coupled resonances are evaluated for an unforced finite panel set in the baffle. Fluid loading leads to a complex modal coupling coefficient in the coupled equation of motion. This equation is formulated in the matrix form for the first four modes and determinant is evaluated, the real part zero crossing gives resonance frequencies.

The expression for determining uncoupled natural frequency is derived from the coupled equation. Using coupled equation, both uncoupled and coupled frequencies are evaluated for lower order modes using analytical expressions of the coupling coefficient (chapter 4). It is found that the real part of the coupled equation gives natural frequency.

The frequency obtained from real part of equation results compared with the frequency obtained by simulation shows a close match.

It is further shown that the cross mode coupling is minimal and hence the off diagonal term of the coupled matrix can be neglected while evaluating the resonance frequency. Diagonal terms with imaginary term alone of the coupling coefficient in the coupled matrix gives natural frequency with reasonable accuracy. In the practical frequency range (10000Hz), it is found that corner-corner and edge-edge mode interactions are good enough for coupled resonance estimation for a given standard size plate. The coupled equation is presented and the frequency evaluated from it for a given mode, matches well when compared with the frequencies obtained through simulation.

6.4 Future research directions

- The topic of fluid loading on finite vibating panels although amenable numerically, is not physically well understood because it was so far not tractable analytically. The fluid loading on infinite panels has been studied using perturbation methods. However, there seems to be little that can be carried over from infinite panels to finite panels. With Anoop's work and the current extension, the closed form solutions of the coupling coefficients can be used to bring out the physics of the fluid and finite panel coupling.

- The problem can be extended to understand sound structure coupling in finite cylindrical vibrating structures.

References

[1] Mark J. Ablowitz and Athanassios S. Fokas. *Complex Variables: Introduction and Applications*. Cambridge Texts in Applied Mathematics. Cambridge University Press, 2 edition, 2003.

[2] Alain Berry. A new formulation for the vibrations and sound radiation of fluid-loaded plates with elastic boundary conditions. *The Journal of the Acoustical Society of America*, 96(2):889–901, 1994.

[3] Alain Berry, Louis Guyader, Jean, and Jean Nicolas. A general formulation for the sound radiation from rectangular, baffled plates with arbitrary boundary conditions. *The Journal of the Acoustical Society of America*, 88(6):2792–2802, 1990.

[4] L. Cremer, M. Heckl, and B.A.T. Petersson. *Structure-Borne Sound: Structural Vibrations and Sound Radiation at Audio Frequencies*. Springer, Berlin, Heidelberg, 3 edition, 2005.

[5] D.G. Crighton and D. Innes. Low frequency acoustic radiation and vibration response of locally excited fluid-loaded structures. *Journal of Sound and Vibration*, 91(2):293–314, 1983.

[6] H. G. Davies. Low frequency random excitation of water-loaded rectangular plates. *Journal of Sound and Vibration*, 15(1):107–126, 1971.

[7] Frank Fahy and Paolo Gardonio. *Sound and Structural Vibration - Radiation, Transmission and Response*. Academic Press, UK, second edition, 2007.

[8] W. R. Graham. High-frequency vibration and acoustic radiation of fluid-loaded plates. *Philosophical Transactions of the Royal Society of London A: Mathematical, Physical and Engineering Sciences*, 352(1698):1–43, 1995. ISSN 0962-8428.

[9] W. R. Graham. Analytical approximations for the modal acoustic impedances of simply supported, rectangular plates. *The Journal of the Acoustical Society of America*, 122(2):719–730, 2007. doi: 10.1121/1.2747094. URL https://doi.org/10.1121/1.2747094.

[10] Robert H. Kraichnan. Noise transmission from boundary layer pressure fluctuations. *The Journal of the Acoustical Society of America*, 29(1):65–80, 1957.

[11] N. S. Lomas and S. I. Hayek. Vibration and acoustic radiation of elastically supported rectangular plates. *Journal of Sound and Vibration*, 52(1):1–25, 1977.

[12] Anoop A. M. *Structural acoustics of perforated panels*. PhD thesis, Indian Institute of Science, Bangalore, India, May 2019.

[13] Gideon Maidanik. Response of ribbed panels to reverberant acoustic fields. *The Journal of the Acoustical Society of America*, 34(6):809–826, 1962.

[14] L. Meirovitch. *Fundamentals of Vibration.* Mcgraw-Hill Publ.Comp., 2003.

[15] Larry D. Pope and Ralph C. Leibowitz. Intermodal coupling coefficients for a fluid-loaded rectangular plate. *The Journal of the Acoustical Society of America*, 56(2):408–415, 1974.

[16] B. E. Sandman. Fluid-loaded vibration of an elastic plate carrying a concentrated mass. *The Journal of the Acoustical Society of America*, 61(6):1503–1510, 1977.

[17] Abhijit Sarkar. *Asymptotic analysis of the dispersion characteristics of structural acoustic waveguides*. PhD thesis, Indian Institute of Science, Bangalore, India, January 2009.

[18] D. Takahashi. Effects of panel boundedness on sound transmission problems. *The Journal of the Acoustical Society of America*, 98(5):2598–2606, 1995.

[19] Chong Wang. Modal sound transmission loss of a single leaf panel: Effects of inter-modal coupling. *The Journal of the Acoustical Society of America*, 137(6): 3514–3522, 2015.

Appendix A

Line integrals and residues in $I_1^{mp}(\mu : |\mu| < k)$ (case 1)

A.1 Line integrals of $\Gamma_1, \Gamma_2, \Gamma_3$ and Γ_4

Consider the contour integrals of case 1 as shown in Fig. 4.10.

$$
\begin{aligned}
\Gamma_1 &= \int_{\mathrm{i}\infty}^{0} \frac{\left[1-(-1)^m\, e^{\mathrm{i}\lambda a}\right]\,(\lambda_1^2-\lambda^2)^{\frac{1}{2}}}{(\lambda^2-k_m^2)\left(\lambda^2-k_p^2\right)}\,\mathrm{d}\lambda,\\
\Gamma_2 &= \int_{0}^{\lambda_1} \frac{\left[1-(-1)^m\, e^{\mathrm{i}\lambda a}\right]\,(\lambda_1^2-\lambda^2)^{\frac{1}{2}}}{(\lambda^2-k_m^2)\left(\lambda^2-k_p^2\right)}\,\mathrm{d}\lambda,\\
\Gamma_3 &= \int_{\lambda_1}^{0} \frac{\left[1-(-1)^m\, e^{\mathrm{i}\lambda a}\right]\,(\lambda_1^2-\lambda^2)^{\frac{1}{2}}}{(\lambda^2-k_m^2)\left(\lambda^2-k_p^2\right)}\,\mathrm{d}\lambda,\\
\text{and}\quad \Gamma_4 &= \int_{0}^{\mathrm{i}\infty} \frac{\left[1-(-1)^m\, e^{\mathrm{i}\lambda a}\right]\,(\lambda_1^2-\lambda^2)^{\frac{1}{2}}}{(\lambda^2-k_m^2)\left(\lambda^2-k_p^2\right)}\,\mathrm{d}\lambda.
\end{aligned}
\tag{A.1}
$$

We have from Eq. (4.10)

$$
\left(\lambda_1^2-\lambda^2\right)^{1/2} = \begin{cases}
|\lambda_1-\lambda|^{1/2}\,|\lambda_1+\lambda|^{1/2}\,\mathrm{e}^{\mathrm{i}(\gamma+\theta)/2} & \text{for } \mathrm{Re}(\lambda)>0 \text{ and } \mathrm{Im}(\lambda)>0\\
-|\lambda_1-\lambda|^{1/2}\,|\lambda_1+\lambda|^{1/2}\,\mathrm{e}^{\mathrm{i}(\gamma+\theta)/2} & \text{for } \mathrm{Re}(\lambda)<0 \text{ and } \mathrm{Im}(\lambda)>0\\
|\lambda_1-\lambda|^{1/2}\,|\lambda_1+\lambda|^{1/2}\,\mathrm{e}^{\mathrm{i}(\gamma+\theta)/2} & \text{for } \mathrm{Re}(\lambda)<0 \text{ and } \mathrm{Im}(\lambda)<0\\
-|\lambda_1-\lambda|^{1/2}\,|\lambda_1+\lambda|^{1/2}\,\mathrm{e}^{\mathrm{i}(\gamma+\theta)/2} & \text{for } \mathrm{Re}(\lambda)>0 \text{ and } \mathrm{Im}(\lambda)<0
\end{cases}
$$

where γ and θ vary from 0 to 2π.

It can be seen that along the contour Γ_1, $\gamma+\theta = 2\pi$ (Fig. 4.5) and $\lambda = \mathrm{i}y$. Therefore,

$$\left(\lambda_1^2 - \lambda^2\right)^{\frac{1}{2}} = \left|\lambda_1^2 - \lambda^2\right|^{\frac{1}{2}} e^{\mathrm{i}\,(\gamma+\theta)/2} = -\left|\lambda_1^2 + y^2\right|^{\frac{1}{2}}.$$

Thus,

$$\Gamma_1 = \mathrm{i}\int_0^\infty \frac{\left[1-(-1)^m\,\mathrm{e}^{-ay}\right]\,|\lambda_1^2 + y^2|^{\frac{1}{2}}}{\left(y^2+k_m^2\right)\left(y^2+k_p^2\right)}\,\mathrm{d}y. \tag{A.2}$$

Now, along the contour of Γ_2, $\gamma = 2\pi$, $\theta = 0$ (Fig. 4.5) and $\lambda = x$. Therefore,

$$\left(\lambda_1^2 - \lambda^2\right)^{\frac{1}{2}} = \left|\lambda_1^2 - \lambda^2\right|^{\frac{1}{2}} e^{\mathrm{i}\,\frac{(\gamma+\theta)}{2}} = -\left|\lambda_1^2 - x^2\right|^{\frac{1}{2}}.$$

Thus,

$$\Gamma_2 = -\int_0^{\lambda_1} \frac{\left[1-(-1)^m\,e^{\mathrm{i}ax}\right]\,|\lambda_1^2 - x^2|^{\frac{1}{2}}}{\left(x^2-k_m^2\right)\left(x^2-k_p^2\right)}\,\mathrm{d}x. \tag{A.3}$$

Along the contour of Γ_3, $\gamma = 0$, $\theta = 2\pi$ (Fig. 4.5) and $\lambda = x$. Therefore,

$$\left(\lambda_1^2 - \lambda^2\right)^{\frac{1}{2}} = -\left|\lambda_1^2 - \lambda^2\right|^{\frac{1}{2}} e^{\mathrm{i}\,\frac{(\gamma+\theta)}{2}} = \left|\lambda_1^2 - x^2\right|^{\frac{1}{2}}.$$

Thus,

$$\Gamma_3 = -\int_0^{\lambda_1} \frac{\left[1-(-1)^m\,e^{\mathrm{i}ax}\right]\,|\lambda_1^2 - x^2|^{\frac{1}{2}}}{\left(x^2-k_m^2\right)\left(x^2-k_p^2\right)}\,\mathrm{d}x. \tag{A.4}$$

And along the contour of Γ_4, $\gamma + \theta = 2\pi$ (Fig. 4.5) and $\lambda = \mathrm{i}y$. Therefore,

$$\left(\lambda_1^2 - \lambda^2\right)^{1/2} = -\left|\lambda_1^2 - \lambda^2\right|^{1/2} e^{\mathrm{i}\,\frac{(\gamma+\theta)}{2}} = \left|\lambda_1^2 + y^2\right|^{\frac{1}{2}}.$$

Thus,

$$\Gamma_4 = \mathrm{i}\int_0^\infty \frac{\left[1-(-1)^m\,\mathrm{e}^{-ay}\right]\,|\lambda_1^2 + y^2|^{1/2}}{\left(y^2+k_m^2\right)\left(y^2+k_p^2\right)}\,\mathrm{d}y. \tag{A.5}$$

A.2 The small circular contour around λ_1

Consider the small circular contour C_ϵ connecting Γ_2 and Γ_3 in Fig. 4.10. Along the contour

$$\lambda = \lambda_1 + \epsilon\, e^{\mathrm{i}\phi},$$

where $\epsilon \to 0$ is a small real quantity and $\phi : \pi$ to $-\pi$. Along the contour

$$\left(\lambda_1^2 - \lambda^2\right)^{1/2} = \left|\lambda_1^2 - \lambda^2\right|^{1/2} e^{\mathrm{i}\,\frac{(\gamma+\theta)}{2}},$$

where γ and θ can vary from 0 to 2π. The integral around the contour is

$$I_{\mathrm{C}_\epsilon} = \lim_{\epsilon \to 0} \int\limits_{\mathrm{C}_\epsilon} \underbrace{\frac{\left[1 - (-1)^m\, e^{\mathrm{i}\lambda a}\right]\, \left(\lambda_1^2 - \lambda^2\right)^{1/2}}{\left(\lambda^2 - k_m^2\right)\, \left(\lambda^2 - k_p^2\right)}}_{f(\lambda)} \mathrm{d}\lambda. \tag{A.6}$$

Now evaluating $|\,(\lambda - \lambda_1)\, f(\lambda)|$ in the limit $\epsilon \to 0$,

$$\begin{aligned} \lim_{\epsilon \to 0} |(\lambda - \lambda_1)\, f(\lambda)| &= \lim_{\epsilon \to 0} \left| \frac{\epsilon\, e^{\mathrm{i}\phi} \left[1 - (-1)^m\, e^{\mathrm{i}\lambda_1 \mathrm{a}}\right] \left|\lambda_1^2 - \left(\lambda_1 + \epsilon\, e^{\mathrm{i}\phi}\right)^2\right|^{1/2} e^{\mathrm{i}\,\frac{(\gamma+\theta)2}{}}}{\left(\lambda_1^2 - k_m^2\right)\, \left(\lambda_1^2 - k_p^2\right)} \right| \\ &= 0. \end{aligned}$$

Therefore [1]

$$\lim_{\epsilon \to 0} \int\limits_{\mathrm{C}_\epsilon} f(\lambda)\, \mathrm{d}\lambda = 0.$$

Thus,

$$I_{\mathrm{C}_\epsilon} = 0. \tag{A.7}$$

A.3 Residues at the simple poles when $k_m \neq k_p$

The integrand of case 1 can be obtained from Eq. (4.6) as

$$f(\lambda) = \frac{\left[1 - (-1)^m\, e^{\mathrm{i}\lambda a}\right]\, \left(\lambda_1^2 - \lambda^2\right)^{1/2}}{\left(\lambda^2 - k_m^2\right)\, \left(\lambda^2 - k_p^2\right)}.$$

The poles are at $\lambda = \pm k_m$ and $\pm\, k_p$, where $k_m = m\pi/a$ and $k_p = p\pi/a$. The residue at k_m can be obtained as

$$\mathrm{Res}(k_m) = \left.(\lambda - k_m)\, f(\lambda)\right|_{\lambda = k_m} = \frac{\left[1 - (-1)^{2m}\right]\, \left(\lambda_1^2 - k_m^2\right)^{1/2}}{2\, k_m\, \left(k_m^2 - k_p^2\right)}$$

which is equal to zero. Thus,

$$\mathrm{Res}(k_m) = 0. \tag{A.8}$$

Similarly, we can also arrive at

$$\mathrm{Res}(-k_m) = \mathrm{Res}(k_p) = \mathrm{Res}(-k_p) = 0. \tag{A.9}$$

A.4 Residues at the poles when $k_m = k_p$

When $k_m = k_p$, the integrand of case 1 is

$$f(\lambda) = \frac{\left[1 - (-1)^m \, e^{\mathrm{i}\lambda a}\right] \, (\lambda_1^2 - \lambda^2)^{1/2}}{(\lambda^2 - k_m^2)^2}.$$

The poles at $\lambda = \pm k_m$ are of multiplicity two. The residue at $\lambda = k_m$ can be obtained from

$$\mathrm{Res}(k_m) = \frac{\mathrm{d}}{\mathrm{d}\lambda} \left[(\lambda - k_m)^2 \, f(\lambda)\right]\Big|_{\lambda = k_m}.$$

We see from Figs. 4.5 and 4.10 that near $\lambda = k_m$, $\gamma = \pi$ and $\theta = 0$. Thus, the square root function

$$\left(\lambda_1^2 - \lambda^2\right)^{1/2} = \left|\lambda_1^2 - \lambda^2\right|^{1/2} \, e^{\mathrm{i}\,(\gamma+\theta)/2} = \mathrm{i} \, \left|\lambda_1^2 - \lambda^2\right|^{1/2}.$$

Therefore,

$$\mathrm{Res}(k_m) = \frac{\mathrm{d}}{\mathrm{d}\lambda} \left[\frac{\left[1 - (-1)^m \, e^{\mathrm{i}\lambda a}\right] \, \mathrm{i} \, |\lambda_1^2 - \lambda^2|^{1/2}}{(\lambda + k_m)^2}\right]\Bigg|_{\lambda = k_m}.$$

Thus, knowing that $k_m = m\pi/a$ we get

$$\mathrm{Res}(k_m) = \frac{a \, |\lambda_1^2 - k_m^2|^{1/2}}{4 \, k_m^2}. \tag{A.10}$$

Similarly, the residue at $\lambda = -k_m$ can be obtained from

$$\mathrm{Res}(-k_m) = \frac{\mathrm{d}}{\mathrm{d}\lambda} \left[(\lambda + k_m)^2 \, f(\lambda)\right]\Big|_{\lambda = -k_m}.$$

Near $\lambda = -k_m$, $\gamma = 2\pi$ and $\theta = \pi$. Thus, the square root function

$$\left(\lambda_1^2 - \lambda^2\right)^{1/2} = -\left|\lambda_1^2 - \lambda^2\right|^{1/2} \, e^{\mathrm{i}\,\frac{(\gamma+\theta)}{2}} = \mathrm{i} \, \left|\lambda_1^2 - \lambda^2\right|^{1/2}.$$

Therefore,

$$\mathrm{Res}(-k_m) = \frac{\mathrm{d}}{\mathrm{d}\lambda}\left[\frac{\left[1-(-1)^m\ e^{\mathrm{i}\lambda a}\right]\ \mathrm{i}\ |\lambda_1^2-\lambda^2|^{1/2}}{(\lambda-k_m)^2}\right]\Bigg|_{\lambda=-k_m}.$$

And by knowing that $k_m = m\pi/a$ we arrive at

$$\mathrm{Res}(-k_m) = \frac{a\ |\lambda_1^2-k_m^2|^{1/2}}{4\,k_m^2}. \tag{A.11}$$

Appendix B

Line integrals and residues in $I_1^{mp}(\mu : |\mu| > k)$ (case 2)

B.1 Line integrals of Γ_1 and Γ_2

The integrals Γ_1 and Γ_2, along the contours as shown in Fig. 4.11, are given by

$$\begin{aligned} \Gamma_1 &= \int_{\mathrm{i}\infty}^{\lambda_1} \frac{\left[1-(-1)^m\ e^{\mathrm{i}\lambda \mathrm{a}}\right]\ \left(\lambda_1^2-\lambda^2\right)^{1/2}}{\left(\lambda^2-k_m^2\right)\left(\lambda^2-k_p^2\right)}\,\mathrm{d}\lambda, \\ \text{and}\quad \Gamma_2 &= \int_{\lambda_1}^{\mathrm{i}\infty} \frac{\left[1-(-1)^m\ e^{\mathrm{i}\lambda \mathrm{a}}\right]\ \left(\lambda_1^2-\lambda^2\right)^{1/2}}{\left(\lambda^2-k_m^2\right)\left(\lambda^2-k_p^2\right)}\,\mathrm{d}\lambda, \end{aligned} \tag{B.1}$$

where $\lambda_1 = \mathrm{i}\lambda_1'$. We have from Eq. (4.11)

$$\left(\lambda_1^2-\lambda^2\right)^{1/2} = \left|\lambda_1^2-\lambda^2\right|^{1/2}\ e^{\mathrm{i}\,\frac{(\gamma+\theta)}{2}},$$

where γ and θ vary from $-\frac{\pi}{2}$ to $\frac{3\pi}{2}$.

We can see that along Γ_1, $\gamma = 3\pi/2$ and $\theta = \pi/2$ (Fig. 4.9) and $\lambda = \mathrm{i}y$. Therefore

$$\left(\lambda_1^2-\lambda^2\right)^{1/2} = \left|\lambda_1^2-\lambda^2\right|^{1/2}\ e^{\mathrm{i}\,\frac{(\gamma+\theta)}{2}} = -\left|\lambda_1'^2-y^2\right|^{1/2}.$$

Thus,

$$\Gamma_1 = \mathrm{i}\int_{\lambda_1'}^{\infty} \frac{\left[1-(-1)^m\ \mathrm{e}^{-ay}\right]\ \left|\lambda_1'^2-y^2\right|^{1/2}}{\left(y^2+k_m^2\right)\left(y^2+k_p^2\right)}\,\mathrm{d}y. \tag{B.2}$$

Similarly, along Γ_2, $\gamma = -\pi/2$ and $\theta = \pi/2$ (Fig. 4.9) and $\lambda = \mathrm{i}y$. Therefore

$$\left(\lambda_1^2 - \lambda^2\right)^{1/2} = \left|\lambda_1^2 - \lambda^2\right|^{1/2} e^{\mathrm{i}\,\frac{(\gamma+\theta)}{2}} = \left|\lambda_1'^2 - y^2\right|^{1/2}.$$

Thus,

$$\Gamma_2 = \mathrm{i} \int\limits_{\lambda_1'}^{\infty} \frac{\left[1 - (-1)^m \, \mathrm{e}^{-ay}\right] \left|\lambda_1'^2 - y^2\right|^{1/2}}{\left(y^2 + k_m^2\right) \left(y^2 + k_p^2\right)} \, \mathrm{d}y. \tag{B.3}$$

B.2 The small circular contour around λ_1

Consider the small circular contour C_ϵ connecting Γ_1 and Γ_2 in Fig. 4.11. Along the contour

$$\lambda = \lambda_1 + \epsilon \, e^{\mathrm{i}\phi},$$

where $\epsilon \to 0$ is a small real quantity and $\phi : \pi/2$ to $-3\pi/2$. Also, along the contour

$$\left(\lambda_1^2 - \lambda^2\right)^{1/2} = \left|\lambda_1^2 - \lambda^2\right|^{1/2} e^{\mathrm{i}\,\frac{(\gamma+\theta)}{2}},$$

where γ and θ can vary from $-\frac{\pi}{2}$ to $\frac{3\pi}{2}$.

The integral around the contour is

$$I_{\mathrm{C}_\epsilon} = \lim_{\epsilon \to 0} \int\limits_{\mathrm{C}_\epsilon} \underbrace{\frac{\left[1 - (-1)^m \, e^{\mathrm{i}\lambda \mathrm{a}}\right] \left(\lambda_1^2 - \lambda^2\right)^{1/2}}{\left(\lambda^2 - k_m^2\right) \left(\lambda^2 - k_p^2\right)}}_{f(\lambda)} \, \mathrm{d}\lambda. \tag{B.4}$$

Now evaluating $|(\lambda - \lambda_1) \, f(\lambda)|$ in the limit $\epsilon \to 0$,

$$\begin{aligned}\lim_{\epsilon \to 0} |(\lambda - \lambda_1) \, f(\lambda)| &= \lim_{\epsilon \to 0} \left| \frac{\epsilon \, e^{\mathrm{i}\phi} \left[1 - (-1)^m \, e^{\mathrm{i}\lambda_1 \mathrm{a}}\right] \left|\lambda_1^2 - \left(\lambda_1 + \epsilon \, e^{\mathrm{i}\phi}\right)^2\right|^{1/2} e^{\mathrm{i}\,\frac{(\gamma+\theta)}{2}}}{\left(\lambda_1^2 - k_m^2\right) \left(\lambda_1^2 - k_p^2\right)} \right| \\ &= 0.\end{aligned}$$

Therefore [1]

$$\lim_{\epsilon \to 0} \int\limits_{\mathrm{C}_\epsilon} f(\lambda) \, \mathrm{d}\lambda = 0.$$

Thus,

$$I_{\mathrm{C}_\epsilon} = 0. \tag{B.5}$$

B.3 Residues at the simple poles when $k_m \neq k_p$

The integrand of case 2 is (from Eq. (4.6))

$$f(\lambda) = \frac{\left[1 - (-1)^m \, e^{\mathrm{i}\lambda \mathrm{a}}\right] \, (\lambda_1^2 - \lambda^2)^{1/2}}{(\lambda^2 - k_m^2) \, \left(\lambda^2 - k_p^2\right)}.$$

The poles are at $\lambda = \pm k_m$ and $\pm\, k_p$, where $k_m = m\pi/a$ and $k_p = p\pi/a$. Now, the residue at k_m is given by

$$\mathrm{Res}(k_m) = \left. (\lambda - k_m) \, f(\lambda) \right|_{\lambda = k_m} = \frac{\left[1 - (-1)^{2m}\right] \, (\lambda_1^2 - k_m^2)^{1/2}}{2 \, k_m \, \left(k_m^2 - k_p^2\right)}$$

which is equal to zero. Thus,

$$\mathrm{Res}(k_m) = 0. \tag{B.6}$$

Similarly, we find that

$$\mathrm{Res}(-k_m) = \mathrm{Res}(k_p) = \mathrm{Res}(-k_p) = 0. \tag{B.7}$$

B.4 Residues at the poles when $k_m = k_p$

When $k_m = k_p$ the integrand of case 2 is

$$f(\lambda) = \frac{\left[1 - (-1)^m \, e^{\mathrm{i}\lambda \mathrm{a}}\right] \, (\lambda_1^2 - \lambda^2)^{1/2}}{(\lambda^2 - k_m^2)^2}.$$

The poles at $\lambda = \pm k_m$ are of multiplicity two. Fig. B.1 illustrates $\lambda_1 - \lambda$ and $\lambda_1 + \lambda$ near these poles.

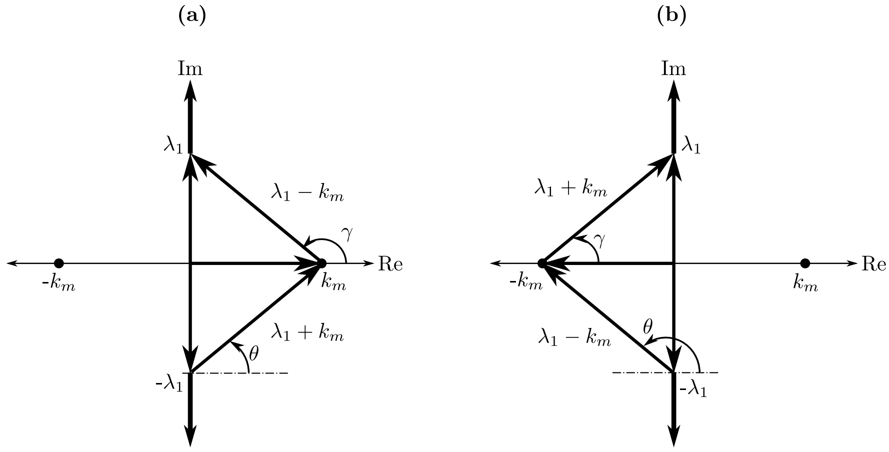

Fig. B.1 Illustrations of $\lambda_1 - \lambda$ and $\lambda_1 + \lambda$ near the poles $\lambda = \pm k_m$ in the complex λ plane (case 2).

It can be seen that along the real axis $\gamma + \theta = \pi$. Therefore, the value of the square root function (as given by Eq. (4.11)) along the real axis is

$$\left(\lambda_1^2 - \lambda^2\right)^{1/2} = \left|\lambda_1^2 - \lambda^2\right|^{1/2} e^{\mathrm{i}\,(\gamma+\theta)/2} = \mathrm{i}\,\left|\lambda_1^2 - \lambda^2\right|^{1/2}.$$

Now, the residue at $\lambda = k_m$ can be obtained from (see Fig. B.1a)

$$\mathrm{Res}(k_m) = \frac{\mathrm{d}}{\mathrm{d}\lambda}\left[(\lambda - k_m)^2 f(\lambda)\right]\bigg|_{\lambda = k_m}.$$

Substituting for $f(\lambda)$ with the appropriate square root term we obtain

$$\mathrm{Res}(k_m) = \frac{\mathrm{d}}{\mathrm{d}\lambda}\left[\frac{\left[1 - (-1)^m\, e^{\mathrm{i}\lambda \mathrm{a}}\right]\,\mathrm{i}\,|\lambda_1^2 - \lambda^2|^{1/2}}{(\lambda + k_m)^2}\right]\bigg|_{\lambda = k_m}.$$

Thus, knowing that $k_m = m\pi/a$ we get

$$\mathrm{Res}(k_m) = \frac{a\,|\lambda_1^2 - k_m^2|^{1/2}}{4\,k_m^2}. \tag{B.8}$$

Similarly, the residue at $\lambda = -k_m$ can be obtained from (see Fig. B.1b)

$$\mathrm{Res}(-k_m) = \frac{\mathrm{d}}{\mathrm{d}\lambda}\left[(\lambda + k_m)^2 f(\lambda)\right]\bigg|_{\lambda = -k_m} = \frac{\mathrm{d}}{\mathrm{d}\lambda}\left[\frac{\left[1 - (-1)^m\, e^{\mathrm{i}\lambda \mathrm{a}}\right]\,\mathrm{i}\,|\lambda_1^2 - \lambda^2|^{1/2}}{(\lambda - k_m)^2}\right]\bigg|_{\lambda = -k_m}.$$

And by knowing that $k_m = m\pi/a$ we arrive at

$$\mathrm{Res}(-k_m) = \frac{a\,\left|\lambda_1^2 - k_m^2\right|^{1/2}}{4\,k_m^2}. \tag{B.9}$$

Appendix C

About the Kraichnan's assumption

We have the integral (from Eq. (4.4))

$$I^{mnpq} = 4 \int_0^\infty \int_0^\infty \frac{\left[1-(-1)^m \cos \lambda a\right] \left[1-(-1)^n \cos \mu b\right] \left(k^2-\lambda^2-\mu^2\right)^{\frac{1}{2}}}{\left(\lambda^2-k_m^2\right)\left(\lambda^2-k_p^2\right)\left(\mu^2-k_n^2\right)\left(\mu^2-k_q^2\right)} \,\mathrm{d}\lambda \,\mathrm{d}\mu. \quad \text{(C.1)}$$

Note that the limits are now from 0 to ∞. The function

$$I^{nq}(\mu) = \frac{\left[1-(-1)^n \cos \mu b\right]}{\left(\mu^2-k_n^2\right)\left(\mu^2-k_q^2\right)} \quad \text{(C.2)}$$

has a behavior as shown in Fig. C.1. It can be found that [6]

$$\int_0^\infty I^{nq}(\mu)\,\mathrm{d}\mu = \begin{cases} \frac{\pi b}{4k_n^2} & \text{if } k_n = k_q \\ 0 & \text{if } k_n \neq k_q. \end{cases} \quad \text{(C.3)}$$

Kraichnan used this behavior of the function $I^{nq}(\mu)$ to approximate it using a Dirac delta function. He used the following approximation [10]

$$\left.\frac{\left[1-(-1)^n \cos \mu b\right]}{\left(\mu^2-k_n^2\right)\left(\mu^2-k_q^2\right)}\right|_{n=q} = \frac{\pi b}{4k_n^2}\,\delta(\mu-k_n). \quad \text{(C.4)}$$

In this thesis, the above approximation is referred to as the Kraichnan's approximation. The integration (Eq. (C.1)) is lot more easier if we make this approximation in the outer integral (either over the λ domain or over the μ domain). Here, the Kraichnan's approximation is used in the integration over the μ domain. The modal interaction cases and hence the modal wavenumbers k_m, k_n, k_p and k_q are selected in such a way

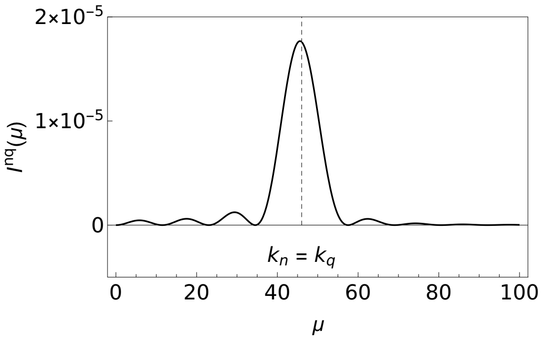

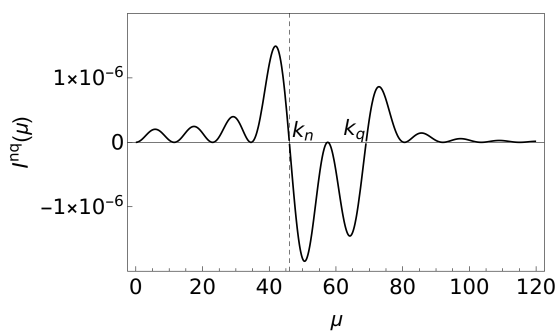

Fig. C.1 Plots of the function $I^{nq}(\mu)$ when $k_n = k_q$ and $k_n \neq k_q$ [6].

that we can make this approximation in the outer integral (μ domain), whenever the requirement arises. Before making the Kraichnan's assumption it has to be ensured that the modal wavenumbers k_n and k_q lie within the integral domain.

Using the above described behavior of $I^{nq}(\mu)$, one can assume that $I^{mnpq} \approx 0$ when $k_n \neq k_q$ for the Y edge - Y edge interaction. For the Y edge - Y edge interaction the integral I^{mnpq} is given by Eq. (4.17):

$$I^{mnpq} = 2\int_0^k \frac{[1-(-1)^n \cos \mu b]}{\left(\mu^2 - k_n^2\right)\left(\mu^2 - k_q^2\right)} I_1^{mp}(\mu : |\mu| < k)\, \mathrm{d}\mu + 2\int_k^\infty \frac{[1-(-1)^n \cos \mu b]}{\left(\mu^2 - k_n^2\right)\left(\mu^2 - k_q^2\right)} I_1^{mp}(\mu : |\mu| > k)\, \mathrm{d}\mu.$$

Here, $k_m, k_p > k$ and $k_n, k_q < k$. When $k_n = k_q$, we can use the Kraichnan's approximation to reduce the integral to

$$I^{mnpq} = \frac{\pi b}{2k_n^2} I_1^{mp}(k_n : k_n < k).$$

Here, by the Kraichnan's approximation and since $k_n < k$, only the contribution from the first integral on the right hand side of Eq. (4.17) is included. Since $k_n < k$, the value of the function $\frac{[1-(-1)^n \cos \mu b]}{(\mu^2 - k_n^2)^2}$ can be assumed to be negligible for $\mu > k$. This is true even when $k_n \neq k_q$, since $k_n, k_q < k$. It follows that when $k_n \neq k_q$ we can still approximate the integral I^{mnpq} including only the contribution from the first term on the right hand side of Eq. (4.17), i.e.,

$$I^{mnpq} = 2\int_0^k \frac{[1-(-1)^n \cos \mu b]}{\left(\mu^2 - k_n^2\right)\left(\mu^2 - k_q^2\right)} I_1^{mp}(\mu : |\mu| < k)\, \mathrm{d}\mu.$$

Since $k_n, k_q < k$ we can find that

$$\int_0^k \frac{[1-(-1)^n \cos \mu b]}{(\mu^2 - k_n^2)\left(\mu^2 - k_q^2\right)} \mathrm{d}\mu \approx 0$$

The integral $I_1^{mp}(\mu : |\mu| < k)$ is largely defined by the values of k_m and k_p $(k_m, k_p > k)$. Hence, we can assume that I_1^{mp} does not vary much in the domain $\mu : 0 \to k$. Therefore, when $k_n \neq k_q$, we can approximate

$$I^{mnpq} \approx 0.$$

Note that to obtain the above approximation no direct substitution of the Kraichnan's assumption is made. The above approximation is obtained by making use of the cues which led to the Kraichnan's assumption.

Appendix D

Detailed derivation of I^{mnpq} in closed form for various modal interactions

D.1 Y edge - Y edge

In this case $k_m, k_p > k$ and $k_n, k_q < k$.

D.1.1 $k_m \neq k_p$ and $k_n = k_q$

Eq. (4.14) is rewritten here

$$I_1^{mp}(\mu : |\mu| < k) = 2 \underbrace{\int_0^{\lambda_1} \frac{[1 - (-1)^m \ \cos ax] \ |\lambda_1^2 - x^2|^{1/2}}{(x^2 - k_m^2) \left(x^2 - k_p^2\right)} \mathrm{d}x}_{T_1(\mu)}$$

$$- 2\,\mathrm{i} \left[\underbrace{\int_0^{\lambda_1} \frac{(-1)^m \ \sin ax \ |\lambda_1^2 - x^2|^{1/2}}{(x^2 - k_m^2) \left(x^2 - k_p^2\right)} \mathrm{d}x}_{T_2(\mu)} + \underbrace{\int_0^{\infty} \frac{[1 - (-1)^m \ \mathrm{e}^{-ay}] \ |\lambda_1^2 + y^2|^{1/2}}{(y^2 + k_m^2) \left(y^2 + k_p^2\right)} \mathrm{d}y}_{T_3(\mu)} \right].$$

This can be used to evaluate $I_1^{mp}(k_n : k_n < k)$, by substituting $\mu = k_n$. In the following, closed form expressions are obtained for each of the integrals appearing in the above equation when $\mu = k_n$.

Integral $T_1(\mu : \mu = k_n)$

Consider first the integral

$$\int_0^{\lambda_1} \frac{\left[1-(-1)^m \cos ax\right] \left|\lambda_1^2 - x^2\right|^{1/2}}{\left(x^2-k_m^2\right)\left(x^2-k_p^2\right)} \, \mathrm{d}x.$$

The integrand can be written as

$$\frac{\left[1-(-1)^m \cos ax\right] \left|\lambda_1^2 - x^2\right|^{1/2}}{\left(x^2-k_m^2\right)\left(x^2-k_p^2\right)} = \frac{(-1)^{m+1}\sqrt{\lambda_1^2-x^2}\cos ax}{\left(x^2-k_m^2\right)\left(x^2-k_p^2\right)} + \frac{\sqrt{\lambda_1^2-x^2}}{\left(x^2-k_m^2\right)\left(x^2-k_p^2\right)}. \tag{D.1}$$

Since $k_m, k_p > \lambda_1$, the following approximation is used in the first term [15] (see Appendix E)

$$\left(x^2-k_m^2\right)\left(x^2-k_p^2\right) \approx \left(k_m^2-\lambda_1^2\right)\left(k_p^2-\lambda_1^2\right). \tag{D.2}$$

Now integrating

$$\int_0^{\lambda_1} \frac{(-1)^{m+1}\sqrt{\lambda_1^2-x^2}\cos ax}{\left(x^2-k_m^2\right)\left(x^2-k_p^2\right)} \, \mathrm{d}x \approx -\frac{\pi\lambda_1(-1)^m \mathrm{J}_1\left(a\lambda_1\right)}{2a\left(\lambda_1^2-k_m^2\right)\left(\lambda_1^2-k_p^2\right)},$$

where $\mathrm{J}_1(*)$ represents the Bessel function of the first kind and first order. Integrating the second term in Eq. (D.1) without any approximations yields

$$\int_0^{\lambda_1} \frac{\sqrt{\lambda_1^2-x^2}}{\left(x^2-k_m^2\right)\left(x^2-k_p^2\right)} \, \mathrm{d}x = \frac{\pi\left(k_p\sqrt{k_m^2-\lambda_1^2} - k_m\sqrt{k_p^2-\lambda_1^2}\right)}{2k_m^3 k_p - 2k_m k_p^3}.$$

Therefore

$$\int_0^{\lambda_1} \frac{\left[1-(-1)^m \cos ax\right] \left|\lambda_1^2 - x^2\right|^{1/2}}{\left(x^2-k_m^2\right)\left(x^2-k_p^2\right)} \, \mathrm{d}x \approx -\frac{\pi\lambda_1(-1)^m \mathrm{J}_1\left(a\lambda_1\right)}{2a\left(\lambda_1^2-k_m^2\right)\left(\lambda_1^2-k_p^2\right)} + \frac{\pi\left(k_p\sqrt{k_m^2-\lambda_1^2} - k_m\sqrt{k_p^2-\lambda_1^2}\right)}{2k_m^3 k_p - 2k_m k_p^3}. \tag{D.3}$$

Integral $T_2(\mu : \mu = k_n)$

Consider the integral

$$\int_0^{\lambda_1} \frac{(-1)^m \sin ax \, |\lambda_1^2 - x^2|^{1/2}}{(x^2 - k_m^2)\left(x^2 - k_p^2\right)} \, \mathrm{d}x.$$

Using the approximation Eq. (D.2) and integrating we get

$$\int_0^{\lambda_1} \frac{(-1)^m \sin ax \, |\lambda_1^2 - x^2|^{1/2}}{(x^2 - k_m^2)\left(x^2 - k_p^2\right)} \, \mathrm{d}x \approx \frac{\pi \lambda_1 (-1)^m \mathrm{H}_1(a\lambda_1)}{2a\left(\lambda_1^2 - k_m^2\right)\left(\lambda_1^2 - k_p^2\right)}, \tag{D.4}$$

where $\mathrm{H}_1(*)$ is the Struve function of the first order.

Integral $T_3(\mu : \mu = k_n)$

Consider the integral

$$\int_0^{\infty} \frac{\left[1 - (-1)^m \, \mathrm{e}^{-ay}\right] |\lambda_1^2 + y^2|^{1/2}}{(y^2 + k_m^2)\left(y^2 + k_p^2\right)} \, \mathrm{d}y.$$

For $\mu = k_n$ and $\lambda_1^2 = k^2 - k_n^2$, the integral can be written as

$$\begin{aligned}\int_0^{\infty} \frac{\left[1 - (-1)^m \, \mathrm{e}^{-ay}\right] |\lambda_1^2 + y^2|^{1/2}}{(y^2 + k_m^2)\left(y^2 + k_p^2\right)} \, \mathrm{d}y = &\underbrace{\int_0^{\infty} \frac{\sqrt{k^2 - k_n^2 + y^2}}{(k_m^2 + y^2)\left(k_p^2 + y^2\right)} \, \mathrm{d}y}_{T_3^1(k_n)} \\ &+ \underbrace{\int_0^{\infty} \frac{(-1)^{m+1} \mathrm{e}^{-ay} \sqrt{k^2 - k_n^2 + y^2}}{(k_m^2 + y^2)\left(k_p^2 + y^2\right)} \, \mathrm{d}y}_{T_3^2(k_n)} .\end{aligned} \tag{D.5}$$

Here, the integration domain can be divided into two parts: $\int_0^{\infty} = \int_0^k + \int_k^{\infty}$.

Integral $T_3^1(k_n)$

Consider the integration from 0 to k of $T_3^1(k_n)$. Since $y < k$ and $k_m, k_p > k$, the following approximation holds (see Appendix E)

$$\int_0^{k} \frac{\sqrt{k^2 - k_n^2 + y^2}}{(k_m^2 + y^2)\left(k_p^2 + y^2\right)} \, \mathrm{d}y \approx \int_0^{k} \frac{\sqrt{k^2 - k_n^2 + y^2}}{k_m^2 k_p^2} \, \mathrm{d}y.$$

Integrating and simplifying we get

$$\int_0^k \frac{\sqrt{k^2-k_n^2+y^2}}{(k_m^2+y^2)\left(k_p^2+y^2\right)}\,\mathrm{d}y \approx \frac{2k\sqrt{2k^2-k_n^2}+(k^2-k_n^2)\,\log\left(\frac{\left(\sqrt{2k^2-k_n^2}+k\right)^2}{k^2-k_n^2}\right)}{4k_m^2k_p^2}. \tag{D.6}$$

Now, for the integration from k to ∞, $y \gg k^2-k_n^2$. Therefore, we may approximate $\sqrt{k^2-k_n^2+y^2} \approx y$. Hence (see Appendix E),

$$\int_k^\infty \frac{\sqrt{k^2-k_n^2+y^2}}{(k_m^2+y^2)\left(k_p^2+y^2\right)}\,\mathrm{d}y \approx \int_k^\infty \frac{y}{(k_m^2+y^2)\left(k_p^2+y^2\right)}\,\mathrm{d}y.$$

Thus,

$$\int_k^\infty \frac{\sqrt{k^2-k_n^2+y^2}}{(k_m^2+y^2)\left(k_p^2+y^2\right)}\,\mathrm{d}y \approx \frac{\log\left(\frac{k^2+k_p^2}{k^2+k_m^2}\right)}{2\left(k_p^2-k_m^2\right)}. \tag{D.7}$$

Therefore using Eqs. (D.6) and (D.7) we obtain

$$\begin{aligned}\int_0^\infty \frac{\sqrt{k^2-k_n^2+y^2}}{(k_m^2+y^2)\left(k_p^2+y^2\right)}\,\mathrm{d}y \approx{}& \frac{\log\left(\frac{k^2+k_p^2}{k^2+k_m^2}\right)}{2\left(k_p^2-k_m^2\right)}\\ &+\frac{2k\sqrt{2k^2-k_n^2}+(k^2-k_n^2)\,\log\left(\frac{\left(\sqrt{2k^2-k_n^2}+k\right)^2}{k^2-k_n^2}\right)}{4k_m^2k_p^2}.\end{aligned} \tag{D.8}$$

Integral $T_3^2(k_n)$

Consider the following first order approximation for the exponential function

$$\mathrm{e}^{-ay} \approx \begin{cases} 1-ay & \text{when } ay<1\\ 0 & \text{when } ay\geq 1.\end{cases} \tag{D.9}$$

If $ak \geq \pi$, $\mathrm{e}^{-ay} \approx 0$, $\forall\, y \geq k$ (see Appendix E). Therefore

$$\int_k^\infty \frac{(-1)^{m+1}\mathrm{e}^{-ay}\sqrt{k^2-k_n^2+y^2}}{(k_m^2+y^2)\left(k_p^2+y^2\right)}\,\mathrm{d}y \approx 0.$$

The integration from 0 to k can be expressed as $\int_0^k = \int_0^{\frac{1}{a}} + \int_{\frac{1}{a}}^k$. When $y > 1/a$, i.e., $ay > 1$, we have the approximation $\mathrm{e}^{-ay} \approx 0$. Hence, one can neglect the integration from $1/a$ to k. Thus, by noting that $1/a < k$ and $k_m, k_p > k$ the integral can be approximated as

$$\int_0^\infty \frac{(-1)^{m+1}\mathrm{e}^{-ay}\sqrt{k^2 - k_n^2 + y^2}}{(k_m^2 + y^2)\left(k_p^2 + y^2\right)}\,\mathrm{d}y \approx \int_0^{\frac{1}{a}} \frac{(-1)^{m+1}(1 - ay)\sqrt{k^2 - k_n^2 + y^2}}{k_m^2 k_p^2}\,\mathrm{d}y.$$

Integrating we obtain

$$\begin{aligned}\int_0^\infty \frac{(-1)^{m+1}\mathrm{e}^{-ay}\sqrt{k^2 - k_n^2 + y^2}}{(k_m^2 + y^2)\left(k_p^2 + y^2\right)}\,\mathrm{d}y \approx \frac{(-1)^{m+1}}{12ak_m^2k_p^2}\Bigg\{2\sqrt{\frac{1}{a^2} + k^2 - k_n^2} - \left(k^2 - k_n^2\right)\\ \times\left[-4a^2\sqrt{k^2 - k_n^2} + 4a^2\sqrt{\frac{1}{a^2} + k^2 - k_n^2} - 3a\log\left(\frac{\left(\sqrt{\frac{1}{a^2} + k^2 - k_n^2} + \frac{1}{a}\right)^2}{k^2 - k_n^2}\right)\right]\Bigg\}.\end{aligned} \tag{D.10}$$

Thus, combining Eqs. (D.8) and (D.10) we get

$$\begin{aligned}\int_0^\infty \frac{\left[1 - (-1)^m\ \mathrm{e}^{-ay}\right]\ |\lambda_1^2 + y^2|^{1/2}}{(y^2 + k_m^2)\ \left(y^2 + k_p^2\right)}\,\mathrm{d}y \approx \frac{\log\left(\frac{k^2 + k_p^2}{k^2 + k_m^2}\right)}{2\left(k_p^2 - k_m^2\right)} + \frac{2k\sqrt{2k^2 - k_n^2}}{4k_m^2k_p^2}\\ + \frac{(k^2 - k_n^2)\ \log\left(\frac{\left(\sqrt{2k^2 - k_n^2} + k\right)^2}{k^2 - k_n^2}\right)}{4k_m^2k_p^2} + \frac{(-1)^{m+1}}{12ak_m^2k_p^2}\Bigg\{2\sqrt{\frac{1}{a^2} + k^2 - k_n^2} - \left(k^2 - k_n^2\right)\\ \times\left[-4a^2\sqrt{k^2 - k_n^2} + 4a^2\sqrt{\frac{1}{a^2} + k^2 - k_n^2} - 3a\log\left(\frac{\left(\sqrt{\frac{1}{a^2} + k^2 - k_n^2} + \frac{1}{a}\right)^2}{k^2 - k_n^2}\right)\right]\Bigg\}.\end{aligned} \tag{D.11}$$

Integral I^{mnpq}

We can now evaluate I^{mnpq} from Eq. (4.19). Using Eqs. (4.14), (D.3), (D.4) and (D.11) we obtain

$$I^{mnpq} \approx \frac{\pi b}{2k_n^2}\, I_1^{mp}(k_n : k_n < k) = I_R^{mnpq} + \mathrm{i}\, I_\chi^{mnpq}, \tag{D.12}$$

where the real part of I^{mnpq} is given by

$$I_R^{mnpq} = \frac{\pi^2 b}{2k_n^2}\left[\frac{k_p\sqrt{k_m^2-\lambda_1^2} - k_m\sqrt{k_p^2-\lambda_1^2}}{k_m^3 k_p - k_m k_p^3} - \frac{\lambda_1(-1)^m \mathrm{J}_1(a\lambda_1)}{a\left(\lambda_1^2-k_m^2\right)\left(\lambda_1^2-k_p^2\right)}\right]\delta_{nq}$$

and the imaginary part of I^{mnpq} is given by

$$I_\chi^{mnpq} = -\frac{\pi b}{k_n^2}(A+B+C)\,\delta_{nq}$$

with

$$A = \frac{\pi\lambda_1(-1)^m \mathrm{H}_1(a\lambda_1)}{2a\left(\lambda_1^2-k_m^2\right)\left(\lambda_1^2-k_p^2\right)},$$

$$B = \frac{2k\sqrt{2k^2-k_n^2} + (k^2-k_n^2)\log\left(\frac{\left(\sqrt{2k^2-k_n^2}+k\right)^2}{k^2-k_n^2}\right)}{4k_m^2 k_p^2} + \frac{\log\left(\frac{k^2+k_p^2}{k^2+k_m^2}\right)}{2\left(k_p^2-k_m^2\right)}$$

and

$$C = \frac{(-1)^{m+1}}{12ak_m^2k_p^2}\left\{2\sqrt{\frac{1}{a^2}+k^2-k_n^2} - \left(k^2-k_n^2\right)\right.$$

$$\left.\times\left[-4a^2\sqrt{k^2-k_n^2} + 4a^2\sqrt{\frac{1}{a^2}+k^2-k_n^2} - 3a\log\left(\frac{\left(\sqrt{\frac{1}{a^2}+k^2-k_n^2}+\frac{1}{a}\right)^2}{k^2-k_n^2}\right)\right]\right\}.$$

D.1.2 $k_m = k_p$ and $k_n = k_q$

When $k_m = k_p$, $I_1^{mp}(\mu : |\mu| < k)$ can be obtained from Eq. (4.21)

$$I_1^{mp}(\mu : |\mu| < k) = 2 \underbrace{\int_0^{\lambda_1} \frac{[1-(-1)^m \, \cos ax] \, |\lambda_1^2 - x^2|^{1/2}}{(x^2-k_m^2)^2} \, \mathrm{d}x}_{T_1(\mu)}$$
$$- 2\,\mathrm{i} \left[\frac{-\pi a \, |\lambda_1^2 - k_m^2|^{1/2}}{4\,k_m^2} + \underbrace{\int_0^{\lambda_1} \frac{(-1)^m \, \sin ax \, |\lambda_1^2 - x^2|^{1/2}}{(x^2-k_m^2)^2} \, \mathrm{d}x}_{T_2(\mu)} \right.$$
$$\left. + \underbrace{\int_0^{\infty} \frac{[1-(-1)^m \, \mathrm{e}^{-ay}] \, |\lambda_1^2 + y^2|^{1/2}}{(y^2+k_m^2)^2} \, \mathrm{d}y}_{T_3(\mu)} \right] .$$

$I_1^{mp}(k_n : k_n < k)$ for $k_m = k_p$ can be evaluated from the above equation by substituting $\mu = k_n$. A similar derivation as presented in the $k_m \neq k_p$ and $k_n = k_q$ case is followed for each of the integrals on the right hand side.

Integral $T_1(\mu : \mu = k_n)$

While evaluating the integral

$$\int_0^{\lambda_1} \frac{[1-(-1)^m \, \cos ax] \, |\lambda_1^2 - x^2|^{1/2}}{(x^2-k_m^2)^2} \, \mathrm{d}x$$

we get the following results

$$\int_0^{\lambda_1} \frac{(-1)^{m+1}\sqrt{\lambda_1^2 - x^2}\cos ax}{(x^2-k_m^2)^2} \, \mathrm{d}x \approx -\frac{\pi\lambda_1(-1)^m \mathrm{J}_1\,(a\lambda_1)}{2a\,(k_m^2-\lambda_1^2)^{\,2}}$$

and

$$\int_0^{\lambda_1} \frac{\sqrt{\lambda_1^2 - x^2}}{(x^2-k_m^2)^2} \, \mathrm{d}x = \frac{\pi\lambda_1^2}{4k_m^3\sqrt{k_m^2-\lambda_1^2}}.$$

Therefore

$$\int\limits_{0}^{\lambda_1} \frac{\left[1-(-1)^m \cos ax\right] \left|\lambda_1^2-x^2\right|^{1/2}}{\left(x^2-k_m^2\right)^2}\,\mathrm{d}x \approx -\frac{\pi\lambda_1(-1)^m \mathrm{J}_1\left(a\lambda_1\right)}{2a\left(k_m^2-\lambda_1^2\right)^2}+\frac{\pi\lambda_1^2}{4k_m^3\sqrt{k_m^2-\lambda_1^2}}. \tag{D.13}$$

Integral $T_2(\mu : \mu = k_n)$

Similarly, we can also arrive at

$$\int\limits_{0}^{\lambda_1} \frac{(-1)^m \sin ax \left|\lambda_1^2-x^2\right|^{1/2}}{\left(x^2-k_m^2\right)^2}\,\mathrm{d}x \approx \frac{\pi\lambda_1(-1)^m \mathrm{H}_1\left(a\lambda_1\right)}{2a\left(\lambda_1^2-k_m^2\right)^2}. \tag{D.14}$$

Integral $T_3(\mu : \mu = k_n)$

We can derive that

$$\int_0^\infty \frac{\sqrt{k^2-k_n^2+y^2}}{\left(k_m^2+y^2\right)^2}\,\mathrm{d}y \approx \frac{1}{2\left(k^2+k_m^2\right)}+\frac{2k\sqrt{2k^2-k_n^2}+\left(k^2-k_n^2\right)\log\left(\frac{\left(\sqrt{2k^2-k_n^2}+k\right)^2}{k^2-k_n^2}\right)}{4k_m^4}$$

and

$$\int_0^\infty \frac{(-1)^{m+1}\mathrm{e}^{-ay}\sqrt{k^2-k_n^2+y^2}}{\left(k_m^2+y^2\right)^2}\,\mathrm{d}y \approx \frac{(-1)^{m+1}}{12ak_m^4}\left\{2\sqrt{\frac{1}{a^2}+k^2-k_n^2}-\left(k^2-k_n^2\right)\right.$$
$$\left.\times\left[-4a^2\sqrt{k^2-k_n^2}+4a^2\sqrt{\frac{1}{a^2}+k^2-k_n^2}-3a\log\left(\frac{\left(\sqrt{\frac{1}{a^2}+k^2-k_n^2}+\frac{1}{a}\right)^2}{k^2-k_n^2}\right)\right]\right\}.$$

Thus,

$$\int_0^\infty \frac{\left[1-(-1)^m\ \mathrm{e}^{-ay}\right]\ \left|\lambda_1^2+y^2\right|^{1/2}}{\left(y^2+k_m^2\right)^2}\,\mathrm{d}y \approx \frac{2k\sqrt{2k^2-k_n^2}+(k^2-k_n^2)\log\left(\frac{\left(\sqrt{2k^2-k_n^2}+k\right)^2}{k^2-k_n^2}\right)}{4k_m^4}$$
$$+\frac{1}{2\left(k^2+k_m^2\right)}+\frac{(-1)^{m+1}}{12ak_m^4}\left\{2\sqrt{\frac{1}{a^2}+k^2-k_n^2}-\left(k^2-k_n^2\right)\right.$$
$$\times\left.\left[-4a^2\sqrt{k^2-k_n^2}+4a^2\sqrt{\frac{1}{a^2}+k^2-k_n^2}-3a\log\left(\frac{\left(\sqrt{\frac{1}{a^2}+k^2-k_n^2}+\frac{1}{a}\right)^2}{k^2-k_n^2}\right)\right]\right\}. \tag{D.15}$$

Integral I^{mnpq}

Now, I^{mnpq} (Eq. (4.22)) can be obtained using Eqs. (4.21), (D.13), (D.14) and (D.15) as

$$I^{mnpq} \approx \frac{\pi b}{2k_n^2}\, I_1^{mp}(k_n : k_n < k) = I_R^{mnpq} + \mathrm{i}\, I_\chi^{mnpq}, \tag{D.16}$$

where the real part of I^{mnpq} is given by

$$I_R^{mnpq} = \frac{\pi^2 b}{2k_n^2}\left[\frac{\lambda_1^2}{2k_m^3\sqrt{k_m^2-\lambda_1^2}} - \frac{\lambda_1(-1)^m J_1\left(a\lambda_1\right)}{a\left(k_m^2-\lambda_1^2\right)^2}\right]\delta_{mp}\,\delta_{nq}$$

and the imaginary part of I^{mnpq} is given by

$$I_\chi^{mnpq} = \left[-\frac{\pi b}{k_n^2}(A+B+C)+D\right]\delta_{mp}\,\delta_{nq}$$

with

$$A = \frac{\pi\lambda_1(-1)^m \mathrm{H}_1\left(a\lambda_1\right)}{2a\left(\lambda_1^2-k_m^2\right)^2},$$

$$B = \frac{2k\sqrt{2k^2-k_n^2}+(k^2-k_n^2)\log\left(\frac{\left(\sqrt{2k^2-k_n^2}+k\right)^2}{k^2-k_n^2}\right)}{4k_m^4} + \frac{1}{2\left(k^2+k_m^2\right)},$$

$$C = \frac{(-1)^{m+1}}{12ak_m^4}\left\{2\sqrt{\frac{1}{a^2}+k^2-k_n^2}-\left(k^2-k_n^2\right)\right.$$
$$\left.\times\left[-4a^2\sqrt{k^2-k_n^2}+4a^2\sqrt{\frac{1}{a^2}+k^2-k_n^2}-3a\log\left(\frac{\left(\sqrt{\frac{1}{a^2}+k^2-k_n^2}+\frac{1}{a}\right)^2}{k^2-k_n^2}\right)\right]\right\}$$

and $D = \dfrac{\pi^2 ab\sqrt{k_m^2-\lambda_1^2}}{4k_m^2k_n^2}$.

D.2 Corner - corner

In this case $k_m, k_n, k_p, k_q > k$.

D.2.1 $k_m \neq k_p$ and $k_n = k_q$

Consider Eq. (4.16):

$$I_1^{mp}(\mu : |\mu| > k) = -2\,\mathrm{i}\int\limits_{\lambda_1'}^{\infty}\frac{\left[1-(-1)^m\ \mathrm{e}^{-ay}\right]\left|\lambda_1'^2-y^2\right|^{1/2}}{\left(y^2+k_m^2\right)\left(y^2+k_p^2\right)}\,\mathrm{d}y,$$

where $\lambda_1'^2 = \mu^2 - k^2$. $I_1^{mp}(k_n : k_n > k)$ can be obtained from the above expression after substituting $\mu = k_n$. By neglecting the exponential term (which is small for large values of μ) and by changing the lower limit of integration to k we get [6, 15]

$$I_1^{mp}(k_n : k_n > k) \approx -2\,\mathrm{i}\int\limits_{k}^{\infty}\frac{\left|\lambda_1'^2-y^2\right|^{1/2}}{\left(y^2+k_m^2\right)\left(y^2+k_p^2\right)}\,\mathrm{d}y,$$

where $\lambda_1'^2 = k_n^2 - k^2$. Using the approximation $\left|\lambda_1'^2-y^2\right|^{1/2} \approx y$ (for $y : k \to \infty$) we get

$$I_1^{mp}(k_n : k_n > k) \approx -2\,\mathrm{i}\int\limits_{k}^{\infty}\frac{y}{\left(y^2+k_m^2\right)\left(y^2+k_p^2\right)}\,\mathrm{d}y.$$

Or

$$I_1^{mp}(k_n : k_n > k) \approx -\frac{\mathrm{i}\log\left(\frac{k^2+k_m^2}{k^2+k_p^2}\right)}{k_m^2-k_p^2}. \tag{D.17}$$

D.2.2 $k_m = k_p$ and $k_n = k_q$

Consider Eq. (4.32):

$$I_1^{mp}(\mu : |\mu| > k) = -2\mathrm{i}\left[\frac{-\pi a\ |\lambda_1^2 - k_m^2|^{1/2}}{4\,k_m^2} + \int\limits_{\lambda_1'}^{\infty} \frac{[1-(-1)^m\ \mathrm{e}^{-ay}]\ \left|\lambda_1'^{2} - y^2\right|^{1/2}}{\left(y^2 + k_m^2\right)^2}\,\mathrm{d}y\right]\delta_{mp},$$

where $\lambda_1 = \mathrm{i}\lambda_1' = \mathrm{i}\,(\mu^2 - k^2)$. For $\mu = k_n$, the integral on the right hand side is approximated in the same fashion as before. And thus,

$$I_1^{mp}(k_n : k_n > k) \approx -2\,\mathrm{i}\left[\frac{-\pi a\ |\lambda_1^2 - k_m^2|^{1/2}}{4\,k_m^2} + \int\limits_{k}^{\infty} \frac{y}{\left(y^2 + k_m^2\right)^2}\,\mathrm{d}y\right]\ \delta_{mp}.$$

Or

$$I_1^{mp}(k_n : k_n > k) \approx \mathrm{i}\left[\frac{\pi a\ |k_m^2 + k_n^2 - k^2|^{1/2}}{2\,k_m^2} - \frac{1}{\left(k^2 + k_m^2\right)}\right]\ \delta_{mp}. \qquad \text{(D.18)}$$

Appendix E

About the approximations used to obtain $I_1^{mp}(\mu)$

While deriving I^{mnpq} for different interactions, only the contributions from the dominant terms are considered. Approximations have been made in each case depending upon the range in which the panel modal wavenumbers k_m, k_n, k_p and k_p lie. In this section, some of these assumptions are discussed in detail.

E.1 Y edge - Y edge

Approximation 1

The following approximation has been used in the Y edge - Y edge interaction case (using Eq. (D.2)):

$$\int_0^{\lambda_1} \underbrace{\frac{(-1)^{m+1}\sqrt{\lambda_1^2 - x^2}\cos ax}{\left(x^2 - k_m^2\right)\left(x^2 - k_p^2\right)}}_{t_1(x)} \mathrm{d}x \approx \int_0^{\lambda_1} \underbrace{\frac{(-1)^{m+1}\sqrt{\lambda_1^2 - x^2}\cos ax}{\left(k_m^2 - \lambda_1^2\right)\left(k_p^2 - \lambda_1^2\right)}}_{t_1^{\mathrm{approx}}(x)} \mathrm{d}x.$$

In the above equation $\lambda_1 = \sqrt{k^2 - k_n^2}$. The functions $t_1(x)$ and $t_1^{\mathrm{approx}}(x)$ for x varying from 0 to λ_1 are plotted in Fig. E.1. For plotting, it is assumed that $a = 0.455$ m, $b = 0.546$ m, $m = 10$, $n = 3$, $p = 14$, $q = 3$ and air as the acoustic medium ($c = 343$ m/s). The functions are plotted at 1200 Hz. It can be observed that both the terms $t_1(x)$ and $t_1^{\mathrm{approx}}(x)$ have similar magnitudes in the range 0 to λ_1.

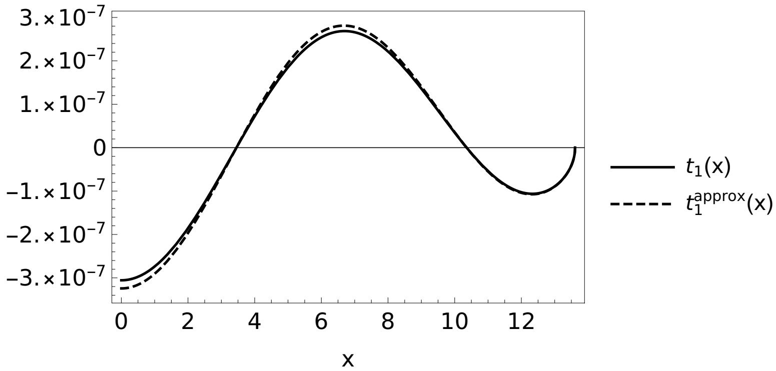

Fig. E.1 Plots of the functions $t_1(x)$ and $t_1^{\text{approx}}(x)$ (Y edge - Y edge case).

Approximation 2

Consider the approximation

$$\int_0^k \underbrace{\frac{\sqrt{k^2 - k_n^2 + y^2}}{\left(k_m^2 + y^2\right)\left(k_p^2 + y^2\right)}}_{t_2(y)} \, \mathrm{d}y \approx \int_0^k \underbrace{\frac{\sqrt{k^2 - k_n^2 + y^2}}{k_m^2 k_p^2}}_{t_2^{\text{approx}}(y)} \, \mathrm{d}y,$$

which has been used while evaluating $T_3^1(k_n)$.

The functions $t_2(y)$ and $t_2^{\text{approx}}(y)$ for y varying from 0 to k are plotted in Fig. E.2. The parameter values used are the same as that for the Approximation 1, above. It can be observed that the above approximation is satisfactory.

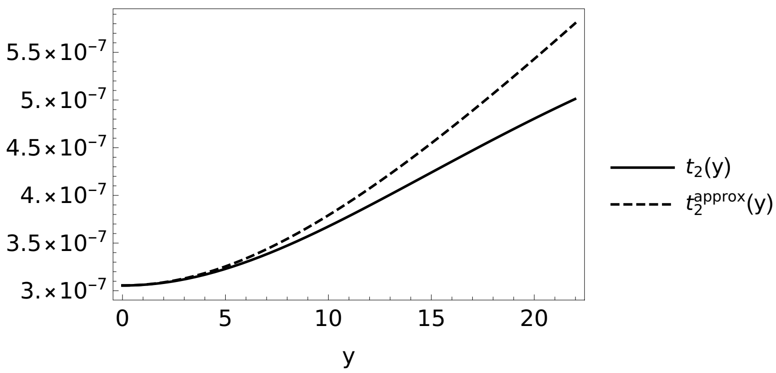

Fig. E.2 Plots of the functions $t_2(y)$ and $t_2^{\text{approx}}(y)$ (Y edge - Y edge case).

Approximation 3

Consider the following approximation which has been used while evaluating $T_3^1(k_n)$:

$$\int_k^\infty \underbrace{\frac{\sqrt{k^2 - k_n^2 + y^2}}{(k_m^2 + y^2)\left(k_p^2 + y^2\right)}}_{t_3(y)} \mathrm{d}y \approx \int_k^\infty \underbrace{\frac{y}{(k_m^2 + y^2)\left(k_p^2 + y^2\right)}}_{t_3^{\mathrm{approx}}(y)} \mathrm{d}y.$$

The functions $t_3(y)$ and $t_3^{\mathrm{approx}}(y)$ for y varying from k to ∞ are plotted in Fig. E.3. The parameter values used are the same as that for the Approximation 1. As seen from the figure, the above approximation holds good for the selected parameter range.

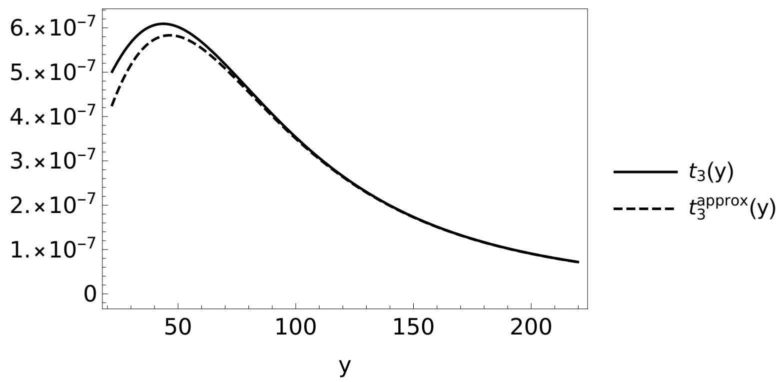

Fig. E.3 Plots of the functions $t_3(y)$ and $t_3^{\mathrm{approx}}(y)$ (Y edge - Y edge case).